High-efficiency photovoltaic cells with wide optical band gap polymers based on fluorinated phenylene-alkoxybenzothiadiazole

Journal:	*Energy & Environmental Science*
Manuscript ID	EE-ART-10-2016-003051.R2
Article Type:	Paper
Date Submitted by the Author:	n/a
Complete List of Authors:	Ko, Seo-Jin; University of California Santa Barbara, Center for Polymers and Organic Solids Hoang, Quoc Viet; Korea Research Institute of Chemical Technology, Energy Materials Research Center; University of Science and Technology, Department of Nanomaterials Science and Engineering Song, Chang Eun; Korea Research Institute of Chemical Technology, Energy Materials Research Center Uddin, Mohammad Afsar; Pusan National University, Department of Nanofusion Technology, Department of Cogno-Mechatronics Engineering (WCU) Lim, Eunhee ; University of California Santa Barbara, Materials Department Park, Song Yi; Ulsan National Institute of Science and Technology (UNIST), Interdisciplinary School of Green Energy Lee, ByoungHoon; University of California, Santa Barbara, Center for Polymers and Organic Solids Song, Seyeong; Ulsan National Institute of Science and Technology (UNIST), Interdisciplinary School of Green Energy Moon, Sang-Jin; Korea Research Institute of Chemical Technology, Hwang, Sungu; Pusan National University, Morin, Pierre-Olivier; Université Laval, Department of Chemistry Université Laval Leclerc, M; Universite Laval, Departement de Chimie Su, Gregory ; E O Lawrence Berkeley National Laboratory Chabinyc, Michael; University of California, Materials Department Woo, Han Young; Korea University, Chemistry Shin, Won Suk; Korea Research Institute of Chemical Technology, Energy Materials Research Center Kim, Jin Young; Ulsan National Institute of Science and Technology, School of Energy and Chemical Engineering

Article type: Full paper

Energy & Environmental Science

ROYAL SOCIETY OF CHEMISTRY

Website www.rsc.org/ees
Impact factor* 25.427

Journal expectations To be suitable for publication in *Energy & Environmental Science* articles must report high quality, agenda-setting research relating to energy conversion and storage, alternative fuel technologies and environmental science.

Article type: Full paper Original scientific work that has not been published previously. Full papers do not have a page limit and should be appropriate in length for scientific content.

Journal scope Visit the *Energy & Environmental Science* website for additional details of the journal scope and expectations.

Energy & Environmental Science is an international journal for the publication of important, very high quality, agenda-setting research relating to energy conversion and storage, alternative fuel technologies and environmental science. For work to be published it must be of significant general interest to our community-spanning readership.

The scope is intentionally broad and the journal recognises the complexity of issues and challenges relating to energy and environmental science and therefore particularly welcomes work of an interdisciplinary nature across both the (bio)chemical and (bio)physical sciences and chemical engineering disciplines. Topics include the following:

- Solar energy conversion and photovoltaics
- Fuel cells
- Hydrogen storage and (bio) hydrogen production
- Materials for energy systems
- Carbon capture and storage
- Catalysis for a variety of feedstocks (for example, oil, gas, coal, biomass and synthesis gas)
- Biofuels and biorefineries
- Global atmospheric chemistry
- Climate change
- Artificial photosynthesis
- Life cycle assessment
- Chemicals from carbon dioxide
- Energy systems and networks
- Nuclear power, including fusion technologies

Reviewer responsibilities Visit the Reviewer responsibilities website for additional details of the reviewing policy and procedure for Royal of Society of Chemistry journals.

When preparing your report, please:

- Focus on the originality, importance, impact and reliability of the science. English language and grammatical errors do not need to be discussed in detail, except where it impedes scientific understanding.
- Use the journal scope and expectations to assess the manuscript's suitability for publication in *Energy & Environmental Science.*
- State clearly whether you think the article should be accepted or rejected and include details of how the science presented in the article corresponds to publication criteria.
- Inform the Editor if there is a conflict of interest, a significant part of the work you cannot review with confidence or if parts of the work have previously been published.

Thank you for evaluating this manuscript, your advice as a reviewer for *Energy & Environmental Science* is greatly appreciated.

Dr Sam Keltie Executive Editor
Royal Society of Chemistry, UK

Professor Nathan Lewis Editorial Board Chair
California Institute of Technology (Caltech), USA

**2015 Journal Citation Reports®, (Thomson Reuters, 2016)*

High-efficiency photovoltaic cells with wide optical band gap polymers based on fluorinated phenylene-alkoxybenzothiadiazole

Seo-Jin Ko,‡[ab] Quoc Viet Hoang,‡[cd] Chang Eun Song,[cd] Mohammad Afsar Uddin,[e,f] Eunhee Lim,[g] Song Yi Park,[b] Byoung Hoon Lee,[a] Seyeong Song,[b] Sang-Jin Moon,[cd] Sungu Hwang,[f] Pierre-Olivier Morin,[h] Mario Leclerc,[h] Gregory M. Su,[i] Michael L. Chabinyc,[g] Han Young Woo,*[e] Won Suk Shin*[cd] and Jin Young Kim*[b]

[a] Center for Polymers and Organic Solids, University of California Santa Barbara (UCSB), Santa Barbara, CA 93106, USA

[b] School of Energy and Chemical Engineering, Ulsan National Institute of Science and Technology (UNIST), Ulsan 44919, Republic of Korea. E-mail) jykim@unist.ac.kr

[c] Energy Materials Research Center, Korea Research Institute of Chemical Technology (KRICT), 141 Gajeong-ro, Yuseong-gu, Daejeon 305-343, Republic of Korea. E-mail) shinws@krict.re.kr

[d] Department of Nanomaterials Science and Engineering, University of Science & Technology (UST), 217 Gajeong-ro, Yuseong-gu, Daejeon, 305-350, Republic of Korea.

[e] Department of Chemistry, Korea University, Seoul 136-713, Republic of Korea. E-mail) hywoo@korea.ac.kr

[f] Department of Nanomechatronics Engineering, Pusan National University, Miryang 627-706, Republic of Korea

[g] Materials Department, University of California Santa Barbara (UCSB), Santa Barbara, CA 93106, USA

[h] Department of Chemistry, Laval University, Quebec City, QC, G1V 0A6, Canada

[i] Advanced Light Source, Lawrence Berkeley National Laboratory, Berkeley, CA 94720, USA

KEYWORDS: wide band gap polymer, semi-crystalline, fluorine, noncovalent interactions, polymer solar cell, tandem solar cell

ABSTRACT

A series of semi-crystalline, wide band gap (WBG) photovoltaic polymers was synthesized with varying number and topology of fluorine substituents. To decrease intramolecular charge transfer and to modulate the resulting band gap of D-A type copolymers, electron-releasing alkoxy substituents were attached to electron-deficient benzothiadiazole (A) and electron-withdrawing fluorine atoms (0 ~ 4F) were substituted onto 1,4-bis(thiophen-2-yl)benzene unit (D). Intra- and/or interchain noncovalent coulombic interactions were also incorporated in the polymer backbone to promote planarity and crystalline intermolecular packing. The resulting optical band gap and the valence level were tuned to 1.93 ~ 2.15 eV and -5.37 ~ -5.67 eV, respectively, and strong interchain organization was observed by differential scanning calorimetry, high-resolution transmission electron microscopy and grazing incidence X-ray scattering measurements. The number of fluorine atoms and their position significantly influenced the photophysical, morphological and optoelectronic properties of bulk heterojunctions (BHJs) with these polymers. BHJ photovoltaic devices showed high power conversion efficiency (PCE) up to 9.8 % with an open-circuit voltage of 0.94 ~ 1.03 V. To our knowledge, this PCE is one of the highest values for fullerene-based single BHJ device with WBG polymers having a band gap over 1.90 eV. A tandem solar cell was also demonstrated successfully to show a PCE of 10.3% by combining a diketopyrrolopyrrole-based low band gap polymer.

1. Introduction

During the last several decades, organic bulk heterojunction (BHJ) polymer solar cells (PSCs) have attracted considerable attention as a portable and flexible energy source because of their light weight, mechanical flexibility and potential for low cost solution fabrication onto a large-area flexible plastic substrate.[1-4] Over the past few years, structural optimization of photovoltaic polymers (or small molecules) and device architecture, morphological control using processing additives and/or thermal (or solvent) annealing, as well as interlayer engineering, have led to power conversion efficiencies (PCE) over 10% in single and multi-junction PSCs.[5-11] The design strategy of Donor-Acceptor (D-A) type alternating copolymers using intramolecular charge transfer (ICT) interactions is an effective way to tune the band gap of photovoltaic materials in PSCs. According to the optical band gap, photovoltaic polymers can be classified into low band gap (LBG, Eg < 1.6 eV), mid band gap (MBG, 1.6 < Eg < 1.8 eV) and wide band gap (WBG, Eg > 1.8 eV) polymers.[12-20] Because the optical absorption of a single polymer is relatively narrow with respect to the solar spectrum, tandem or ternary blend solar cells have been often tried as an alternative method to cover a broader spectral range by combination of polymers with complementary optical absorption.[21-25] It has been predicted that the ultimately achievable PCE of a tandem PSC with two absorbing layers is 15–20%.[26, 27] To achieve such a high PCE in tandem PSCs, it is essential to have both highly efficient WBG and LBG-polymers with deep highest occupied molecular orbital (HOMO) and complementary optical absorption.[26, 27] Various types of MBG and/or LBG polymers have been reported, but relatively fewer WBG polymer have been examined in BHJs.[28, 29]

Development of new WBG conjugated polymers with excellent photovoltaic properties is important for efficient tandem or ternary PSCs. In the most efficient tandem cells reported previously, poly(3-hexylthiophene-2,5-diyl) (P3HT) is a common WBG polymer. However, the open-circuit voltage (V_{OC}) of BHJs with P3HT can be limited by its high-lying HOMO level.[22] Hou *et al*. recently pushed forward the highest PCE of tandem (11.6%) and ternary (12.2%) organic solar cells by utilizing a deep HOMO, WBG polymer instead of P3HT along with complimentary LBG polymer/small molecules with broad absorption spectra; this work demonstrated the importance of using high-efficiency, deep-HOMO WBG polymers in tandem and ternary solar cells.[30] However, very few high-efficiency, deep-HOMO WBG polymers have been currently reported. To design new WBG polymers with deep HOMO level, it is necessary to finely control the ICT interaction in the D-A copolymer structures while still allowing the morphology of BHJs to provide good charge mobility and charge generation to achieve high PCE. It is quite challenging to design an ordered WBG polymer with a deep HOMO that has a planar polymeric backbone. Although increasing the torsional angle between units in the polymer main chain can increase the band gap, the interchain organization can become significantly disturbed and this can disrupt the morphology.

There have been several successful reports on the WBG photovoltaic polymers (see Fig. S1 and Table S1, ESI†). Beaujuge *et al*. and co-workers designed poly(4,8-bis((2-ethylhexyl)oxy)benzo[1,2-b:4,5-b']dithiophene-3,4-difluorothiophene) (PBDT2FT) as an alternative WBG polymer to P3HT based on 3,4-diflurothiophene motifs to extend the optical gap (2.1 eV) and achieved 7% PCE in BHJs.[31] Hou *et al*. developed a new WBG polymer, PM6 by fluorination of a donor segment in the D-A alternating structure and

achieved over 9% PCE.[32] Wang *et al*. also developed an alternative copolymer, PBDTTS-FTAZ with a band gap 1.9 eV by using fluorinated benzotriazole and alkylthio side-chains, showing a PCE over 8% PCE.[33] Jo and coworkers investigated the fluorination (on the D unit) effect in the D−A polymers and obtained ~7% PCE.[34] Recently, Sun *et al*. reported a highly efficient WBG polymer (1.9 eV band gap) with the highest PCE of 9.8% reported so far by extending π-conjugation of benzodithiophene unit of poly[dithieno[2,3-d:2′,3′-d′]benzo[1,2-b:4,5-b′]dithiophene-co-1,3-bis(thiophen-2-yl)-benzo-[1,2-c:4,5 c′]dithiophene-4,8-dione] (PDBT-T1) polymer.[35]

Inspired by the previous reports, we designed new WBG polymers based on our previous design concept using intra- and/or interchain noncovalent coulombic interactions.[31-40] In this contribution, we have designed and synthesized a series of semi-crystalline WBG D-A type conjugated copolymers with fluorine substitution of varying number and position, based on the similar backbone of the previously reported poly[(2,5-bis(2-hexyldecyloxy)phenylene)-alt-(5,6-difluoro-4,7-di(thiophen-2-yl)benzo[c][1,2,5]thiadiazole)] (PPDT2FBT).[39] The band gap was finely tuned by the ICT interaction from the weak donor-weak acceptor design motif. To decrease the electron-deficiency of difluorobenzothiadiazole (2FBT) in PPDT2FBT, the fluorine substituents were replaced with the electron-releasing dialkoxy groups. In addition, the phenylene ring was substituted with varying the number and position of fluorine atoms, which decreases the electron sufficiency of 1,4-bis(thiophen-2-yl)phenylene moiety, resulting in a decreased ICT interaction along the polymeric backbone. The optical gap was successfully adjusted to 1.93~2.15 eV and remarkable photovoltaic PCE up to 9.8% was measured with high V_{OC} of ~1 V. To the best of our knowledge, the PCE of 9.8 % is one

of the highest values reported so far for fullerene-based single-junction BHJ PSCs using polymers with an optical band gap above 1.9 eV. The crystalline blend morphology with nanofibrillar structure formation and face on orientation explains well-balanced charge carrier transport and the resulting photovoltaic characteristics. By combining a diketopyrrolopyrrole (DPP)-based LBG polymer, DT-PDPP2T-TT, a tandem cell was also fabricated, showing a great potential (10.3% PCE) of the WBG polymers as a front subcell component.

2. Results and discussion

2.1 Molecular Design, Synthesis and Characterization.

Synthetic routes to the dialkoxybenzothiadiazole (DOBT) monomer and final polymers are described in Scheme 1. DOBT is substituted with two 2-hexyldecyloxy side-chains for solution processibility where the electron-releasing alkoxy group decreases the electron-withdrawing ability of DOBT and resulting ICT interaction, modulating the band gap of resulting polymers. Additionally, the intrachain dipole-dipole interaction via $S^{\delta+}\cdots O^{\delta-}$ in the neighboring thiophene and DOBT moieties enhances the chain planarity and interchain orderings. The substitution of solubilizing alkoxy side-chains on the electron-deficient BT negligibly increases the HOMO level. As shown in Scheme 1, the DOBT monomer was prepared by two steps using 5,6-difluorobenzothiadiazole (10) as a starting material. First, 5,6-difluorobenzothiadiazole was reacted with 2-hexyldecanol in *N,N*-dimethylformamide (DMF) to form 5,6-bis(2-hexyldecyloxy)benzothiadiazole (11) almost quantitatively, and then the monomer M21 was obtained in ~80% yield by bromination of 11 with bromine in a mixture of dichloromethane : acetic acid (2 : 1 by

volume). Five different kinds of dithienylbenzene intermediates (31~35) with different number and position of fluorine atoms were prepared by Stille coupling (yield: 50~80%) of dibromobenzene compounds (with/without fluorines) and 2-(tributylstannyl)thiophene. The dialkoxy substituents on BT decrease the electron deficiency of BT, resulting in decreased ICT along the polymeric backbone. Similarly, the different number of fluorine substituents with different topology (*syn* or *anti*) modulates the ICT interaction along the polymer backbone and influences the interchain dipole-dipole interactions and intermolecular ordering. The weak donor-weak acceptor design strategy decreases the ICT and increases the band gap (~2 eV), compared to the parent PPDT2FBT (band gap 1.76 eV) structure. Successive stannylation with n-butyllithium and trimethyltin chloride yielded the final M41~M45 monomers in 70~80% yield. The synthetic details are described (see ESI†). The resulting WBG copolymers were synthesized via the Stille coupling of brominated monomer M21 and five corresponding tin monomers (M41~M45) using Pd2dba3/P(o-tolyl)3 as a catalytic system in a microwave reactor, yielding poly[(5,6-bis(2-hexyldecyloxy)benzo[c][1,2,5]thiadiazole-4,7-diyl)-alt-(5,5'-(1,4-phenylene)bis(thiophen-2-yl))] (PDTBTBz-0F) (yield: 78%), poly[(5,6-bis(2-hexyldecyloxy)benzo[c][1,2,5]thiadiazole-4,7-diyl)-*alt*-(5,5'-(2-fluoro-1,4-phenylene)bis(thiophen-2-yl))] (PDTBTBz-1F) (77%), poly[(5,6-bis(2-hexyldecyloxy)benzo[c][1,2,5]thiadiazole-4,7-diyl)-*alt*-(5,5'-(2,3-difluoro-1,4-phenylene)bis (thiophen-2-yl))] (PDTBTBz-2F_{syn}) (77%), poly[(5,6-bis(2-hexyldecyloxy)benzo[c] [1,2,5]thiadiazole-4,7-diyl)-*alt*-(5,5'-(2,5-difluoro-1,4-phenylene)bis(thiophen-2-yl))] (PDTBTBz-2F_{anti}) (81%) and poly[(5,6-bis(2-hexyldecyloxy)benzo[c][1,2,5]thiadiazole-4,7-diyl)-*alt*-(5,5'-(2,3,5,6-tetrafluoro-1,4-

phenylene)bis(thiophen-2-yl))] (PDTBTBz-4F) (78%). All the polymers showed sufficient solubility in common organic solvents such as chloroform, chlorobenzene, and *o*-dichlorobenzene, etc.

Molecular weight and polydispersity index (PDI) of polymers were characterized by gel permeation chromatography (GPC) using *o*-dichlorobenzene as the eluent relative to polystyrene as a standard at 80 °C. Each polymerization was carried out three times and the three batches in the same condition showed similar molecular weights and PDI values. The number-average molecular weights (M_n) of this polymer series were measured to be in the range of 26~48 KDa (see Table 1). The thermal stability of the polymers was tested by thermogravimetric analysis (TGA) under a nitrogen atmosphere, showing decomposition temperatures (with 5% weight loss) of ~280 °C (see Fig. S2, ESI†). Differential scanning calorimetry (DSC) measurements show clear endothermic peaks at 243.3, 251.1, 253.0, 274.6, and 284.7 °C for PDTBTBz-0F, PDTBTBz-1F, PDTBTBz-$2F_{syn}$, PDTBTBz-$2F_{anti}$, and PDTBTBz-4F, respectively, which correspond the melting temperatures of each polymer (see Fig. S3, ESI†). The DSC data strongly support the crystalline nature of polymers, which may originate from strong interchain ordering via intra- and/or interchain noncovalent coulombic attractions (dipole-dipole and hydrogen bonding interaction). The melting point increases with increasing the number of fluorine atoms, suggesting stronger intermolecular interaction with fluorine substitution. In addition, the different symmetry in the fluorine substitution for PDTBTBz-$2F_{anti}$ (C2-symmetric) and PDTBTBz-$2F_{syn}$ (mirror-symmetric) may influence interchain organization in a solid state. According to the DSC data, PDTBTBz-$2F_{anti}$ with C2-

symmetric F substitution is expected to improve the crystalline interchain ordering with a close and tight packing.[12]

2.2 Structural Analysis by Density Functional Theory and Electrochemical Properties

The minimum energy conformation, torsional energy barriers between units, and the frontier orbital structures of five polymers were calculated by density functional theory (DFT; Jaguar quantum chemistry software, B3LYP/6-31G** level of theory). For simplicity, methyl substituents (in place of hexyldecyl groups) were considered for all structures.[37] The torsional angles between the constituting building blocks along the polymeric chain based on a model with two repeats unit are summarized inTable S2, ESI†. Upon addition of fluorine atoms to a benzene ring, the torsional angles (θ_2, θ_3, θ_6 and θ_7) between thiophene and benzene moieties were clearly decreased through the dipole-dipole induced interaction such as $S^{\delta+}\cdots F^{\delta-}$ and $F^{\delta-}\cdots H^{\delta+}$, inducing a more planar polymeric backbone (see dihedral angle: 20 degree for PDTBTBz-0F and 0 degree for PDTBTBz-4F). This planarity of the chain is beneficial for achieving more ordered interchain packing and hence affects the resulting morphology in BHJ films and their photovoltaic properties. Interestingly, the PDTBTBz-$2F_{syn}$ and PDTBTBz-$2F_{anti}$ polymers show clearly different minimum energy conformations where PDTBTBz-$2F_{anti}$ shows more planar structure compared to PDTBTBz-$2F_{syn}$. In addition, the electronic structure of HOMO and lowest unoccupied molecular orbital (LUMO) frontier orbitals were similar for all polymers but their energy levels were gradually down-shifted with substituting more fluorine atoms due to their strong electron-withdrawing effect (see Table S4, ESI†).

2.3 Optical and Electrochemical Properties

The UV-vis absorption spectra of the polymers in chloroform and in thin film are shown in Fig. 1 and summarized in Table 1. The polymers show two absorption bands in which the first absorption peak below 450 nm is attributed to characteristic π-π* transition and the low-energy absorption band in the range of 450-650 nm is attributed to the ICT interaction. With compared to the similarly structured PPDT2FBT reported previously (based on 2FBT and dialkoxy-substituted dithienylbenzene, optical band gap of 1.76 eV),[39] the newly synthesized PDTBTBz series polymers show a blue-shifted absorption due to the decreased ICT from dithienylbenzene (with or without fluorine) to DOBT.[41] The polymers show wide optical band gaps of 1.9-2.0 eV, depending on the number and topology of fluorine substitution. Except PDTBTBz-0F, all fluorine-substituted polymers show a vibrionic shoulder peak in solution, suggesting strong interchain interactions. In chloroform, the absorption maximum was observed at λ_{abs} = 508, 523, 558, 563 and 546 nm for PDTBTBz-0F, PDTBTBz-1F, PDTBTBz-2F$_{syn}$, PDTBTBz-2F$_{anti}$, and PDTBTBz-4F, respectively. With increasing the number of fluorine substitution, the λ_{abs} was measured to be red-shifted except PDTBTBz-4F. In film, the absorption spectra of PDTBTBz-0F and PDTBTBz-1F were further red-shifted with λ_{abs} = 569 and 571 nm. In contrary, PDTBTBz-2F$_{syn}$, PDTBTBz-2F$_{anti}$, and PDTBTBz-4F show similar λ_{abs}'s in solution and in film, which may be due to strong self-aggregation of these polymers even in solution with increasing fluorine substitution. It is noteworthy to mention that PDTBTBz-2F$_{anti}$ and PDTBTBz-4F shows the most pronounced vibrionic shoulder peak in films, suggesting the strongest interchain π–π stacking than other polymers.

Cyclic voltammetry (CV) was utilized to investigate the electrochemical properties and electronic energy levels of the polymers (see Fig. S5, ESI†). The HOMO energy levels of the polymers were determined from the oxidation onsets, by assuming the energy level of ferrocene (Fc) is -4.8 eV relative to the vacuum level. In the anodic scan, the onsets of oxidation for PDTBTBz-0F, PDTBTBz-1F, PDTBTBz-2F$_{syn}$, PDTBTBz-2F$_{anti}$, and PDTBTBz-4F were measured at 0.57, 0.58, 0.62, 0.70, and 0.87 V, corresponding to the ionization potential values of -5.37, -5.38, -5.42, -5.50, and -5.67 eV, respectively. The LUMO energy levels were estimated similarly from the reduction onsets. In the cathodic scan, the onsets of reduction (versus Fc+/Fc) for PDTBTBz-0F, PDTBTBz-1F, PDTBTBz-2F$_{syn}$, PDTBTBz-2F$_{anti}$, and PDTBTBz-4F occur at -1.40, -1.35, -1.36, -1.31, and -1.28 V, corresponding to the LUMO level of -3.40, -3.45, -3.44, -3.49, and -3.52 eV, respectively. The results are summarized in Table 1 and the energy band diagram is sketched in Fig. 1d. It indicates that both HOMO and LUMO of polymers become deeper with increasing F substituents onto the polymer backbone, being consistent with the DFT calculation. A comparison of PDTBTBz-2F$_{syn}$ and PDTBTBz-2F$_{anti}$ reveals that the substitution of two F atoms at *anti* positions leads to a deeper HOMO energy level than that for the *syn* isomer. The HOMO energy levels of PDTBTBz polymers are clearly down-shifted (up to -5.67 eV) and the LUMO levels are up-shifted (up to -3.40 eV) based on the weaker donor and acceptor pairs, resulting in wider band gap, compared to PPDT2FBT (HOMO: -5.45 eV, LUMO: -3.69 eV).[39]

2.4. Photovoltaic Characteristics

To investigate the photovoltaic properties of PDTBTBz-based polymers, the PSC devices using a BHJ blend of PDTBTBz-based polymers as the electron donor and [6,6]-phenyl-C_{71} butyric acid methyl ester ($PC_{71}BM$) as the acceptor were fabricated in a conventional device structure of indium-tin-oxide (ITO)/poly(3,4-ethylenedioxythiophene):polystyrene sulfonate (PEDOT:PSS) /polymers:$PC_{71}BM$/Ca/Al (see Fig. 1c). First, the device fabrication was optimized at a polymer:$PC_{71}BM$ blend ratio of 1:1.5 (by weight) using chlorobenzene as a main solvent without any processing additives. The photovoltaic characteristics were tested under illumination condition of AM 1.5G (100 mW cm^{-2}). Fig. S6a† and S6b† show optimal current density and voltage (*J-V*) curves and external quantum efficiency (EQE) spectra, respectively. As summarized in Table S4†, the device with PDTBTBz-$2F_{anti}$ showed the highest PCE of 5.4 % with J_{SC} of 10.6 mA cm^{-2}, V_{OC} of 0.93, and fill factor (FF) of 0.55. The use of processing additives can modify the BHJ morphology, resulting in improvement of device properties in many cases.[42, 43] We therefore further tested devices with diphenyl ether (DPE) as a processing additive.[39, 44] The devices processed with the solvent mixture of CB and DPE (97:3 vol. %) led to a remarkable increase in all device parameters compared to devices without DPE as shown in Fig. 2 and Fig. S6†. In addition, we investigated the use of other processing additives such as 1,8-diiodooctane and 1-chloronaphthalene with PDTBTBz-$2F_{anti}$:$PC_{71}BM$ blends (morphologies are reported in Fig. S7). These results confirmed that DPE was the most effective processing additive. PDTBTBz-$2F_{anti}$:$PC_{71}BM$ blends processed with DPE exhibited the best performance among all of our WBG polymer blends as shown in Fig. S8† and Table S5†. In particular, PCEs of the devices with incorporation of DPE significantly increased from 2.2, 2.6, 5.2, 5.4, and 2.5% to 7.3, 7.5, 8.1, 9.8, and 4.1% for PDTBTBz-0F, -1F, -$2F_{syn}$, -$2F_{anti}$ and -4F

based PSCs, respectively. The detailed device parameters are listed in Table 2. Remarkably high values of the V_{OC} (over 0.9 V) and good values of the FF (0.6~0.7) were obtained for all devices. The optimized thicknesses of active layers with DPE additive were determined to be 160 nm (PDTBTBz-0F), 145 nm (PDTBTBz-1F), 150 nm (PDTBTBz-2F$_{syn}$), 190 nm (PDTBTBz-2F$_{anti}$) and 150 nm (PDTBTBz-4F).

Among five PDTBTBz-based PSC devices processed with CB:DPE, device using PDTBTBz-2F$_{anti}$:PC$_{71}$BM blend showed the best PCE of 9.8 % with J_{SC} of 14.0 mA cm^{-2}, V_{OC} of 0.97 V and FF of 0.72. The J_{SC} (14.0 mA cm^{-2}) measured from device with PDTBTBz-2F$_{anti}$:PC$_{71}$BM blend is well matched with the calculated J_{SC} (13.8 mA cm^{-2}) from EQE as shown in Fig. 2b and Table 2. To the best of our knowledge, the PCE of 9.8 % is one of the highest values yet reported for fullerene-based single BHJ PSCs using polymers with band gaps over 1.90 eV. Interestingly, difluorinated PDTBTBz-2F$_{anti}$ and PDTBTBz-2F$_{syn}$ showed higher photovoltaic performance, compared with PDTBTBz-0F, -1F and 4F. Furthermore, the *anti*-substitution of two F atoms turned out to be more beneficial for improving the photovoltaic properties. Compared to PPDT2FBT, PDTBTBz-2F$_{anti}$ shows the lower J_{SC} (16.3 →14.0 mA cm^{-2}) due to narrower absorption range but higher V_{OC} (0.79 → 0.97 V) with deeper HOMO. Both polymers show similarly high *FF*, showing well distributed nano-fibrillar, semi-crystalline BHJ film morphology.[39]

2.5. Characterization of Film Morphology

Fig. 3 shows AFM topography images of polymer:PC$_{71}$BM blend films prepared from CB and CB:DPE solvents. The BHJ film of PDTBTBz-0F prepared from CB solvent shows very smooth surface with root-mean-square (rms) roughness of 0.58. With increasing F

substitution, the surface roughens with rms values increasing 1.04, 1.55, 1.83 and 2.43 nm for DTBTBz-1F, -2F_{syn}, -2F_{anti} and 4F blend films respectively. This roughness may be related to the strong interchain interaction and self-agglomeration. In contrast, the optimal BHJ films prepared from a CB:DPE solvent mixture show significantly different nanoscale morphologies. Among the blend films, the PDTBTBz-2F_{anti}:$PC_{71}BM$ blend are the smoothest (rms roughness of 1.58 nm) and finely dispersed surface topology (see Fig. 3i).

To further study the BHJ film morphology of PDTBTBz-2F_{syn} and PDTBTBz-2F_{anti} blend films, HR-TEM images were also measured as shown in Fig. 4. Both PDTBTBz-2F_{syn} and PDTBTBz-2F_{anti} blend films show fibril-like structures and more finely distributed and clear fibrillar structures were observed with addition of DPE (Fig. 4c and 4d). A similar blend morphology of PPDT2FBT was reported previously,[39] which is closely related to the semi-crystalline nature of polymer *via* intra- and/or interchain noncovalent coulombic interactions. The nanofibrillar crystalline morphology can allow efficient charge transport, increasing the J_{SC} and FF values of PSCs.[36, 45] The TEM image of PDTBTBz-2F_{anti} blend film (processed with DPE) showed the more developed fibrillary structures compared to the PDTBTBz-2F_{syn} blend, leading to better device performance of PDTBTBz-2F_{anti}:$PC_{71}BM$. The morphology of PDTBTBz-2F_{anti} blend film, obtained from AFM and HR-TEM measurements helps to provide the high photovoltaic efficiency compared to all polymers examined.

To further investigate the detailed film morphologies of five PDTBTBz-based polymers, the molecular orientation and packing characteristics were studied by 2D-GIWAXS.[46-48] Fig. 5 and Fig. S9† show 2D-GIWAXS images and in-plane and out-of-plane line-cut

profiles of pristine polymers, polymer:$PC_{71}BM$ blended films with and without DPE. The extracted 2D-GIWAXS scattering features are summarized in Table S6†. With regard to pristine films, the scattering from PDTBTBz-0F is characteristic of a glassy film, but increasing order is observed for polymers with F substituents. PDTBTBz-$2F_{anti}$ shows well-resolved lamellar scattering up to (300) in the out-of-plane direction with π-π stacking (010) peaks in both in-plane and out-of-plane directions. The lamellar *d*-spacing for PDTBTBz-1F, -$2F_{syn}$, -$2F_{anti,}$ and -4F neat films were measured to be ~18 to 21 Å. The π-π stacking distances were ~3.7Å for all samples.

In the case of BHJs of the polymers with $PC_{71}BM$, there were no large changes in the packing structure of the polymer, but there were changes in texture of the crystallites. The π-π stacking (010) peak appears mainly in the out-of-plane direction, suggesting preferential face-on orientation in the blends (see PDTBTBz-$2F_{syn}$, PDTBTBz-$2F_{anti}$ and PDTBTBz-4F blend films). The polymer phase in PDTBTBz-0F: $PC_{71}BM$ and PDTBTBz-1F: $PC_{71}BM$ BHJs is disordered, and no clear alkyl or π-π stacking (010) peak are assignable. Aggregates of $PC_{71}BM$ are observed in all BHJs by a characteristic glassy peak around 1.33~1.37$Å^{-1}$ similar to observations for BHJs of PCPDTBT/$PC_{71}BM$ and other systems.[49, 50] Upon addition of a processing additive, DPE, similar scattering patterns with qualitatively stronger scattering were observed. PDTBTBz-$2F_{anti}$:$PC_{71}BM$ and PDTBTBz-$2F_{syn}$:$PC_{71}BM$ blends show the most pronounced lamellar and π-π stacking scatterings. Interestingly, the PDTBTBz-4F:$PC_{71}BM$ also showed a strong and similar 2D-GIWAXS pattern to the difluoro-polymers, but the lowest photovoltaic performance was observed.

The phase separated domain structure is closely correlated with charge separation and extraction in BHJ polymer:fullerene solar cell systems.[47, 51, 52] In-plane periodicities for five PDTBTBz-based BHJ blend thin films were probed using resonant soft X-ray scattering (RSoXS).[47, 51, 52] The five blend samples were prepared using the same film fabrication conditions used to prepare optimized solar cell devices. RSoXS data were obtained at a photon energy of 286.4 eV, which exhibited high scattering contrast. Fig. S10† shows Lorentz corrected RSoXS profiles as a function of scattering vector q. A single dominant peak located in the range of q = 0.010-0.017 $Å^{-1}$ was observed for all five samples, corresponding to length scales of approximately 43, 51, 44, 38, and 60 nm for PDTBTBz-0F, PDTBTBz-1F, PDTBTBz-$2F_{syn}$, PDTBTBz-$2F_{anti}$ and PDTBTBz-4F containing BHJ blend films, respectively. This length scale likely corresponds to an average domain separation distance. The PDTBTBz-$2F_{anti}$:$PC_{71}BM$ blend exhibits the smallest domain separation and the highest PCE in solar cell devices, suggesting that this BHJ blend may form a phase separated morphology with more favorable length scales for charge separation and transport relative to the other BHJ blends. With compared to PDTBTBz-2F polymers, PDTBTBz-4F has the most rigid structure with 4 fluorine atoms in the polymeric backbone and shows the strongest tendency of interchain aggregation with relatively poor solubility. As shown in Fig. S10, the PDTBTBz-4F:$PC_{71}BM$ blend exhibits a larger average domain size. The quick and excessive segregation of PDTBTBz-4F may decrease the domain purity (Fig. S10†) in the blend with $PC_{71}BM$, resulting in poorer photovoltaic performance.

2.6. Charge Carrier Transport and Recombination

To study the charge transport and recombination behaviors in the PDTBTBz-based PSCs, the light intensity dependence of J_{SC} was measured under short-circuit condition.[53-55] Fig. 2c exhibits logarithmic plots of J_{SC}s as a function of the light intensity, showing the power-law dependence of $J_{SC} \propto P_{\alpha}$ (where P is the incident-light intensity and α is an exponential constant, generally 0.85-1 in PSCs).[55] The α values were determined to be 0.90, 0.91, 0.94, 0.94 and 0.92 for the PDTBTBz-0F, -1F, -2F_{anti}, -2F_{syn} and -4F BHJ devices with $PC_{71}BM$ (with DPE), respectively. The devices of PDTBTBz-2F_{syn} and -2F_{anti} showed relatively higher value (α = 0.94) compared to other devices. The higher α value for the PDTBTBz-2F_{anti} and -2F_{syn} devices suggests a weaker bimolecular recombination during charge transport process,[55] showing a good agreement with the measured photovoltaic characteristics for both devices (see Table 2).

The charge carrier transport in both horizontal and vertical directions, was investigated by fabrication of polymer field-effect transistor (PFET) and the SCLC method. The details for PFET fabrication are described in the Experimental section (channel length L = 20 μm, channel width W =1000 μm). Transfer and output characteristics of the PFETs of five PDTBTBz-based polymers are shown in Fig. S11† and Fig. S12†, respectively. As summarized in Table S7†, the hole mobilities were determined to be 2.4×10^{-2}, 4.1×10^{-2}, 5.2×10^{-2}, 5.6×10^{-2} and 9.0×10^{-3} cm^2 V^{-1} s^{-1}, for the PDTBTBz-0F, -1F, -2F_{syn}, -2F_{anti} and -4F pristine polymer films, respectively. PDTBTBz-2F_{anti} and -2F_{syn} show the highest hole mobility. To obtain the vertical mobility, hole-only (ITO/PEDOT:PSS/polymers:$PC_{71}BM$/Au) and electron-only (FTO/polymer:$PC_{71}BM$/Al, FTO: fluorine-doped tin oxide) devices were prepared under the same fabrication condition for the optimized PSC devices. Fig. S13† and Table S8† show the *J-V*

characteristics and extracted mobility values of hole- and electron-only devices, respectively. The vertical hole and electron mobilities were calculated based on the Mott-Gurney equation of $J_{SCL} = 9\varepsilon_0\varepsilon_r\mu V^2/(8L^3)$ (where ε_0 is free-space permittivity, ε_r is dielectric constant of the semiconductor, μ is mobility, V is the applied voltage and L is the thickness of the active layer).[56, 57] The hole (μ_h) (and electron (μ_e)) mobility values obtained from the SCLC method are 1.0×10^{-3} (7.5×10^{-4}), 1.07×10^{-3} (8.3×10^{-4}), 1.0×10^{-3} (9.0×10^{-4}), 1.15×10^{-3} (1.1×10^{-3}) and 1.15×10^{-4} (7.3×10^{-4}) $cm^2\ V^{-1}\ s^{-1}$, for the BHJ devices of PDTBTBz-0F, -1F, -$2F_{syn}$, -$2F_{anti}$ and -4F, respectively (see Table S8†). All the devices showed the efficient vertical transport of charge carriers, showing mobility of $\sim 10^{-3}$ $cm^2\ V^{-1}\ s^{-1}$. The μ_h / μ_e ratio was also calculated to be 1.33 (PDTBTBz-0F), 1.29 (PDTBTBz-1F), 1.11 (PDTBTBz-$2F_{syn}$), 1.05 (PDTBTBz-2_{Fanti}) and 0.16 (PDTBTBz-4F). The PDTBTBz-$2F_{anti}$:$PC_{71}BM$ and PDTBTBz-$2F_{syn}$:$PC_{71}BM$ blends with DPE show the most balanced μ_h / μ_e ratio of 1.05~1.11, suggesting the efficient charge transport and extraction with little electron-hole recombination in the PSC device. On the contrary, the poor photovoltaic properties of device using PDTBTBz-4F:$PC_{71}BM$ may be mainly due to an unbalanced charge carrier transport, build-up of space charges and the resulting electron-hole recombination.

2.7. Tandem Solar Cells

Based on the outstanding photovoltaic performance of a single junction PSC of PDTBTBz-$2F_{anti}$, we also fabricated a tandem PSC by combining the WBG polymer PDTBTBz-$2F_{anti}$ (Eg > 1.9 eV) with a DPP-based LBG polymer, DT-PDPP2T-TT (Eg ~1.4 eV)[58] These two polymers have complementary absorption spectra such that the WBG

front cell absorbs high energy photons and produces a large V_{OC}, while allowing low energy red and infrared photons to pass through to the LBG back cell which produces additional current at a lower V_{OC}. Brabec and coworkers suggested that an optimal combination of bandgaps of 1.3 eV and 1.6 eV would maximize the tandem device efficiency, however, this study did not completely account for the effects of overlapping absorption spectra.[26, 27] The tandem PSC was fabricated using a conventional device structure where the PDTBTBz-2F_{anti}:$PC_{71}BM$ and DT-PDPP2T-TT:$PC_{71}BM$ blend layers were incorporated as a front and back cell, respectively (Fig. 6a). DT-PDPP2T-TT LBG polymer was synthesized following the same synthetic method and the device was fabricated using the same condition as reported in the previous literature.[44, 58] As shown in Fig. 6c, the PDTBTBz-2F_{anti}:$PC_{71}BM$ and DT-PDPP2T-TT:$PC_{71}BM$ blends show complementary absorption, covering a broad range of solar spectrum of UV-vis and near infrared regions up to 900 nm in a tandem device. The front (PDTBTBz-2F_{anti}:$PC_{71}BM$) and back subcell (DT-PDPP2T-TT:$PC_{71}BM$) showed the PCEs of 9.0 % and 8.0 %, respectively (see Fig. 6d and Table S9). By combining both front and back cells, the tandem PSC achieved the PCE of 10.3 % along with J_{SC} = 9.89 mA cm^{-2}, V_{OC} = 1.58 V, and FF = 0.66. We confirmed the great potential of tandem devices using the WBG PDTBTBz polymer and the device optimization is now under investigation by combining various LBG polymers, recombination layer and modulating thickness of each subcell. The detailed results on the tandem devices will be reported separately.

2.8. Inverted Devices and Device Stability

We prepared and characterized inverted devices (Fig. S14) using the architecture of ITO/ZnO/active layer/MoO_3/Au. These devices exhibited slightly reduced photovoltaic performance relative to that of conventional devices, showing a J_{SC} of 11.3 $mAcm^{-2}$, V_{OC} of 0.97 V, FF of 0.66 and PCE of 7.3%. We investigated the air stability of inverted devices and conventional devices (conventional devices with Al or Ca/Al electrodes without sealing and Ca/A1 with UV epoxy sealant; inverted structure devices using MoO_3/Au electrode without sealing). As shown in Fig. S15, the performance degradation of devices with Al and Ca/Al electrodes without encapsulation is similar within 100 h of air exposure. In contrast, the devices with MoO_3/Au without sealing and Ca/Al with UV epoxy sealing show much better long-term stability. The Ca/Al cathode is not stable and is unsuitable for commercialization of PSCs. However, we observed that conventional devices using Ca/Al with proper encapsulation showed similar or better stability compared to inverted devices without encapsulation. These data indicate that our WBG polymers exhibit comparably good stability in the inverted geometry or in the conventional structure with proper encapsulation.

3. Conclusion

In summary, new series of semi-crystalline photovoltaic polymers with wide band gap over 1.90 eV were designed and synthesized based on weak donor-weak acceptor motif by varying number and position of fluorine substituents. In a design of a polymeric main chain, noncovalent coulombic interactions (such as H bonding and dipole-dipole interactions) were considered to enhance the chain planarity and interchain ordering. By attaching the solubilizing alkoxy side chains onto the electron-deficient benzothiadiazole,

the intramolecular charge transfer was modulated to decrease with maintaining a deep conduction band. Five different polymers showed an optical band gap in the range of 1.93 ~ 2.15 eV and the HOMO level decreased gradually with increasing the number of fluorine substituents (-5.37 ~ -5.67 eV). In particular, PDTBTBz-2F_{anti} showed a crystalline nanofibrillar morphology with strong face on π-π stacking in the blend film with $PC_{71}BM$. The best PCE of 9.8% was obtained with PDTBTBz-2F_{anti} with remarkably high a V_{OC} of 0.97 V, J_{SC} of 13.95 mA cm^{-2} and FF of 0.72. The high horizontal mobility of 5.6×10^{-2} cm^2 V^{-1} s^{-1} was measured by PFET fabrication and well balanced hole and electron mobilities (μ_h/μ_e = $1.15 \times 10^{-3}/1.1 \times 10^{-3}$ cm^2 V^{-1} s^{-1}) in a vertical direction were also measured by SCLC method. In addition, PDTBTBz-2F_{anti} showed a great potential as a front subcell, showing the PCE of 10.3 % in a tandem PSC device.

4. Experimental

4.1. General

^1H, ^{13}C and ^{19}F nuclear magnetic resonance (NMR) spectroscopy spectra were recorded on Bruker DRX-300 FT-NMR, Bruker Avance-400 MHz, and Bruker Avance-500 MHz spectrometer at 25 °C. Me_4Si and the residual solvent peak impurity are used as reference of 1H and 13C NMR spectra. Chemical shifts are reported in ppm and coupling constants in Hz as absolute values. UV-Visible spectroscopies were recorded using wither a Shimadzu UV-2550 spectrophotometer at room temperature. All solution UV-vis experiments were carried out in $CHCl_3$. Films were prepared by spin-coating $CHCl_3$ solutions onto quartz substrates. Full scan, low resolution mass spectrometry was carried

out at the analytical center, Korea Research Institute of Chemical Technology. DSC was determined using a TA Instruments DSC (Model Q-1000) with about 5 mg samples at a rate of 10 °C / min in the temperature range of 0 to 300 °C, unless otherwise stated. TGA was carried out at the Analytical Center, Korea Research Institute of Chemical Technology. Samples were run under N_2 and heated from room temperature to 600 °C at a rate of 10 °C min^{-1}. All electrochemical measurements were performed using IVIUMSTAT instrument model PV-08 in a standard three-electrode, one compartment configuration equipped with $Ag/AgNO_3$ electrode, Pt wire and Pt electrode (dia. 1.6 mm), as the pseudo reference, counter electrode and working electrode respectively. Pt working electrodes were polished with alumina. The measurements were carried out in anhydrous acetonitrile with tetrabutyl ammonium hexafluorophosphate (0.1 M) as the supporting electrolyte under an argon atmosphere at a scan rate of 20 mV s^{-1}. Polymer films were prepared by drop casting onto the Pt working electrode from chloroform solution and dried before measurements. The electrochemical onsets were determined at the position where the current starts to differ from the baseline. The potential of the $Ag/AgNO_3$ reference electrode was internally calibrated by using the ferrocene/ferrocenium redox couple (Fc / Fc+), which has a known reduction potential of −4.8 eV. The HOMO of copolymers were calculated from the onset oxidation potentials ($E_{oxonset}$) according to: HOMO= $-(E_{oxonset} + 4.8)$ (eV). The LUMO of copolymers were calculated from the onset reduction potentials ($E_{redonset}$) according to: LOMO= $-(E_{redonset} + 4.8)$ (eV).

4.2. Film characterization

AFM images were collected using a Veeco Multimode microscope with 300 kHz silicon tips operating in tapping mode. HR-TEM images were obtained using a JEOL JEM-2100 TEM operated at 200 kV. 2D-GIWAXS experiments were performed at the Advanced Light Source (ALS) at beamline 7.3.3. The incident beam energy is 10keV, and the incident angle used was 0.12-0.14˚. The sample-to-detector distance was 30cm, and a Pilatus 2M area detector was used for 2D diffraction pattern collection. Samples were kept under Helium environment during X-ray scattering was to minimize background scattering and beam damage. Exposure times were 5 to 60 seconds. Samples for 2D-GIWAXS measurements were prepared by spin-coating pristine polymer and polymers:$PC_{71}BM$ blend solutions on top of PEDOT:PSS/Si substrates.

Resonant Soft X-ray Scattering (RSoXS) was performed at beamline 11.0.1.2 at the Advanced Light Source. Thin film samples were prepared on 100 nm thick 1.5 mm x 1.5 mm silicon nitride membranes supported by a 5 mm x 5 mm silicon frame (Norcada Inc.). Scattering was collected in a transmission geometry with a 150 mm sample-detector distance. Data was collected on an in-vacuum CCD camera (Princeton Instrument PI-MTE) thermoelectrically cooled to -45 °C. Images were taken near the carbon K edge, in the range of 280-300 eV. 2D data waere reduced by azimuthally averaging over all q values.

4.3. Fabrication and characterization of PSCs

Photovoltaic devices were fabricated according to the following procedures. First, the glass/ITO substrates were cleaned with detergent, then ultra-sonicated in acetone and isopropyl alcohol and subsequently dried in an oven overnight at 100 °C. PEDOT:PSS hole transport layers were spin-coated (after passing through a 0.45 μm cellulose acetate syringe filter) at 5000 rpm for 40s

followed by baking at 150 °C for 30 min in air and then moved into a glove box. For the single-junction active layer, blend solutions of PDTBTBz-based polymers (1.0 wt%):$PC_{71}BM$ (1.5 wt%) dissolved in CB (with 1.5~3 vol% DPE) were spin-coated (1500 to 3000 rpm for optimization) on top of the PEDOT:PSS layer in a nitrogen-filled glove box. The device was pumped down in vacuum (< 10^{-6} torr), and the Ca/Al (20 nm/100 nm thick) electrode for conventional architecture was deposited on top of the active layer by thermal evaporation. The deposited Ca/Al electrode area defined the active area as 13 mm^2. Photovoltaic characteristics measurements were carried out inside the glove box using a high quality optical fiber to guide the light from the solar simulator equipped with a Keithley 2635A source measurement unit. J-V curves were measured under AM 1.5G illumination at 100 mW cm^{-2} using an aperture to define the illuminated area. EQE measurements were conducted in ambient air using an EQE system (Model QEX7) by PV measurements Inc. (Boulder, Colorado). The monochromatic light intensity was calibrated using a Si photodiode and chopped at 100 Hz. A Mask (1.70 mm^2) made of thin black plastic was attached to each cell for measurement of the *J-V* characteristics and the EQE spectra. All devices were tested in ambient air after UV-epoxy encapsulation.

4.4. Fabrication of Tandem-junction PSC

The device structure of the tandem cell is shown in Fig. 6a. The PDTBTBz-$2F_{anti}$(1.0 wt%):$PC_{71}BM$ (1.5 wt%) dissolved in CB (with 3 vol% DPE) was spin-cast on top of PEDOT:PSS layer at a spin rate of 2500 ~ 3000 rpm as an active layer in a front cell. The ZnO nanoparticles solution was prepared following the previous literature[59] and spin-coated at 3000 rpm on top of the front cell. The neutral PEDOT:PSS solution was also prepared as by mixing isopropyl alcohol (IPA) and deionized water (DI water) with a mixing ratio of neutral PEDOT:PSS (1.0): IPA(0.8): DI water (1.4) as volume fraction, and then spin-coated on top of

ZnO layer at 4000 rpm for 40 s . The DT-PDPP2T-TT:$PC_{71}BM$ active layer was fabricated under the same condition reported in the previous literature.[44] Finally, the device fabrication was completed by deposition of 100 nm thick Al as cathode.

4.5. Fabrication and characterization of PFETs

The PFETs were fabricated onto n^{++}Si (500 μm)/SiO2 (300 nm) substrates (International Wafer Services Co.). The Ni (5 nm)/Au (50 nm) source and drain electrodes were patterned on the dielectrics by electron beam evaporation at 7×10^{-7} Torr. After ultraviolet/ozone treatment of pre-cleaned SiO_2 substrates for 10 min, the substrates were passivated with the n-decyltrichlorosilane (Gelest Inc.) in toluene solution (1% by volume) at 80°C for 20 min in air. The semiconductor solutions were then spin cast from a chloroform solution (5 mg mL^{-1}) at 1200 rpm for 40 s in a nitrogen-filled glove box. The devices were then cured at 200°C for 5 min prior to measurements, and were tested using a probe station (Signatone Co.) in a nitrogen-filled glove box. Data were collected by a Keithley 4200 system.

Acknowledgements

We thank Prof. Alan J. Heeger for guidance. This work was supported by the NASA Small Buisiness Technology Transfer (STTR) UCSB (07012013-01) and National Research Foundation (NRF) of Korea (2015R1D1A1A09056905, 2015M1A2A2057506, 2015M1A2A2056214). E.L. acknowledges support from the National Science Foundation Graduate Research Fellowship (DGE-1144085). Portions of the research were carried out at the Advanced Light Source, supported by the Director, Office of Science, Office of

Basic Energy Sciences, of the U.S. Department of Energy under Contract No. DE-AC02-05CH11231.

Author contributions

S.-J.K. and Q.V.H. contributed equally to this work. S.-J.K. proposed the research, conducted most of the characterizations, fabricated solar cells and also contributed to data analysis and preparation of manuscript. Q.V.H and C.E.S. synthesized and five kinds of WBG polymers and conducted characterization related to synthesis. M.A.U. contributed to data analysis, participated to the discussion and manuscript preparation with S.-J.K. S.Y.P. performed HR-TEM and B.H.L fabricated PFET. S.S. measured AFM. S.-J.M. designed WBG polymers. S.H. conducted DFT calculation. E.L. and M.L.C. measured and analysed 2D-GIWAXS and also fully revised manuscript. G.M.S. measured and analysed RSoXS. P.-O.M and M.L. prepared LBG polymer for tandem device fabrication. W.S.S. supervised synthesis of five kinds of WBG polymers. H.Y.W. and J.Y.K. supervised the whole project. All authors discussed the results and commented on the manuscript.

References

1. N. Sariciftci, L. Smilowitz, A. J. Heeger and F. Wudl, *Science*, 1992, **258**, 1474-1476.
2. G. Yu, J. Gao, J. C. Hummelen, F. Wudl and A. J. Heeger, *Science*, 1995, **270**, 1789-1791.
3. B. C. Thompson and J. M. J. Fréchet, *Angew. Chem. Int. Ed.*, 2008, **47**, 58-77.
4. M. C. Scharber and N. S. Sariciftci, *Prog. Polym. Sci.*, 2013, **38**, 1929-1940.
5. Y. Liu, J. Zhao, Z. Li, C. Mu, W. Ma, H. Hu, K. Jiang, H. Lin, H. Ade and H. Yan, *Nat. Commun.*, 2014, **5**, DOI:10.1038/ncomms6293.
6. J.-D. Chen, C. Cui, Y.-Q. Li, L. Zhou, Q.-D. Ou, C. Li, Y. Li and J.-X. Tang, *Adv. Mater.*, 2015, **27**, 1035-1041.

7. C. Liu, C. Yi, K. Wang, Y. Yang, R. S. Bhatta, M. Tsige, S. Xiao and X. Gong, *ACS Appl. Mater. Interfaces*, 2015, **7**, 4928-4935.
8. X. Ouyang, R. Peng, L. Ai, X. Zhang and Z. Ge, *Nat. Photon.*, 2015, **9**, 520-524.
9. S. Zhang, L. Ye and J. Hou, *Adv. Energy Mater.*, 2016, **6**, 1502529.
10. J. Zhao, Y. Li, G. Yang, K. Jiang, H. Lin, H. Ade, W. Ma and H. Yan, *Nat. Energy*, 2016, **1**, 15027.
11. H. Hu, K. Jiang, G. Yang, J. Liu, Z. Li, H. Lin, Y. Liu, J. Zhao, J. Zhang, F. Huang, Y. Qu, W. Ma and H. Yan, *J. Am. Chem. Soc.*, 2015, **137**, 14149-14157.
12. Z. Li, K. Jiang, G. Yang, J. Y. L. Lai, T. Ma, J. Zhao, W. Ma and H. Yan, *Nat. Commun.*, 2016, **7**, 13094.
13. Y.-J. Cheng, S.-H. Yang and C.-S. Hsu, *Chem. Rev.*, 2009, **109**, 5868-5923.
14. P. M. Beaujuge and J. M. J. Fréchet, *J. Am. Chem. Soc.*, 2011, **133**, 20009-20029.
15. G. Li, R. Zhu and Y. Yang, *Nat. Photon.*, 2012, **6**, 153-161.
16. Y. Li, *Acc. Chem. Res.*, 2012, **45**, 723-733.
17. H. Zhou, L. Yang and W. You, *Macromolecules*, 2012, **45**, 607-632.
18. X. Guo, M. Baumgarten and K. Müllen, *Prog. Polym. Sci.*, 2013, **38**, 1832-1908.
19. J. You, L. Dou, Z. Hong, G. Li and Y. Yang, *Prog. Polym. Sci.*, 2013, **38**, 1909-1928.
20. K. Müllen and W. Pisula, *J. Am. Chem. Soc.*, 2015, **137**, 9503-9505.
21. J. Y. Kim, K. Lee, N. E. Coates, D. Moses, T.-Q. Nguyen, M. Dante and A. J. Heeger, *Science*, 2007, **317**, 222-225.
22. J. You, L. Dou, K. Yoshimura, T. Kato, K. Ohya, T. Moriarty, K. Emery, C.-C. Chen, J. Gao, G. Li and Y. Yang, *Nat. Commun.*, 2013, **4**, 1446.
23. J. Zhang, Y. Zhang, J. Fang, K. Lu, Z. Wang, W. Ma and Z. Wei, *J. Am. Chem. Soc.*, 2015, **137**, 8176-8183.
24. Q. An, F. Zhang, J. Zhang, W. Tang, Z. Deng and B. Hu, *Energy Environ. Sci.*, 2016, **9**, 281-322.
25. Z. Zheng, S. Zhang, J. Zhang, Y. Qin, W. Li, R. Yu, Z. Wei and J. Hou, *Adv. Mater.*, 2016, **28**, 5133-5138.
26. G. Dennler, M. C. Scharber, T. Ameri, P. Denk, K. Forberich, C. Waldauf and C. J. Brabec, *Adv. Mater.*, 2008, **20**, 579-583.
27. N. Li, D. Baran, G. D. Spyropoulos, H. Zhang, S. Berny, M. Turbiez, T. Ameri, F. C. Krebs and C. J. Brabec, *Adv. Energy Mater.*, 2014, **4**, 1400084.
28. J. W. Jung, J. W. Jo, E. H. Jung and W. H. Jo, *Org. Electron.*, 2016, **31**, 149-170.
29. G. Li, X. Gong, J. Zhang, Y. Liu, S. Feng, C. Li and Z. Bo, *ACS Appl. Mater. Interfaces*, 2016, **8**, 3686-3692.
30. W. Zhao, S. Li, S. Zhang, X. Liu and J. Hou, *Adv. Mater.*, 2016, DOI: 10.1002/adma.201604059, n/a-n/a.
31. J. Wolf, F. Cruciani, A. El Labban and P. M. Beaujuge, *Chem. Mater.*, 2015, **27**, 4184-4187.
32. M. Zhang, X. Guo, W. Ma, H. Ade and J. Hou, *Adv. Mater.*, 2015, **27**, 4655-4660.
33. Z. Genene, J. Wang, X. Meng, W. Ma, X. Xu, R. Yang, W. Mammo and E. Wang, *Adv. Electron. Mater.*, 2016, **2**, 1600084.
34. J. W. Jo, S. Bae, F. Liu, T. P. Russell and W. H. Jo, *Adv. Funct. Mater.*, 2015, **25**, 120-125.
35. L. Huo, T. Liu, X. Sun, Y. Cai, A. J. Heeger and Y. Sun, *Adv. Mater.*, 2015, **27**, 2938-2944.

36. H.-Y. Chen, J. Hou, S. Zhang, Y. Liang, G. Yang, Y. Yang, L. Yu, Y. Wu and G. Li, *Nat. Photon.*, 2009, **3**, 649-653.
37. H. Zhou, L. Yang, A. C. Stuart, S. C. Price, S. Liu and W. You, *Angew. Chem. Int. Ed.*, 2011, **50**, 2995-2998.
38. S. Albrecht, S. Janietz, W. Schindler, J. Frisch, J. Kurpiers, J. Kniepert, S. Inal, P. Pingel, K. Fostiropoulos, N. Koch and D. Neher, *J. Am. Chem. Soc.*, 2012, **134**, 14932-14944.
39. T. L. Nguyen, H. Choi, S. J. Ko, M. A. Uddin, B. Walker, S. Yum, J. E. Jeong, M. H. Yun, T. J. Shin, S. Hwang, J. Y. Kim and H. Y. Woo, *Energy Environ. Sci.*, 2014, **7**, 3040-3051.
40. F. Meyer, *Prog. Polym. Sci.*, 2015, **47**, 70-91.
41. Q. T. Zhang and J. M. Tour, *J. Am. Chem. Soc.*, 1998, **120**, 5355-5362.
42. J. Peet, N. S. Cho, S. K. Lee and G. C. Bazan, *Macromolecules*, 2008, **41**, 8655-8659.
43. C. Piliego, T. W. Holcombe, J. D. Douglas, C. H. Woo, P. M. Beaujuge and J. M. J. Fréchet, *J. Am. Chem. Soc.*, 2010, **132**, 7595-7597.
44. H. Choi, S.-J. Ko, T. Kim, P.-O. Morin, B. Walker, B. H. Lee, M. Leclerc, J. Y. Kim and A. J. Heeger, *Adv. Mater.*, 2015, **27**, 3318-3324.
45. X. Yang, J. Loos, S. C. Veenstra, W. J. H. Verhees, M. M. Wienk, J. M. Kroon, M. A. J. Michels and R. A. J. Janssen, *Nano Lett.*, 2005, **5**, 579-583.
46. W. Chen, M. P. Nikiforov and S. B. Darling, *Energy Environ. Sci.*, 2012, **5**, 8045-8074.
47. L. Ye, S. Zhang, W. Ma, B. Fan, X. Guo, Y. Huang, H. Ade and J. Hou, *Adv. Mater.*, 2012, **24**, 6335-6341.
48. H. Zhou, Y. Zhang, J. Seifter, S. D. Collins, C. Luo, G. C. Bazan, T.-Q. Nguyen and A. J. Heeger, *Adv. Mater.*, 2013, **25**, 1646-1652.
49. M. R. Hammond, R. J. Kline, A. A. Herzing, L. J. Richter, D. S. Germack, H.-W. Ro, C. L. Soles, D. A. Fischer, T. Xu, L. Yu, M. F. Toney and D. M. DeLongchamp, *ACS Nano*, 2011, **5**, 8248-8257.
50. F. Buss, B. Schmidt-Hansberg, M. Sanyal, C. Munuera, P. Scharfer, W. Schabel and E. Barrena, *Macromolecules*, 2016, **49**, 4867-4874.
51. S. Swaraj, C. Wang, H. Yan, B. Watts, J. Lüning, C. R. McNeill and H. Ade, *Nano Lett.*, 2010, **10**, 2863-2869.
52. H. Yan, B. A. Collins, E. Gann, C. Wang, H. Ade and C. R. McNeill, *ACS Nano*, 2012, **6**, 677-688.
53. P. Schilinsky, C. Waldauf and C. J. Brabec, *Appl. Phys. Lett.*, 2002, **81**, 3885-3887.
54. Z. Li, J. D. A. Lin, H. Phan, A. Sharenko, C. M. Proctor, P. Zalar, Z. Chen, A. Facchetti and T.-Q. Nguyen, *Adv. Funct. Mater.*, 2014, **24**, 6989-6998.
55. L. Lu, T. Xu, W. Chen, E. S. Landry and L. Yu, *Nat. Photon.*, 2014, **8**, 716-722.
56. P. W. M. Blom, M. J. M. de Jong and M. G. van Munster, *Phys. Rev. B*, 1997, **55**, R656-R659.
57. Y. Shen, A. R. Hosseini, M. H. Wong and G. G. Malliaras, *ChemPhysChem*, 2004, **5**, 16-25.
58. W. Li, K. H. Hendriks, W. S. C. Roelofs, Y. Kim, M. M. Wienk and R. A. J. Janssen, *Adv. Mater.*, 2013, **25**, 3182-3186.
59. Y. Sun, J. H. Seo, C. J. Takacs, J. Seifter and A. J. Heeger, *Adv. Mater.*, 2011, **23**, 1679-1683.

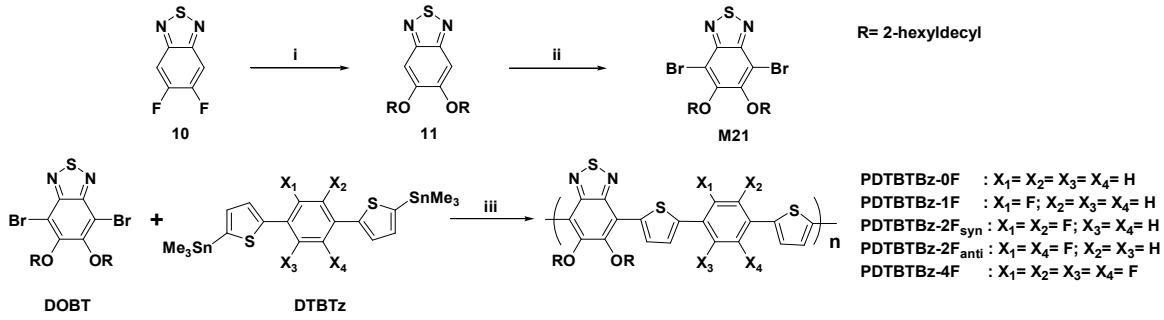

Scheme 1 The synthetic route to the monomer M21 and polymers. i) 2-Hexyldecanol, NaH (60% dispersion in paraffin), DMF. ii) Bromine, CH2Cl2:CH3COOH (1:1). iii) Pd2(dba)3, P(o-Tol)3, chlorobenzene, MW 150 ºC.

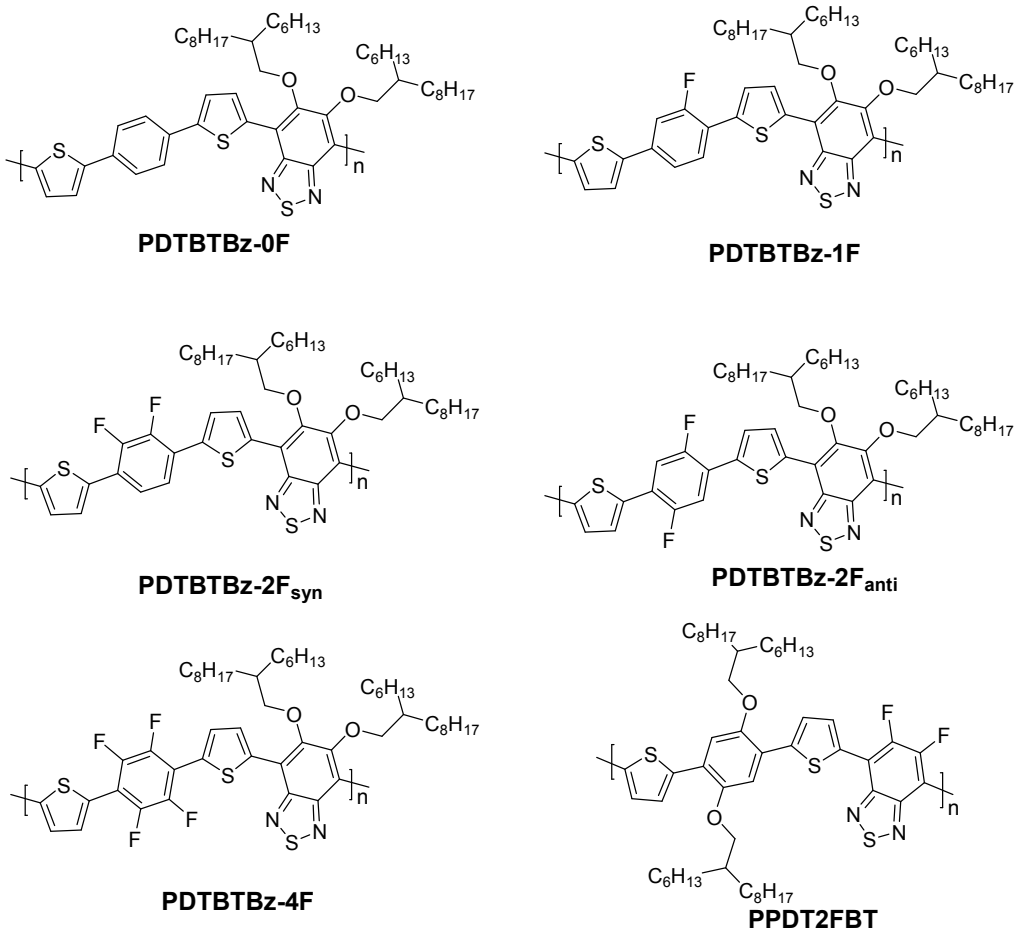

Scheme 2 Molecular structures of polymers in this study and PPDT2FBT[39]

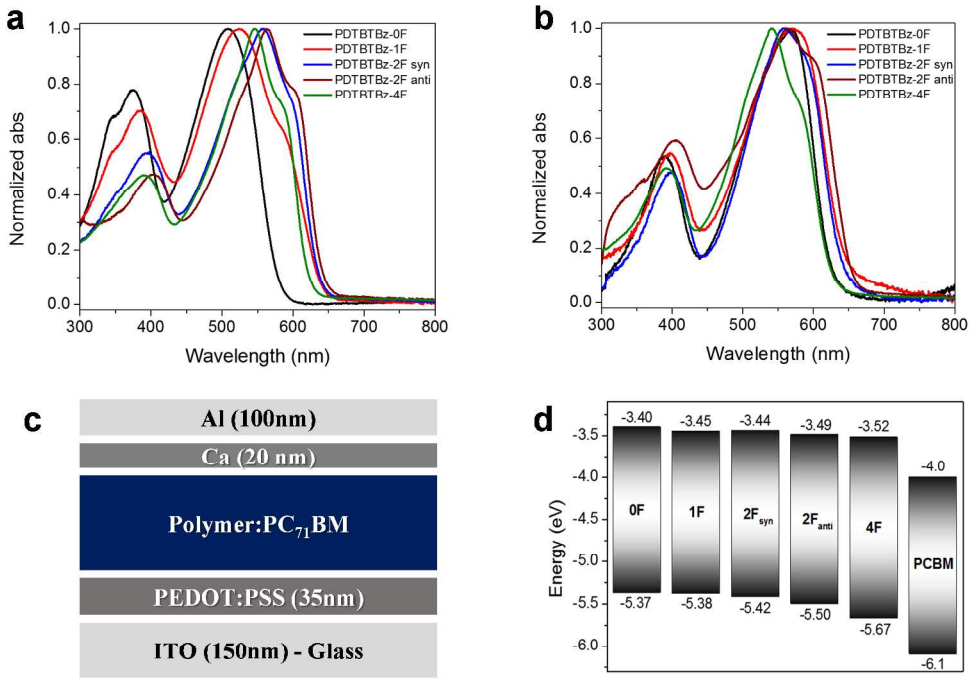

Fig. 1 Normalized optical absorption spectra of the polymers (a) in chloroform solution and (b) in thin film. (c) Device structure of PSCs used in this study. (d) Energy diagram of polymer series and $PC_{71}BM$.

Table 1 Physical properties of the WBG polymers

Polymer	M_n (M_w)[a] [kg.mol^{-1}]	T_d (^{0}C)[b]	$\lambda_{max}^{abs,sol}$ (nm)	$\lambda_{max}^{abs,film}$ (nm)	$\lambda_{onset}^{abs,film}$ (nm)	E_g^{opt} (eV)	HOMO[c] (eV)	LUMO[c] (eV)	E_g^{ec} (eV)
PDTBTBz-0F	28.6 (43.7)	283	508	569	631	1.97	- 5.37	- 3.40	1.97
PDTBTBz-1F	46.2(109.4)	283	523	571	646	1.92	- 5.38	- 3.45	1.93
PDTBTBz-2F$_{syn}$	111.9(347.2)	283	558	558	646	1.92	- 5.42	-3.44	1.98
PDTBTBz-2F$_{anti}$	182.6(382.1)	285	563	564	652	1.90	- 5.50	- 3.49	2.01
PDTBTBz-4F	182.3(557.0)	285	546	541	629	1.97	- 5.67	-3.52	2.15

[a]Number-average molecular weight (Mn) and Weight-average molecular weight (Mw) determined by GPC with o-dichlorobenzene as the eluent at 80 °C. [b]Decomposition temperature (Td) was determined by TGA in a nitrogen atmosphere (with 5% weight-loss). [c]HOMO and LUMO level was estimated from the tangential onset of oxidation ($E_{ox\ onset}$) and onset of reduction ($E_{red\ onset}$) by cyclic voltammetry using equation HOMO(eV)=-($E_{ox\ onset}$-E1/2ferrocene+4.8).

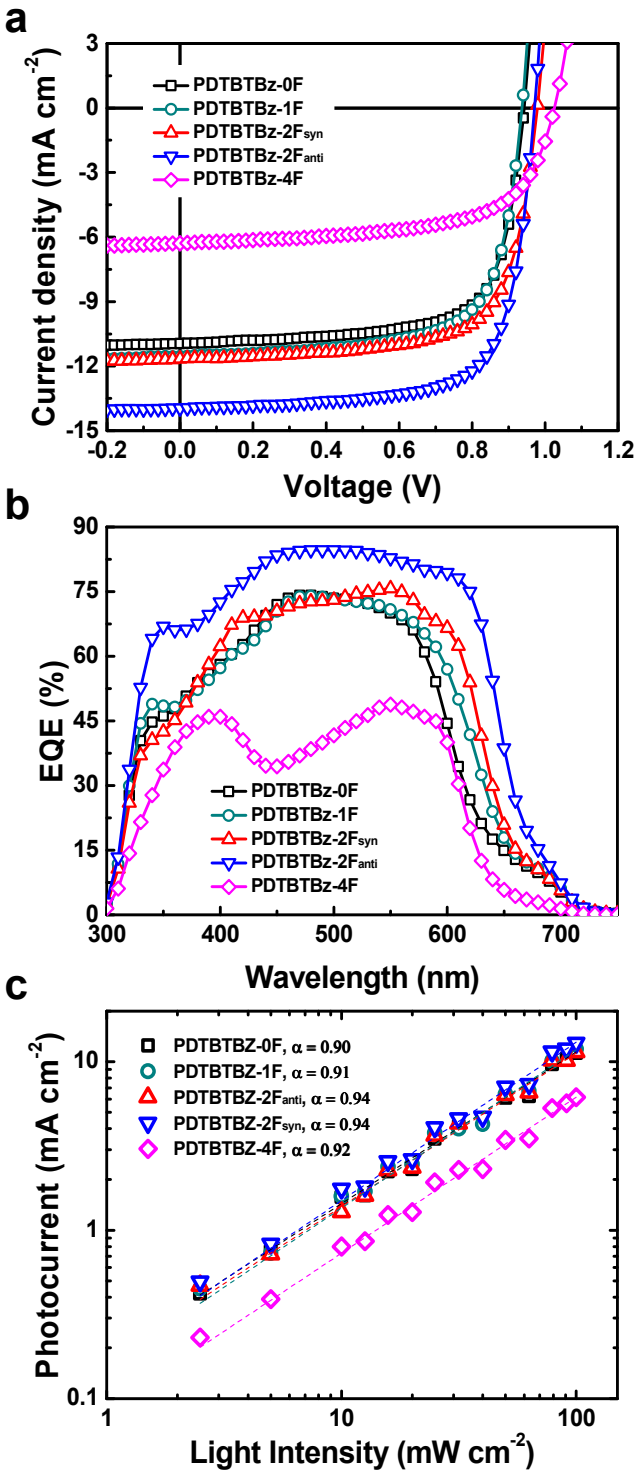

Fig. 2 (a) Current density–voltage (*J–V*) curves, (b) external quantum efficiency (EQE) and (c) light intensity dependence of J_{SC} for optimum devices using polymers:$PC_{71}BM$ blend prepared from CB solvent with DPE.

Table 2 Summary of device parameter for optimum device using polymers:$PC_{71}BM$ blend prepared from CB solvent with DPE.

Donor:$PC_{71}BM$	J_{SC} (mA/cm^2)	[*Cal.*] J_{SC}[a)] (mA/cm^2)	V_{OC} (V)	FF	PCE (%) Best (Ave.)[b)]
PDTBTBz-0F	11.0 (11.1±0.4)	10.2	0.94 (0.93±0.01)	0.71 (0.69±0.02)	7.3 (7.2±0.1)
PDTBTBz-1F	11.6 (11.5±0.5)	11.1	0.94 (0.93±0.1)	0.70 (0.69±0.01)	7.5 (7.4±0.2)
PDTBTBz-2F_{syn}	11.7 (11.5±0.1)	11.4	0.98 (0.97±0.01)	0.71 (0.70±0.01)	8.1 (7.9±0.1)
PDTBTBz-2F_{anti}	14.0 (13.8±0.2)	13.8	0.97 (0.97±0.0)	0.72 (0.72±0.01)	9.8 (9.5±0.2)
PDTBTBz-4F	6.3 (6.4±0.4)	6.4	1.03 (0.99±0.02)	0.63 (0.61±0.01)	4.1 (4.0±0.2)

a) Calculated J_{SC} from a EQE curve, [b)]Average PCE values obtained from 15 devices.

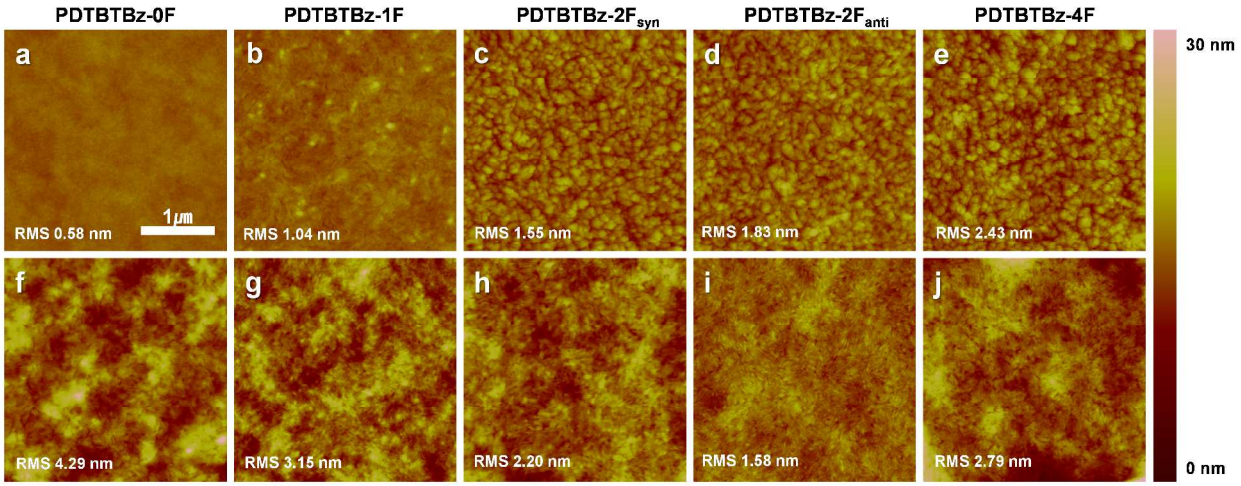

Fig. 3 Tapping-mode AFM topography of polymers:$PC_{71}BM$ blend films (solvent: CB without and with DPE). Without DPE: (a) PDTBTBz-0F, (b) PDTBTBz-1F,(c) PDTBTBz-2F_{syn}, (d) PDTBTBz-2F_{anti}, and (e) PDTBTBz-4F. With DPE: f) PDTBTBz-0F, g) PDTBTBz-1F, h) PDTBTBz-2F_{syn}, i) PDTBTBz-2F_{anti}, and j) PDTBTBz-4F. The size of all images is 3.0 μm × 3.0 μm.

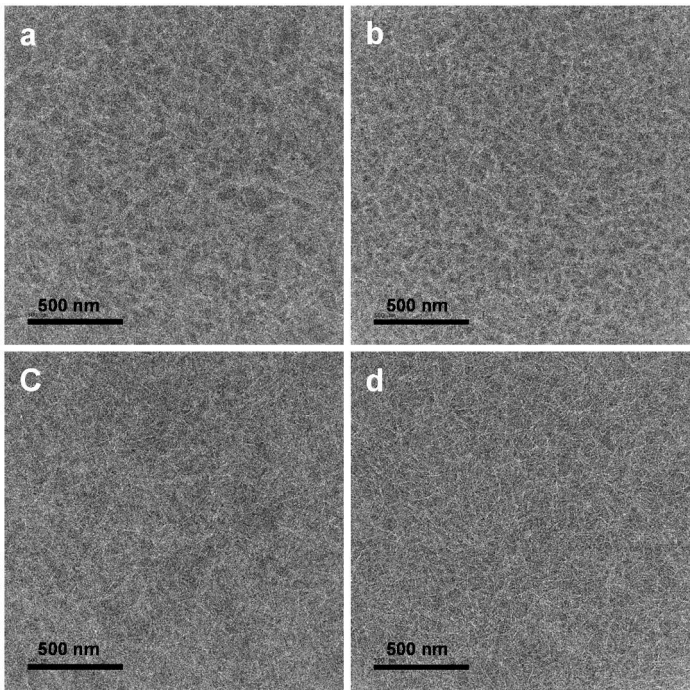

Fig. 4 HR-TEM images of PDTBTBz-2F$_{syn}$ and -2F$_{anti}$ polymers:PC$_{71}$BM films without (a and b) and with DPE (c and d), respectively. The size of all images is 1.8 μm × 1.8 μm.

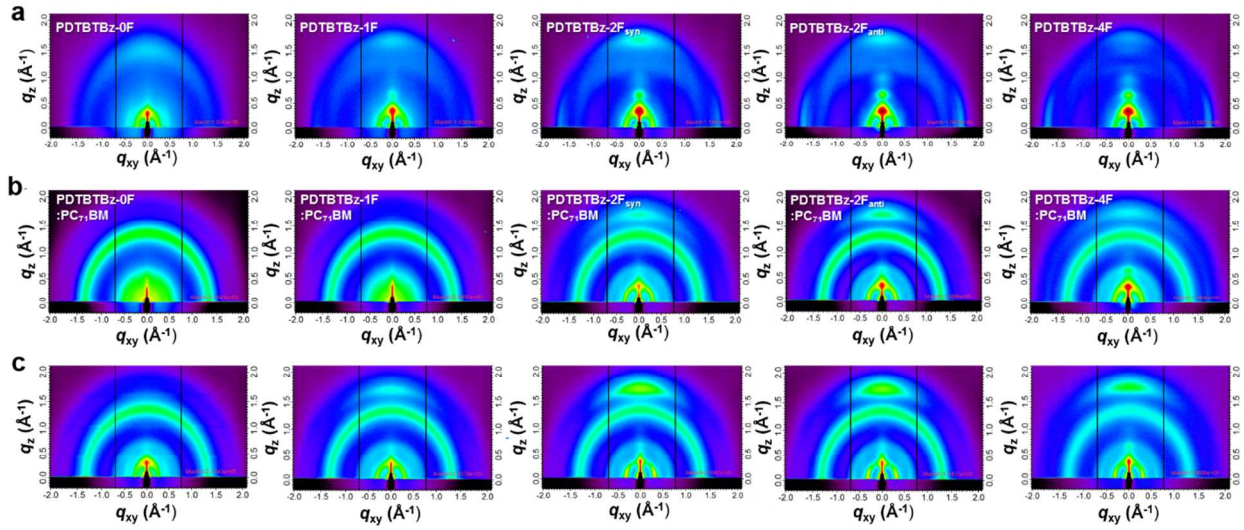

Fig. 5 Two-dimensional grazing incidence wide angle X-ray scattering (2D-GIWAXS) images. (a) 2D-GIWAXS images of pristine polymer films, (b) polymers:PC$_{71}$BM blend films, and (c) polymers:PC$_{71}$BM blend films with DPE. Each panel from left to right shows the 2D-GIWAXS images for PDTBTBz-0F, PDTBTBz-1F, PDTBTBz-2F$_{syn}$, PDTBTBz-2F$_{anti}$, and PDTBTBz-4F, respectively. Note that images have not been corrected for the inaccessible region of reciprocal space near the q_z axis.

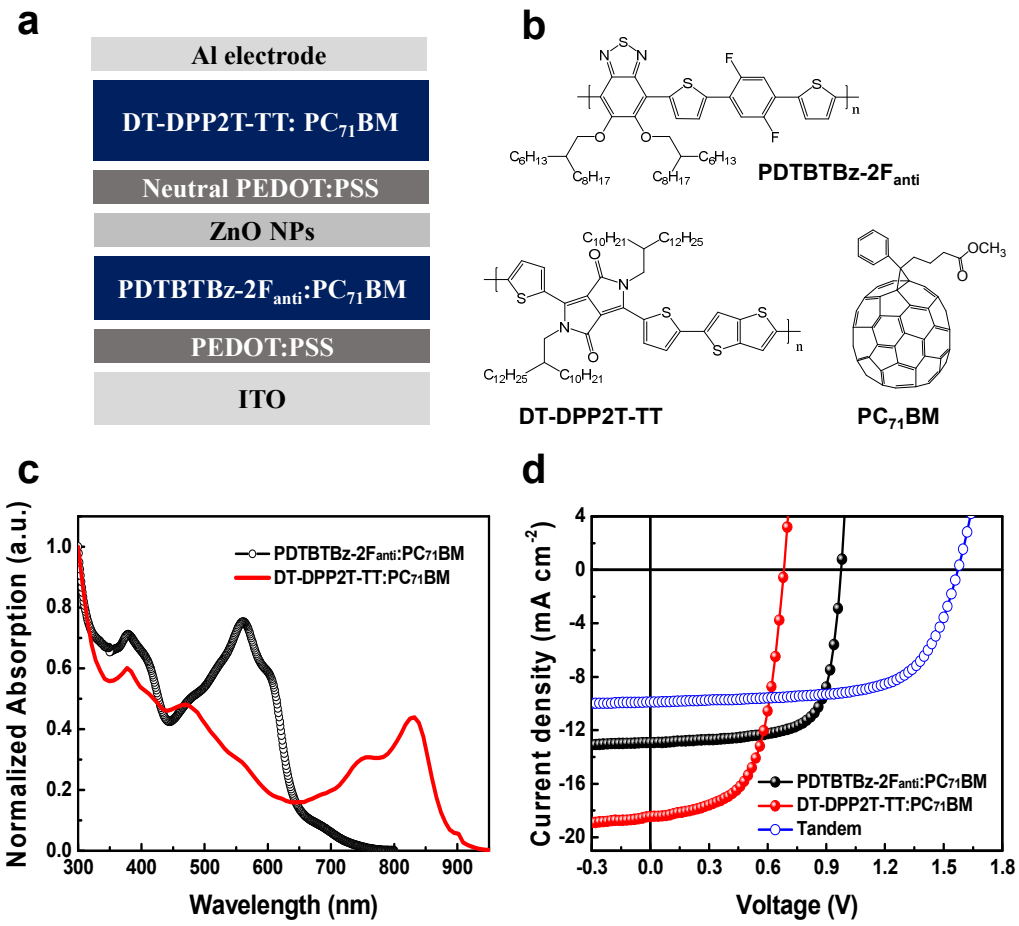

Fig. 6 (a) Tandem PSC device structure and (b) chemical structures of the active layer materials. (c) Absorption spectra of the active layers and (d) *J*–*V* curves of single (front and back) and tandem devices.

The table of contents:

A new series of wide band gap based on fluorinated phenylene-alkoxybenzothiadiazole unit with optical band gap over 1.90 eV is designed and utilized for high-performance single- and multi-junction bulk heterojunction polymer solar cells.

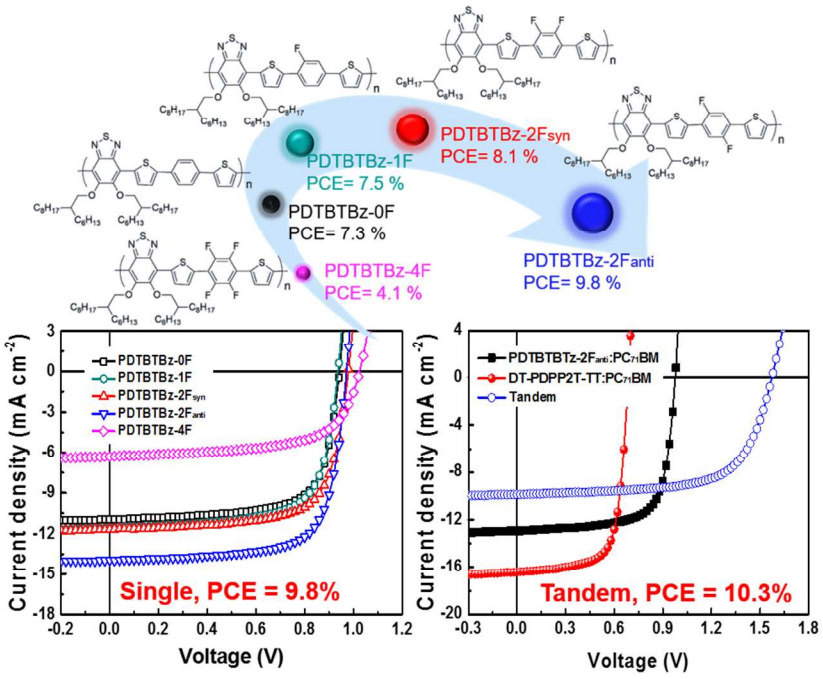

Supporting Information for

High-efficiency photovoltaic cells with wide optical band gap polymers based on fluorinated phenylene-alkoxybenzothiadiazole

Seo-Jin Ko,‡[ab] Quoc Viet Hoang,‡[cd] Chang Eun Song,[cd] Mohammad Afsar Uddin,[e,f] Eunhee Lim,[g] Song Yi Park,[b] Byoung Hoon Lee,[a] Seyeong Song,[b] Sang-Jin Moon,[cd] Sungu Hwang,[f] Pierre-Olivier Morin,[h] Mario Leclerc,[h] Gregory M. Su,[i] Michael L. Chabinyc,[g] Han Young Woo,*[e] Won Suk Shin*[cd] and Jin Young Kim*[b]

[a] Center for Polymers and Organic Solids, University of California Santa Barbara (UCSB), Santa Barbara, CA 93106, USA

[b] School of Energy and Chemical Engineering, Ulsan National Institute of Science and Technology (UNIST), Ulsan 44919, Republic of Korea. E-mail) jykim@unist.ac.kr

[c] Energy Materials Research Center, Korea Research Institute of Chemical Technology (KRICT), 141 Gajeong-ro, Yuseong-gu, Daejeon 305-343, Republic of Korea. E-mail) shinws@krict.re.kr

[d] Department of Nanomaterials Science and Engineering, University of Science & Technology (UST), 217 Gajeong-ro, Yuseong-gu, Daejeon, 305-350, Republic of Korea.

[e] Department of Chemistry, Korea University, Seoul 136-713, Republic of Korea. E-mail) hywoo@korea.ac.kr

[f] Department of Nanomechatronics Engineering, Pusan National University, Miryang 627-706, Republic of Korea

[g] Materials Department, University of California Santa Barbara (UCSB), Santa Barbara, CA 93106, USA

[h] Department of Chemistry, Laval University, Quebec City, QC, G1V 0A6, Canada

[i] Advanced Light Source, Lawrence Berkeley National Laboratory, Berkeley, CA 94720, USA

Material Syntheses

5,6-Difluorobenzo[c][1,2,5]thiadiazole was purchased from *Newell* Company. All other chemicals were purchased from Aldrich, Alfa Aesar and TCI Chemical Co. A series of 1,4-Bis(5-trimethylstannylthiophen-2-yl)benzene derivatives were synthesized by modifying the previous literatures.[1]

Syntheses of monomers

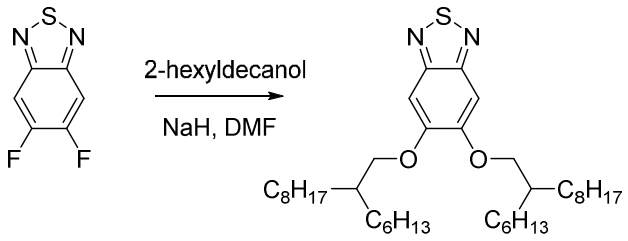

11

5,6-Bis(2-hexyldecyloxy)benzo[c][1,2,5]thiadiazole (11).

2-Hexyldecanol (7.0 g, 29 mmol) was added into 2-neck round bottom flask containing 200 mL anhydrous *N,N*-dimethylformamide (DMF) under argon. After cooling down to 0 ^{o}C, sodium hydride (1.16 g, 29 mmol, 60% dispersion in paraffin) was added as one portion and the reaction mixture was stirred for 1 h at 0 ^{o}C. 5,6-Difluorobenzo[c][1,2,5]thiadiazole (2.0 g, 11.6 mmol) was added and the reaction mixture was warmed up to room temperature. After stirring overnight, the mixture was quenched by addition of 100 mL water and extracted with diethyl ether. The organic extract was dried over anhydrous magnesium sulfate and concentrated by rotary evaporator. The crude product was purified by column chromatography on silica gel using dichloromethane:hexane (1:3, by volume) as eluent, yielding a colorless oil (7 g, 98% yield). ^{1}H NMR (400 MHz, $CDCl_3$): δ (ppm) 7.11 (s, 2H), 3.95 (d, J= 5.3 Hz, 4H), 1.89 (m, 2H), 1.28 (m, 48H), 0.87 (m, 12H). ^{13}C NMR (125 MHz, $CDCl_3$): δ (ppm) 154.52, 151.41, 97.96, 71.41, 37.81, 31.91, 31.87, 31.35, 30.06, 29.72, 29.63, 29.37, 26.88, 26.85, 22.68, 14.11. MS (EI): Calcd m/z = 616.5; found M^+ = 617.

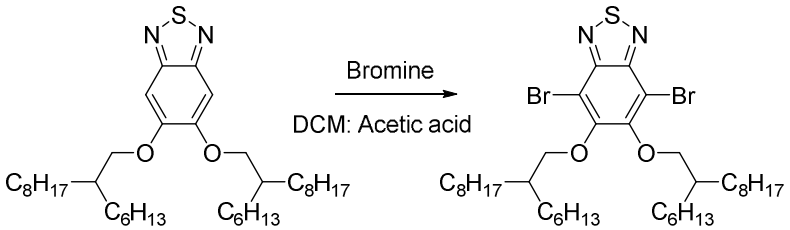

M21

4,7-dibromo-5,6-bis(2-hexyldecyloxy)benzo[c][1,2,5]thiadiazole (M21).

Bromine (1.7 mL, 34.0 mmol) was added into a solution of 5,6-bis((2-hexyldecyl)oxy)benzo[c][1,2,5]thiadiazole (7.0 g, 11.3 mmol) in a mixture of dichloromethane:acetic acid (200 mL : 100 mL) at room temperature. After stirring overnight under dark, the mixture was quenched by addition of aq. sodium sulfite solution and then extracted with diethyl ether (100 mL × 3 times). The organic phase was dried over anhydrous magnesium sulfate then concentrated. The crude product was purified by silica gel column chromatography using dichloromethane:hexane (1:4, by volume) as eluent. After evaporation of solvent, 7.1 g of colorless oil was obtained (81% yield). ^{1}H NMR (400 MHz, $CDCl_3$): δ (ppm) 4.02 (d, J= 6.1 Hz, 4H), 1.92 (m, 2H), 1.56 (m, 4H), 1.30 (m, 44H), 0.89 (m, 12H). ^{13}C NMR (100 MHz, $CDCl_3$): δ (ppm) 154.84, 150.39, 106.01, 78.43, 39.22, 31.94, 1.09, 30.12, 29.79, 29.68, 29.39, 26.92, 26.89, 22.71, 14.13. MS (EI): Calcd m/z = 774.3; found $(M+1)^+$ = 775.

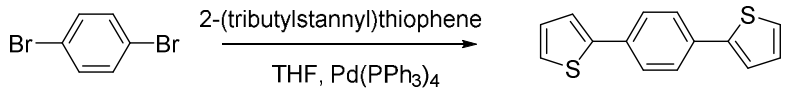

31

1,4-Bis(thiophen-2-yl)benzene (31).

1,4-Dibromobenzene (3 g, 12.7 mmol) and 2-(tributylstannyl)thiophene (12.3 g, 33.0 mmol) were added into a 2-neck round bottom flask. The reaction mixture was purged with argon and anhydrous tetrahydrofuran (100 mL) and tetrakis(triphenylphosphine)palladium(0) (730 mg) were added. After purging for another 10 min, the reaction mixture was heated at 90 ^{o}C for 24 h under argon. After cooling down the reaction solution to room temperature, the mixture was concentrated and passed through a short silica gel column by eluting with hexane and then with dichloromethane. The residue was recrystallized from hexane to obtain 2.26 g of colorless crystal (79% yield). ^{1}H NMR (400 MHz, $CDCl_3$): δ (ppm) 7.61 (s, 4H), 7.33 (d, J= 3.3 Hz, 2H), 7.28 (d, J= 5.0 Hz, 2H), 7.08 (t, J= 4.2 Hz, 2H). MS (EI): Calcd m/z = 242.0; found M^+ = 242.

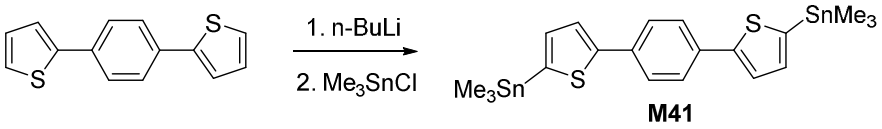

M41

1,4-Bis(5-(trimethylstannyl)thiophen-2-yl)benzene (M41).

1,4-Bis(thiophen-2-yl)benzene (1.0 g, 4.13 mmol) was dissolved in 100 mL anhydrous THF under argon. The solution was cooled down to −78 °C with a dry ice–acetone bath, and 1.6 M *n*-BuLi solution in hexane (6.5 mL, 10.3 mmol) was added dropwise for 10 min. After stirring at −78 °C for 1 h, trimethyltin chloride solution (10.3 mL, 10.3 mmol, 1 M in THF) was added rapidly. The mixture was allowed to warm up to room temperature and stirred overnight. The reaction was quenched by addition of 50 mL cold water and extracted with dichloromethane three times. The organic extract was washed with water twice and then dried by anhydrous magnesium sulfate. After removing the solvent under vacuum, recrystallization of the residue from hexane twice yielded the compound **M41** (1.75 g, 75%) as a pale green crystal. ^{1}H NMR (300 MHz, $CDCl_3$): δ (ppm) 7.62 (s, 4H), 7.45 (d, J= 3.4 Hz, 2H), 7.18 (d, J= 3.4 Hz, 2H), 0.41 (t, J= 28.2 Hz, 18H). MS (EI): Calcd m/z = 568.0; found M^+ = 568.

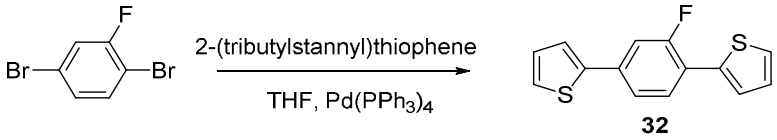

32

1,4-Bis(thiophen-2-yl)-2-fluorobenzene (32).

1,4-Dibromo-2-fluorobenzene (3 g, 11.8 mmol) and 2-(tributylstannyl)thiophene (11.5 g, 30.7 mmol) were added in a 2-neck round bottom flask. The mixture was purged with argon and anhydrous THF (100 mL) and tetrakis(triphenylphosphine)palladium(0) (680 mg) were added. The compound **32** was prepared similarly as described for **31**. The crude compound was recrystallized from methanol to obtain 1.85 g of colorless crystal (60% yield). ^{1}H NMR (400 MHz, $CDCl_3$): δ (ppm) 7.63 (t, J= 8.6 Hz, 1H), 7.50 (d, J= 3.8 Hz, 1H), 7.38 (m, 5H), 7.11 (m, 2H). MS (EI): Calcd m/z = 260.0; found M^+ = 260.

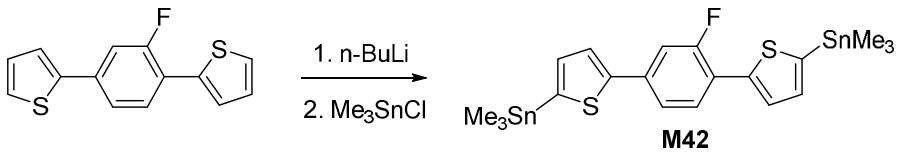

M42

1,4-Bis(5-(trimethylstannyl)thiophen-2-yl)-2-fluorobenzene (M42).

1,4-Bis(thiophen-2-yl)-2-fluorobenzene (1.0 g, 3.84 mmol) was dissolved in 100 mL anhydrous THF under argon. The solution was cooled down to −78 ^{o}C using a dry ice–acetone bath, and 1.6 M *n*-BuLi in hexane (6.0 mL, 9.6 mmol) was added dropwise for 10 min. After stirring at −78 °C for 1 h, trimethyltin chloride solution (9.6 mL, 9.6 mmol, 1 M in THF) was added rapidly. **M42** was prepared similarly as described for **M41**. Recrystallization from ethanol yielded the compound **M42** (1.65 g, 73%) as a pale yellow crystal. ^{1}H NMR (300 MHz, $CDCl_3$): δ (ppm) 7.61 (m, 2H), 7.40 (m, 3H), 7.20 (m, 2H), 0.40 (t, J= 28.2 Hz, 18H). MS (EI): Calcd m/z = 586.0; found M^+ = 586.

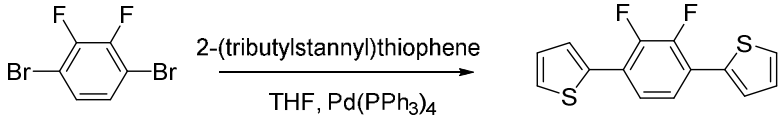

33

1,4-Bis(thiophen-2-yl)-2,3-difluorobenzene (33).

1,4-Dibromo-2,3-difluorobenzene (3 g, 11.0 mmol) and 2-(tributylstannyl)thiophene (10.7 g, 28.7 mmol) were added in a 2-neck round bottom flask. The mixture was purged with argon and anhydrous THF (100 mL) and tetrakis(triphenylphosphine)palladium(0) (640 mg) were added. The compound **33** was prepared similarly as described for **31**. The crude compound was recrystallized from ethanol to obtain 1.63 g of a colorless crystal (53% yield). ^{1}H NMR (400 MHz, $CDCl_3$): δ (ppm) 7.53 (d, J= 3.6 Hz, 2H), 7.40 (m, 4H), 7.14 (m, 2H). MS (EI): Calcd m/z = 278.0; found M^+ = 278.

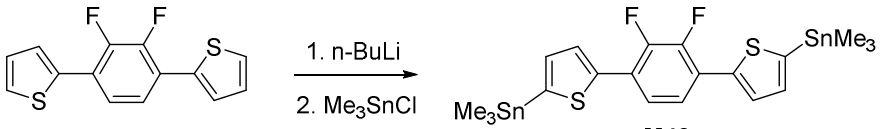

M43

1,4-Bis(5-(trimethylstannyl)thiophen-2-yl)-2,3-difluorobenzene (M43).

1,4-Bis(thiophen-2-yl)-2,3-difluorobenzene (0.8 g, 2.87 mmol) was dissolved in 100 mL anhydrous THF under argon. **M43** was prepared similarly as described for **M41** as a pale yellow needle crystal (1.42 g, 82%). ^{1}H NMR (400 MHz, $CDCl_3$): δ (ppm) 7.61 (d, J= 3.3 Hz, 2H), 7.38 (d, J= 4.7 Hz, 2H), 7.22 (d, J= 3.6 Hz, 2H), 0.41 (t, J= 28 Hz, 18H). MS (EI): Calcd m/z = 604.0; found M^+ = 604.

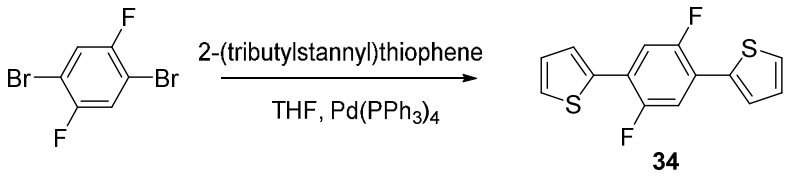

34

1,4-bis(thiophen-2-yl)-2,5-difluorobenzene (34).

1,4-Dibromo-2,5-difluorobenzene (3 g, 11.0 mmol) and 2-(tributylstannyl)thiophene (10.7 g, 28.7 mmol) were added in a 2-neck round bottom flask. The compound **34** was prepared similarly as described for **31**. The crude compound was recrystallized from hexane to obtain 1.95 g of a colorless crystal (64% yield). ^{1}H NMR (400 MHz, $CDCl_3$): δ (ppm) 7.51 (d, J= 3.7 Hz, 2H), 7.41 (m, 4H), 7.13 (m, 2H). MS (EI): Calcd m/z = 278.0; found M^+ = 278.

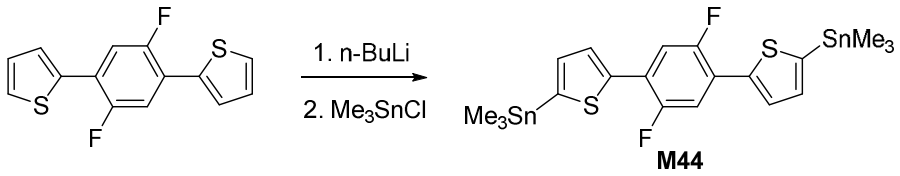

M44

1,4-Bis(5-(trimethylstannyl)thiophen-2-yl)-2,5-difluorobenzene (M44).

1,4-Bis(thiophen-2-yl)-2,5-difluorobenzene (1.0 g, 3.59 mmol) was dissolved in 100 mL anhydrous THF under argon. **M44** was prepared similarly as described for **M41** and recrystallized from hexane to yield a pale green needle crystal (1.53 g, 71%). ^{1}H NMR (400 MHz, $CDCl_3$): δ (ppm) 7.60 (d, J= 3.5 Hz, 2H), 7.40 (t, J= 9.2 Hz, 2H), 7.21 (d, J= 3.5 Hz, 2H), 0.41 (t, J= 28 Hz, 18H). MS (EI): Calcd m/z = 604.0; found M^+ = 604.

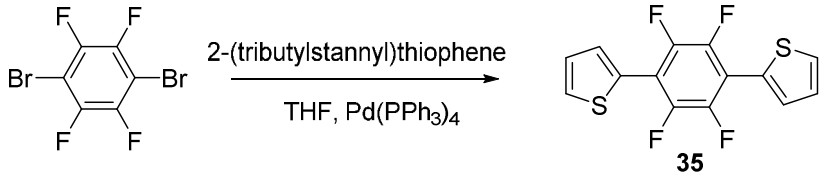

35

1,4-Bis(thiophen-2-yl)-2,3,5,6-tetrafluorobenzene (35).

1,4-Dibromo-2,3,5,6-tetrafluorobenzene (3 g, 9.7 mmol) and 2-(tributylstannyl)thiophene (9.5 g, 25.3 mmol) were added in a 2-neck round bottom flask. The compound **35** was prepared similarly as described for **31**. The crude product was recrystallized from ethanol to obtain 1.80 g of a colorless crystal (59%

yield). ^{1}H NMR (400 MHz, $CDCl_3$): δ (ppm) 7.68 (d, J= 3.7 Hz, 2H), 7.56 (dd, J^1= 5.2 Hz, J^2= 1.0 Hz, 2H), 7.20 (t, J= 4.5 Hz, 2H). MS (EI): Calcd m/z = 314.0; found M^+ = 314.

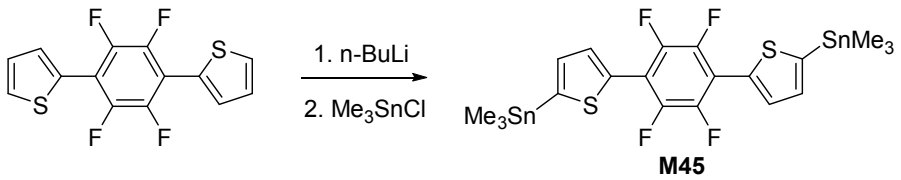

M45

1,4-Bis(5-(trimethylstannyl)thiophen-2-yl)-2,3,5,6-tetrafluorobenzene (M45).

1,4-Bis(thiophen-2-yl)-2,3,5,6-tetrafluorobenzene (1.0 g, 3.18 mmol) was dissolved in 100 mL anhydrous THF under argon protection. **M45** was prepared similarly as described for **M41** and recrystallized from ethanol to yield a pale yellow needle crystal (1.46 g, 72%). ^{1}H NMR (400 MHz, $CDCl_3$): δ (ppm) 7.76 (d, J= 3.3 Hz, 2H), 7.27 (d, J= 3.6 Hz, 2H), 0.43 (t, J= 28.2 Hz, 18H). MS (EI): Calcd m/z = 639.9; found M^+ = 640.

Syntheses of Polymers

Poly[(5,6-bis(2-hexyldecyloxy)benzo[c][1,2,5]thiadiazole-4,7-diyl)-alt-(5,5'-(1,4-phenylene)bis(thiophen-2-yl))] (PDTBTBz-0F).

4,7-Dibromo-5,6-bis(2-hexyldecyloxy)benzo[c][1,2,5]thiadiazole (**M21**) (155 mg, 0.20 mmol) and 1,4-bis(5-(trimethylstannyl)thiophen-2-yl)benzene **(M41)** (114 mg, 0.20 mmol) was added into a 2 mL microwave tube. $Pd_2(dba)_3$ (3.7 mg) and P(*o*-Tol)$_3$ (4.8 mg) were added to the above reaction mixture in a glovebox . After capping the microwave tube, anhydrous chlorobenzene (1.5 mL) was added via a syringe. The polymerization was carried out in a microwave reactor at 150 °C for 90 min. The resulting polymer was precipitated into methanol and collected by filtration. The precipitate was dissolved in chlorobenzene and precipitated again into methanol. The precipitate was then subjected to Soxhlet extraction with methanol, hexanes, dichloromethane, and chloroform. The final polymer was obtained by precipitating into methanol and drying in vacuum for 12 h, yielding **PDTBTBz-0F** (134 mg, 78%). M_n = 28,600 Da and PDI = 1.53.

The other polymers were similarly synthesized as described for **PDTBTBz-0F**.

Poly[(5,6-bis(2-hexyldecyloxy)benzo[c][1,2,5]thiadiazole-4,7-diyl)-alt-(5,5'-(2-fluoro-1,4-phenylene)bis(thiophen-2-yl))] (PDTBTBz-1F).

4,7-Dibromo-5,6-bis(2-hexyldecyloxy)benzo[c][1,2,5]thiadiazole (**M21**) (155 mg, 0.20 mmol) and 1,4-bis(5-(trimethylstannyl)thiophen-2-yl)-2-fluorobenzene **(M42)** (117 mg, 0.20 mmol) was reacted using $Pd_2(dba)_3$ (3.7 mg) and P(*o*-Tol)$_3$ (4.8 mg) as a catalyst. Yield: 135 mg, 77%. GPC: M_n = 46,200 Da, PDI = 2.37.

Poly[(5,6-bis(2-hexyldecyloxy)benzo[c][1,2,5]thiadiazole-4,7-diyl)-alt-(5,5'-(2,3-difluoro-1,4-phenylene)bis (thiophen-2-yl))] (PDTBTBz-2F$_{syn}$).

4,7-Dibromo-5,6-bis(2-hexyldecyloxy)benzo[c][1,2,5]thiadiazole (**M21**) (155 mg, 0.20 mmol) and 1,4-bis(5-(trimethylstannyl)thiophen-2-yl)-2,3-difluorobenzene **(M43)** (121 mg, 0.20 mmol) was reacted using $Pd_2(dba)_3$ (3.7 mg) and P(*o*-Tol)$_3$ (4.8 mg) as a catalyst. Yield: 138 mg, 77%. M_n = 111,900 Da, PDI = 3.10.

Poly[(5,6-bis(2-hexyldecyloxy)benzo[c][1,2,5]thiadiazole-4,7-diyl)-alt-(5,5'-(2,5-difluoro-1,4-phenylene)bis(thiophen-2-yl))] (PDTBTBz-2F$_{anti}$).

4,7-Dibromo-5,6-bis(2-hexyldecyloxy)benzo[c][1,2,5]thiadiazole (**M21**) (155 mg, 0.20 mmol) and 1,4-bis(5-(trimethylstannyl)thiophen-2-yl)-2,5-difluorobenzene **(M44)** (121 mg, 0.20 mmol) was reacted. Yield: 144 mg, 81%. M_n = 182,600 Da, PDI = 2.09.

Poly[(5,6-bis(2-hexyldecyloxy)benzo[c][1,2,5]thiadiazole-4,7-diyl)-alt-(5,5'-(2,3,5,6-tetrafluoro-1,4-phenylene)bis(thiophen-2-yl))] (PDTBTBz-4F).

4,7-Dibromo-5,6-bis(2-hexyldecyloxy)benzo[c][1,2,5]thiadiazole (**M21**) (155 mg, 0.20 mmol) and 1,4-bis(5-(trimethylstannyl)thiophen-2-yl)-2,3,5,6-tetrafluorobenzene **(M45)** (128 mg, 0.20 mmol) was polymerized. Yield: 142 mg, 78%. M_n = 182,300 Da, PDI = 3.06.

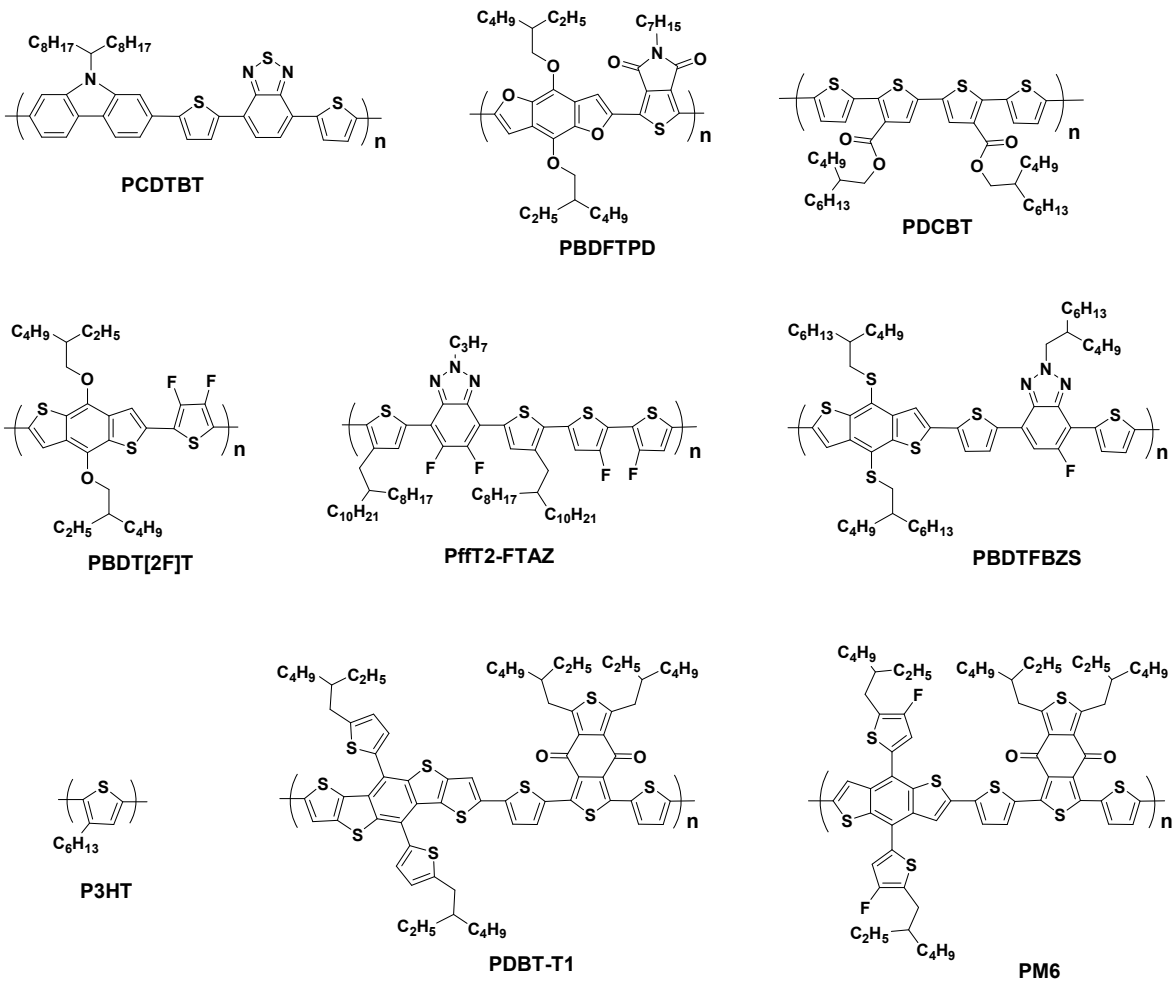

Fig. S1 Reported wide band gap polymers with high PCEs.

Table S1 Summary of previously reported high PCE wide band gap polymers.

Polymer	E_g^{opt} (eV)	V_{OC} (V)	J_{SC} (mA cm^{-2})	FF (%)	PCE (%)	Reference
P3HT	1.90	0.85	10.6	74	6.7	2
PCDTBT	1.88	0.88	10.6	66	6.1	3
PBDFTPD	1.97	0.97	11.2	68	7.4	4
PDCBT	1.90	0.91	11.0	72	7.2	5
PBDTFBZS	1.81	0.88	12.4	71	7.7	6
PBDT[2F]T	2.10	0.90	10.7	72	7.0	7
PDBT-T1	1.85	0.92	14.1	75	9.7	8
PM6	1.80	0.98	12.7	74	9.2	9
PffT2-FTAZ	1.88	0.80	13.3	69	7.8	10

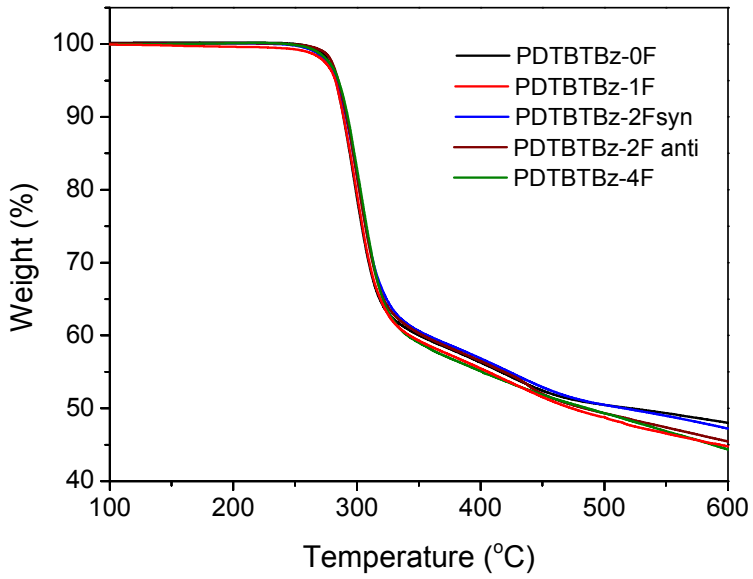

Fig. S2 TGA thermograms of polymers.

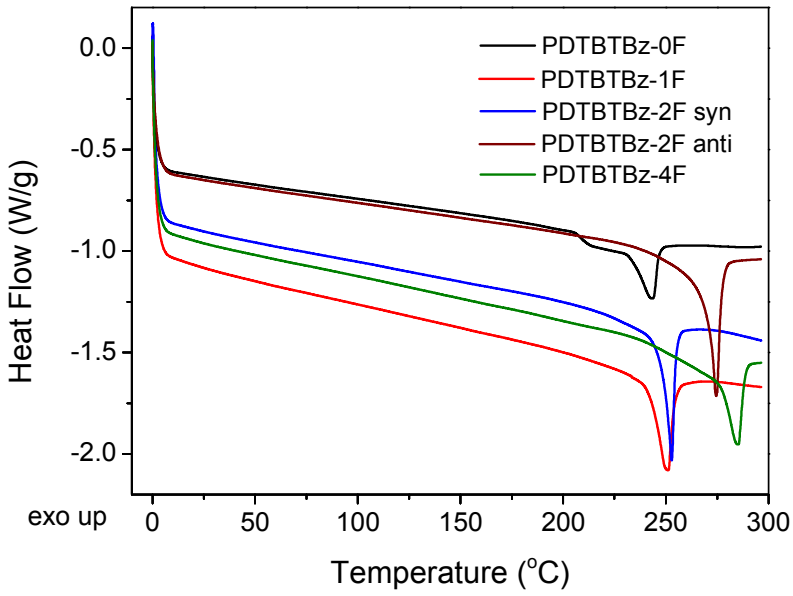

Fig. S3 DSC thermograms of polymers.

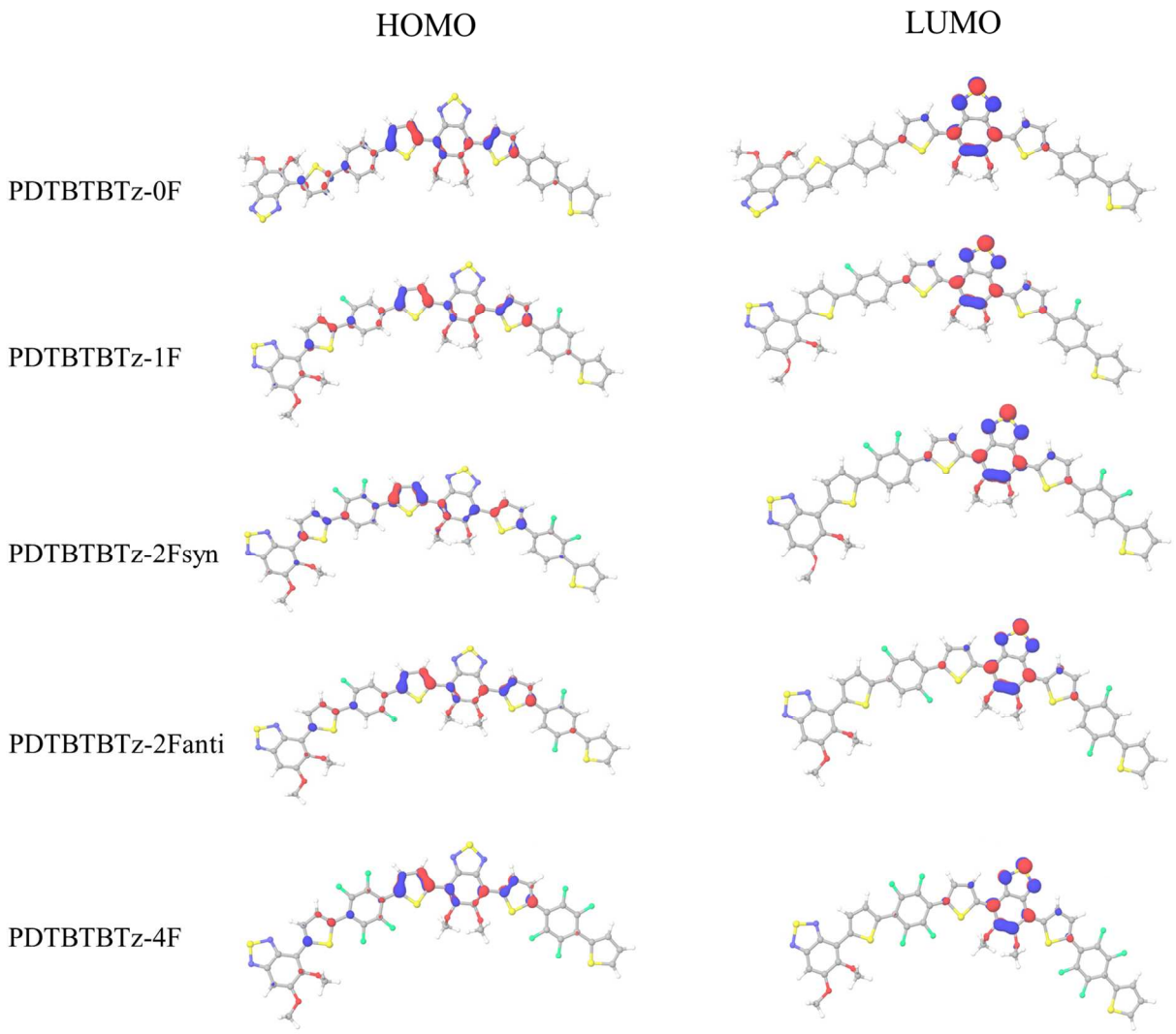

Fig. S4 Calculated HOMO and LUMO electronic structures of polymers (B3LYP/6-31G** level).

Table S2 Summary of torsional profiles of energy minimum conformations.

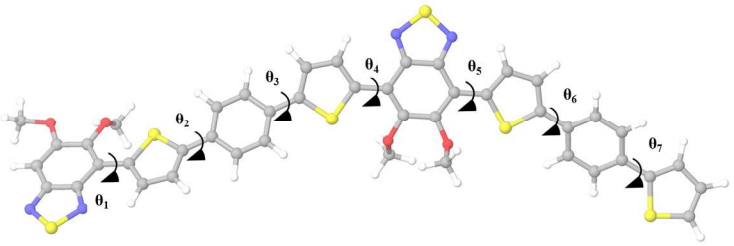

Polymer	θ_1 (degree)	θ_2 (degree)	θ_3 (degree)	θ_4 (degree)	θ_5 (degree)	θ_6 (degree)	θ_7 (degree)
PDTBTBz-0F	-173	20	-159	-178	-174	20	-26
PDTBTBz-1F	-172	163	-161	-172	-168	168	-156
PDTBTBz-2F$_{syn}$	-171	168	170	-170	-170	-164	165
PDTBTBz-2F$_{anti}$	-171	179	-1	-173	-174	-179	1
PDTBTBz-4F	-172	0	-1	-175	-173	2	0

Table S3 Calculated frontier orbital levels based on two repeating units by DFT.

Polymer	HOMO (eV)	LUMO (eV)	Band gap (eV)
PDTBTBz-0F	-4.87	-2.55	2.32
PDTBTBz-1F	-4.95	-2.63	2.32
PDTBTBz-2F$_{syn}$	-5.03	-2.69	2.34
PDTBTBz-2F$_{anti}$	-4.97	-2.67	2.30
PDTBTBz-4F	-5.11	-2.75	2.36

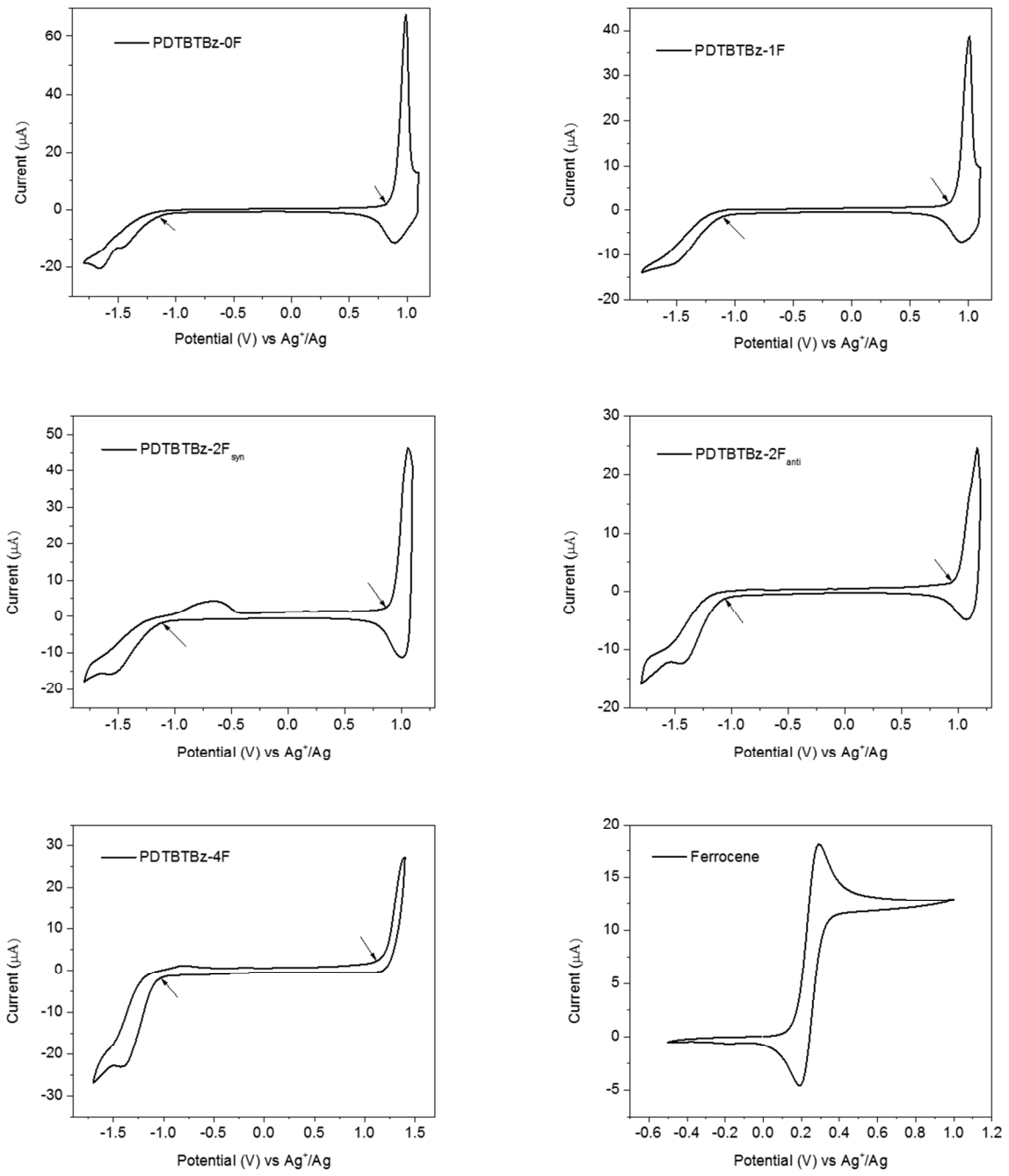

Fig. S5 Cyclic voltammograms of polymers and ferrocene as a reference.

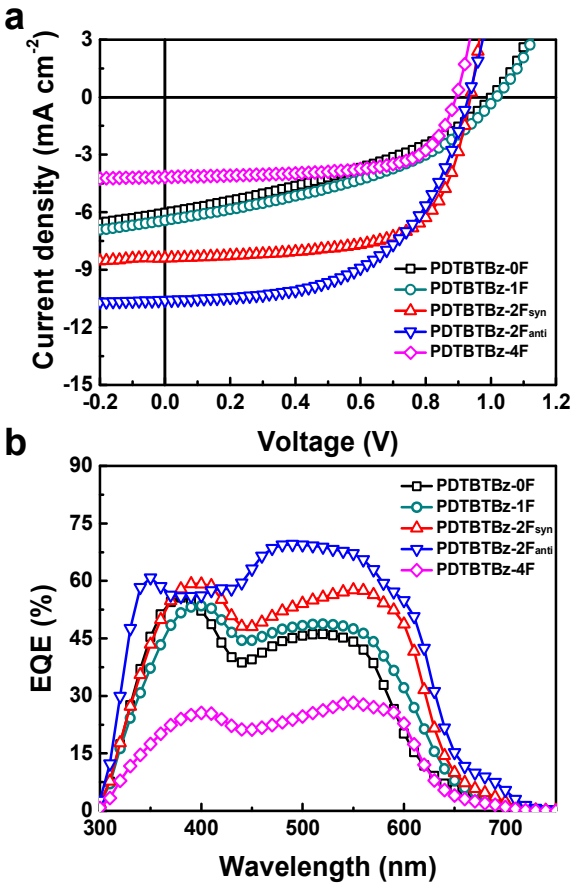

Fig. S6 (a) *J–V* curves and (b) EQE spectra of optimum polymer:$PC_{71}BM$ devices prepared from CB solvent without DPE.

Table S4 Summary of device parameters (CB solvent without DPE).

Donor:$PC_{71}BM$	J_{SC} (mA cm^{-2})	[*Cal.*] J_{SC} [a] (mA cm^{-2})	V_{OC} (V)	FF	PCE (%) Best (Ave.)[b]
PDTBTBz-0F	6.0	6.1	1.00	0.37	2.2 (2.1)
PDTBTBz-1F	6.4	6.9	1.02	0.40	2.6 (2.6)
PDTBTBz-$2F_{syn}$	8.4	8.3	0.94	0.66	5.2 (5.0)
PDTBTBz-$2F_{anti}$	10.6	10.1	0.93	0.55	5.4 (5.2)
PDTBTBz-4F	4.2	3.7	0.89	0.66	2.5 (2.2)

[a][*Cal.*] J_{SC}, calculated J_{SC} from a EQE curve. [b]Average PCE values obtained from 15 devices.

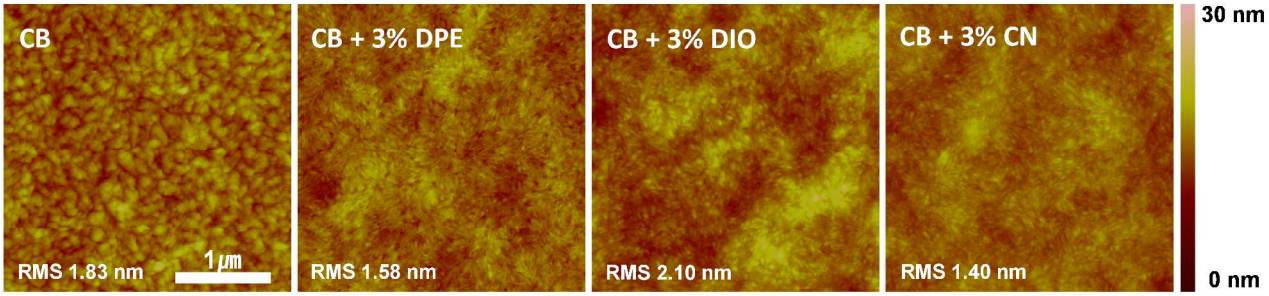

Fig. S7. Tapping-mode AFM topography images of polymer:$PC_{71}BM$ blend films (solvent: CB without and with DPE, DIO and CN (from left to right).

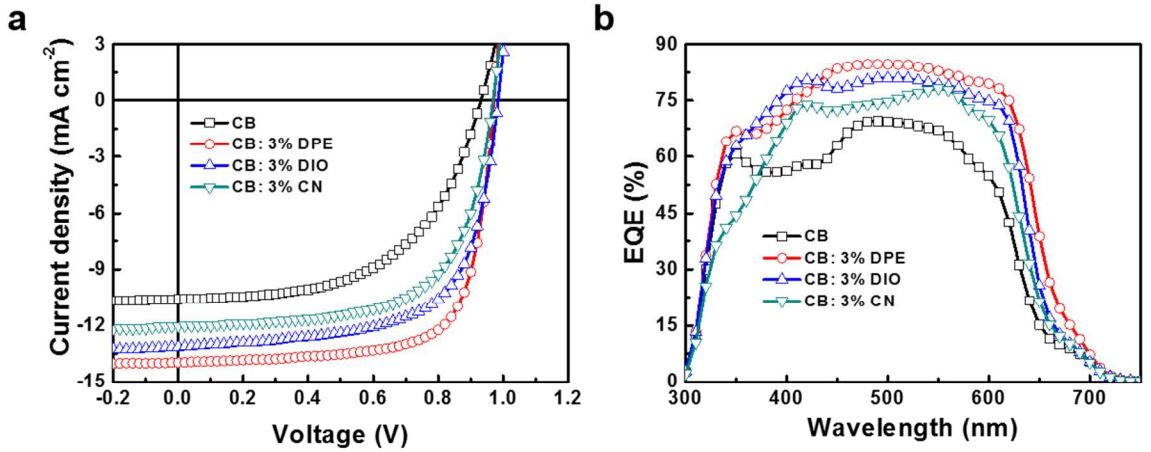

Fig. S8 (a) *J–V* curves and (b) EQE spectra for PDTBTBz-2F_{anti}:$PC_{71}BM$ prepared from CB solvent without and with DPE, DIO and CN.

Table S5 Summary of device parameters for PDTBTBz-2F_{anti}:$PC_{71}BM$ with various processing additives

Solvent	J_{SC} (mA cm^{-2})	[*Cal.*] J_{SC}[a)] (mA cm^{-2})	V_{OC} (V)	FF	Best PCE (%)
CB	10.6	10.1	0.93	0.55	5.4
CB : 3% DPE	14.0	13.8	0.97	0.72	9.8
CB : 3% DIO	13.1	12.9	0.98	0.66	8.5
CB : 3% CN	12.0	11.8	0.97	0.65	7.5

[a)] [*Cal.*] J_{SC}, calculated J_{SC} from a EQE curve

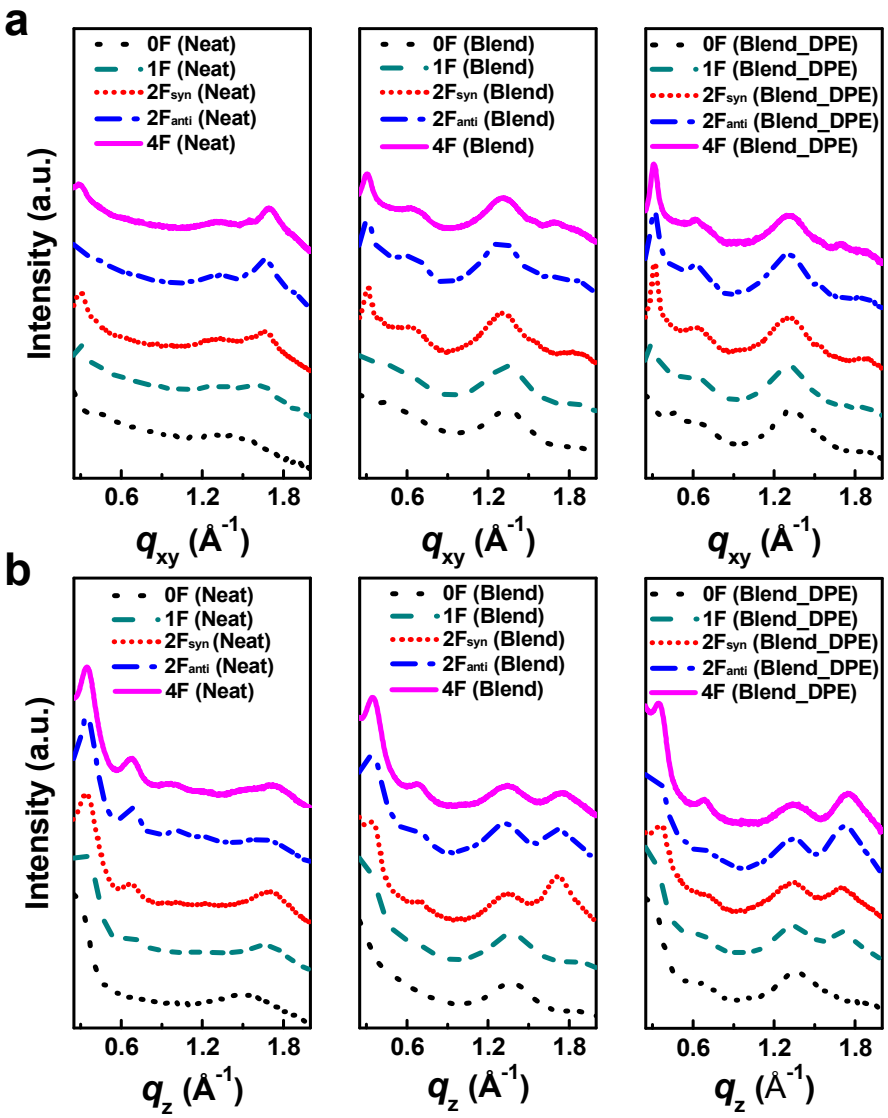

Fig. S9 In-plane (a) and out-of-plane (b) GIWAXS line-cut data for pristine polymers (left panel), polymer:$PC_{71}BM$ (middle), and polymer:$PC_{71}BM$ films with DPE (right panel).

Table S6 Packing parameters derived from GIWAXS measurements. ($q_{vertical}$ was taken near the vertical direction, but not exactly at q_{xy}=0 because of the inaccessible region of reciprocal space.)

Films	Polymers	Packing parameters				
		Axis	π-π stack [Å^{-1}]	d-spacing [Å]	Lamella stack [Å^{-1}]	d-spacing [Å]
Pristine polymer	PDTBTBz-0F	q_{xy}	-	-	0.22	28.55
		$q_{vertical}$	1.69	3.72	-	-
	PDTBTBz-1F	q_{xy}	1.66	3.79	0.31	20.20
		$q_{vertical}$	1.68	3.74	0.33	18.48
	PDTBTBz-2F$_{syn}$	q_{xy}	1.67	3.76	0.31	20.27
		$q_{vertical}$	1.69	3.72	0.34	18.48
	PDTBTBz-2F$_{anti}$	q_{xy}	1.68	3.74	0.32	19.63
		$q_{vertical}$	1.69	3.72	0.35	17.95
	PDTBTBz-4F	q_{xy}	1.70	3.70	0.30	20.94
		$q_{vertical}$	1.72	3.65	0.34	18.48
Polymer:$PC_{71}BM$ blend	PDTBTBz-0F	q_{xy}	-	-	-	-
		$q_{vertical}$	-	-	-	-
	PDTBTBz-1F	q_{xy}	-	-	-	-
		$q_{vertical}$	-	-	-	-
	PDTBTBz-2F$_{syn}$	q_{xy}	-	-	0.32	19.63
		$q_{vertical}$	1.72	3.65	0.36	17.45
	PDTBTBz-2F$_{anti}$	q_{xy}	-	-	0.32	19.63
		$q_{vertical}$	1.73	3.63	0.35	17.95
	PDTBTBz-4F	q_{xy}	1.69	3.72	0.31	20.27
		$q_{vertical}$	1.75	3.59	0.34	18.48
Polymer:$PC_{71}BM$ blend with DPE	PDTBTBz-0F	q_{xy}	-	-	0.24	26.17
		$q_{vertical}$	-	-	-	-
	PDTBTBz-1F	q_{xy}	-	-	0.31	20.20
		$q_{vertical}$	1.72	3.65	0.32	19.63
	PDTBTBz-2F$_{syn}$	q_{xy}	-	-	0.32	19.63
		$q_{vertical}$	1.72	3.65	0.35	17.95
	PDTBTBz-2F$_{anti}$	q_{xy}	-	-	0.32	19.63
		$q_{vertical}$	1.72	3.65	0.35	17.95
	PDTBTBz-4F	q_{xy}	1.70	3.70	0.31	20.27
		$q_{vertical}$	1.75	3.59	0.34	18.48

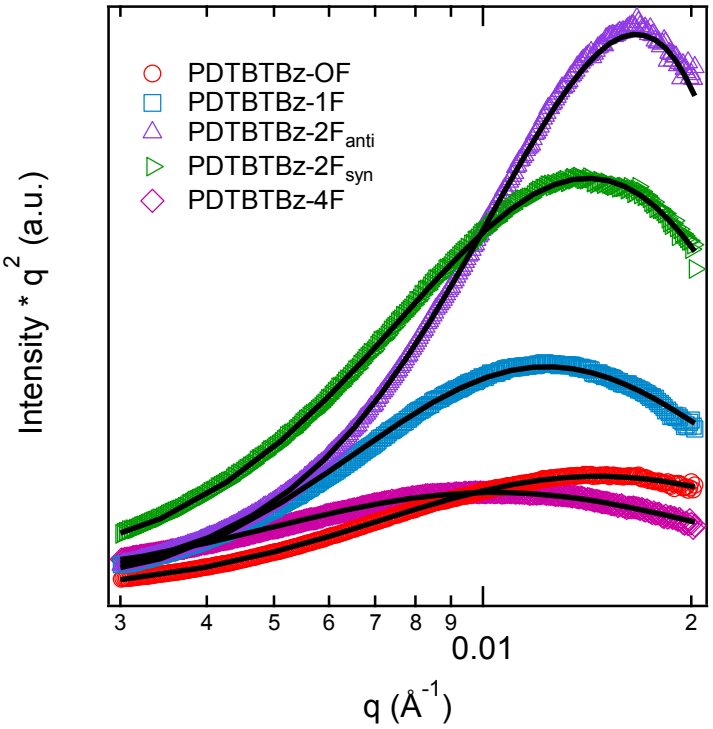

Fig. S10 Resonant soft X-ray scattering (RSoXS) profiles of PDTBTBz-based polymer:$PC_{71}BM$ blends spin cast from a CB solvent with DPE additive. The Lorentz corrected curves were fit with log-normal distributions (solid black traces). The length scales based on the peak positions are 43, 51, 44, 38, and 60 nm for PDTBTBz-0F, PDTBTBz-1F, PDTBTBz-$2F_{syn}$, PDTBTBz-$2F_{anti}$, and PDTBTBz-4F, respectively.

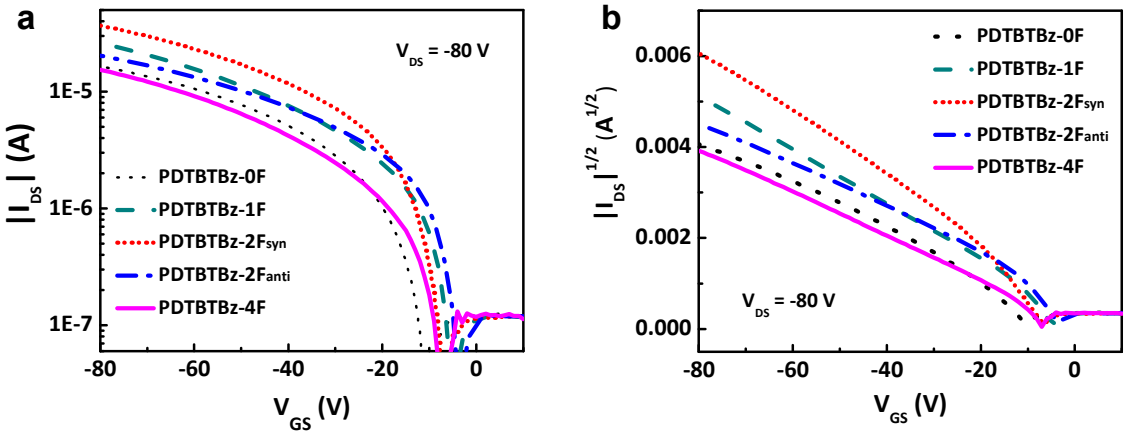

Fig. S11 Transfer characteristic of PFET devices at V_{DS} = −80 V (W/L = 1000/20 μm).

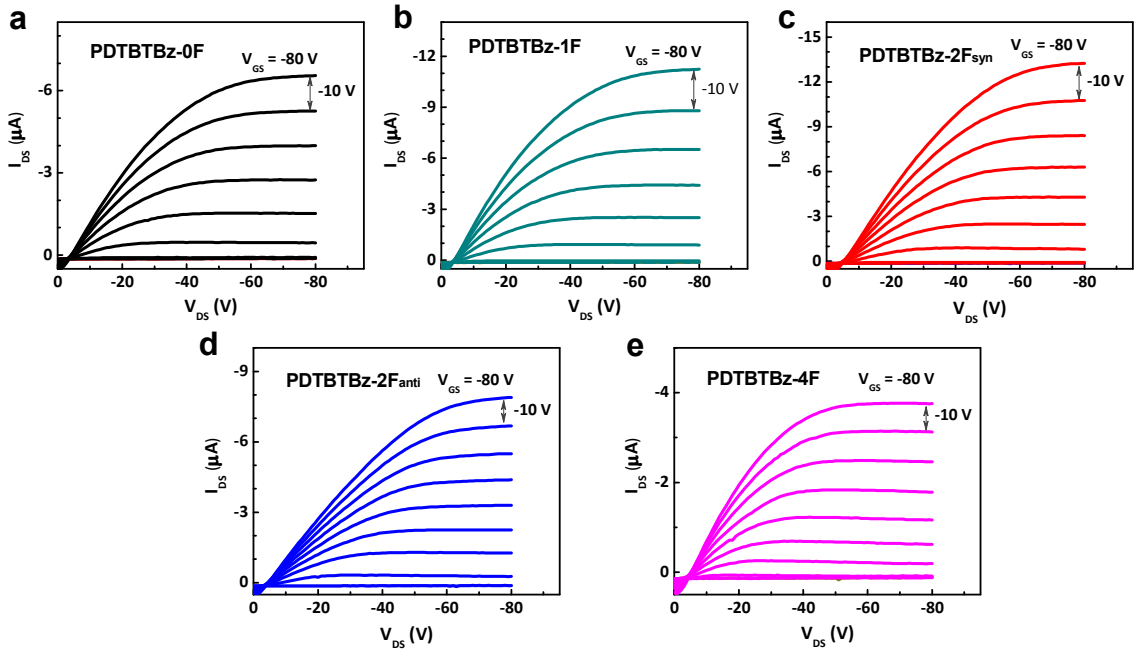

Fig. S12 Output curves of PFET devices. (a) PDTBTBz-0F, (b) PDTBTBz-1F, (c) PDTBTBz-2F$_{syn}$, (d) PDTBTBz-2F$_{anti}$, and (e) PDTBTBz-4F.

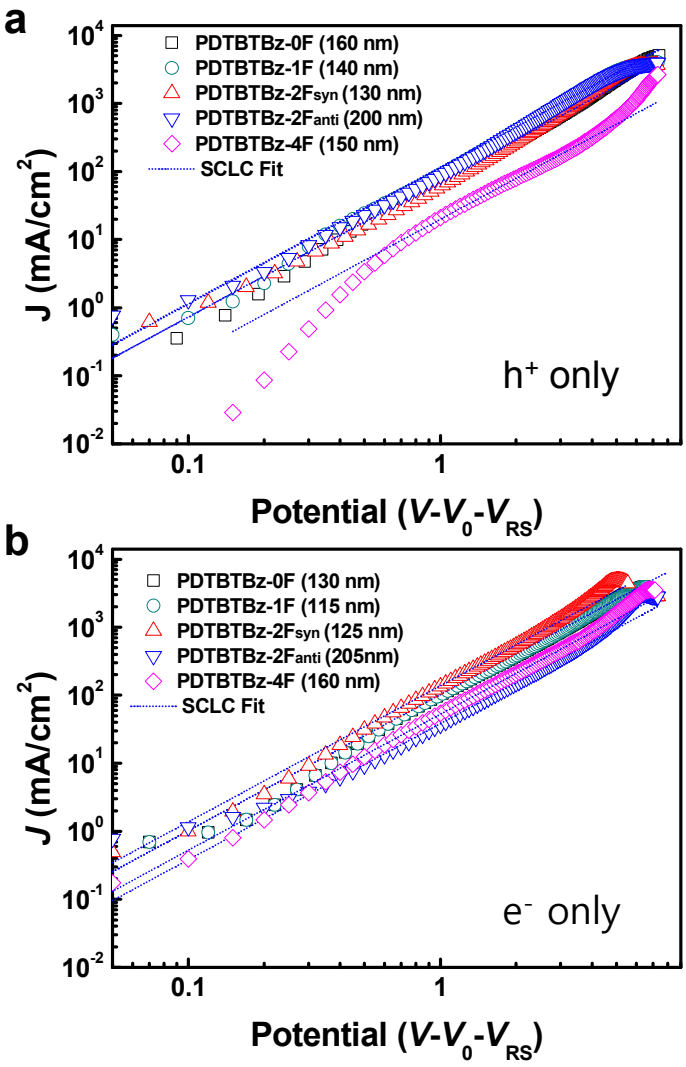

Fig. S13 *J–V* characteristics of (a) hole- and (b) electron-only devices based on polymer:$PC_{71}BM$ blend films (CB:DPE = 97 : 3 vol%). Blue lines represent the best fit based on the Mott–Gurney relationship.

Table S7 Field effect hole mobilities for polymers.

Sample	μ_h (cm^2 $V^{-1}s^{-1}$)	V_T (V)
PDTBTBz-0F	2.4×10^{-2}	-8.1
PDTBTBz-1F	4.1×10^{-2}	-3.4
PDTBTBz-$2F_{syn}$	5.2×10^{-2}	-2.0
PDTBTBz-$2F_{anti}$	5.6×10^{-2}	-7.7
PDTBTBz-4F	9.0×10^{-3}	-4.5

Table S8 SCLC charge mobilities for polymer:$PC_{71}BM$ blend films.

Polymer:$PC_{71}BM$ with DPE	Hole mobility (μ_h) (cm^2 V^{-1} s^{-1})	Electron Mobility (μ_e) (cm^2 V^{-1} s^{-1})	μ_h/μ_e
PDTBTBz-0F	1.0×10^{-3}	7.5×10^{-4}	1.33
PDTBTBz-1F	1.07×10^{-3}	8.3×10^{-4}	1.29
PDTBTBz-$2F_{syn}$	1.0×10^{-3}	9.0×10^{-4}	1.11
PDTBTBz-$2F_{anti}$	1.15×10^{-3}	1.1×10^{-3}	1.05
PDTBTBz-4F	1.15×10^{-4}	7.3×10^{-4}	0.16

Table S9 Summary of reference subcells and tandem PSCs.

Device	J_{SC} (mA cm^{-2})	V_{OC} (V)	FF	PCE (%)
Ref. front cell (PDTBTBz-$2F_{anti}$)	13.0	0.98	0.70	9.0
Ref. back cell (DT-PDPP2T-TT)	16.4	0.69	0.71	8.0
Tandem	9.9	1.58	0.66	10.3

Inverted structure:
ITO/ZnO/Active Layer/MoO_3/Au

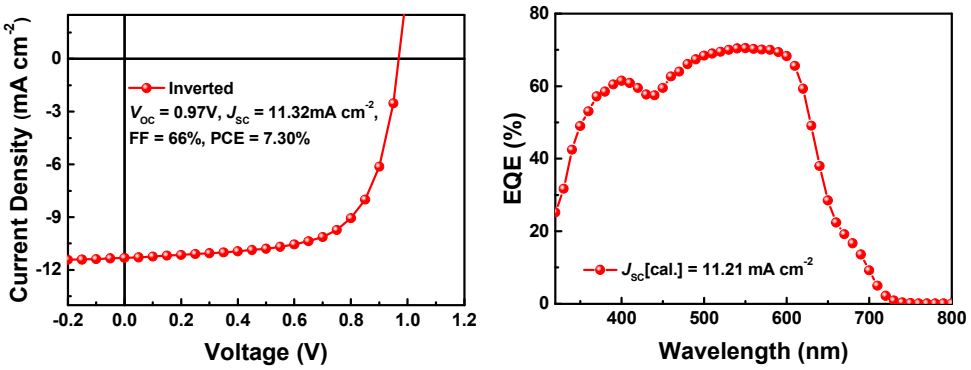

Fig. S14 *J-V* curve and EQE of devices using PDTBTBz-2F_{anti}:PC_{71}BM blend in an inverted structure.

Air stability test
- Five types of devices (conventional (Al), Inverted (MoO_3/Au), conventional (Ca/Al) without sealing and conventional (Ca/Al) with sealing by UV epoxy for single-junction device and conventional device (Al) for tandem-junction device) in Air

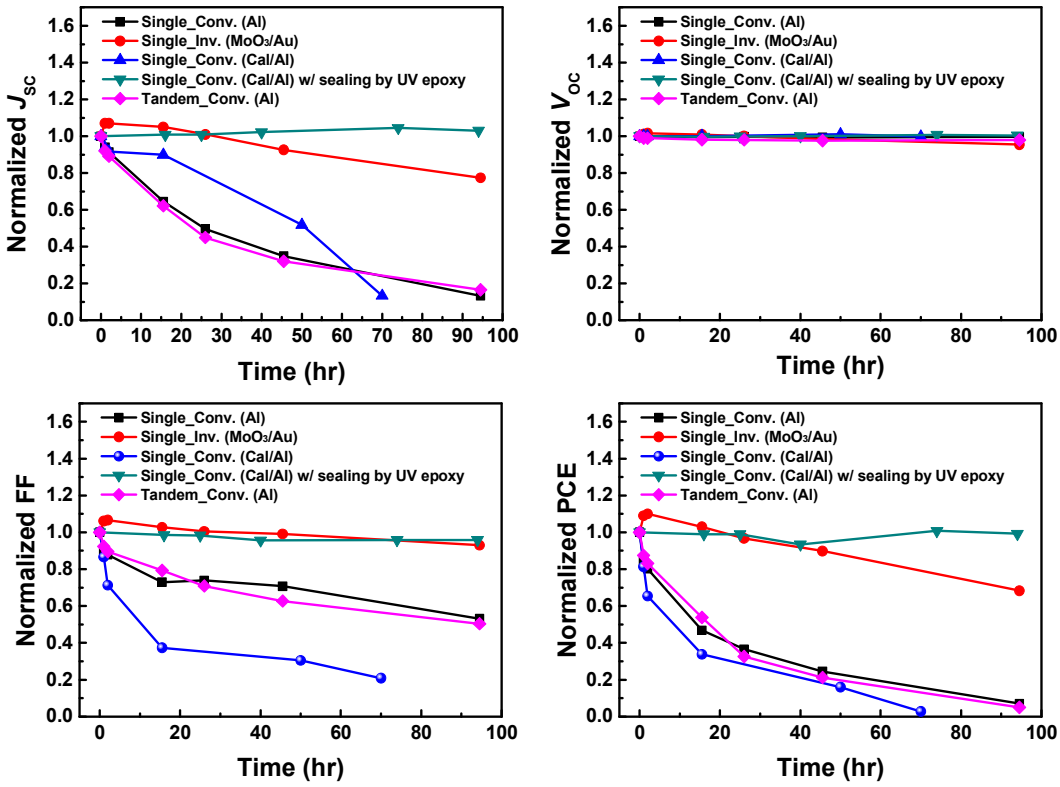

Fig. S15 Comparison of air stabilities for single- and tandem-junction solar cells with different electrodes and device structures.

Reference

1. B.-G. Kim, E. J. Jeong, J. W. Chung, S. Seo, B. Koo and J. Kim, *Nat. Mater.*, 2013, **12**, 659-664.
2. X. Fan, C. Cui, G. Fang, J. Wang, S. Li, F. Cheng, H. Long and Y. Li, *Adv. Funct. Mater.*, 2012, **22**, 585-590.
3. S. H. Park, A. Roy, S. Beaupre, S. Cho, N. Coates, J. S. Moon, D. Moses, M. Leclerc, K. Lee and A. J. Heeger, *Nat. Photon.*, 2009, **3**, 297-302.
4. J. Warnan, C. Cabanetos, A. E. Labban, M. R. Hansen, C. Tassone, M. F. Toney and P. M. Beaujuge, *Adv. Mater.*, 2014, **26**, 4357-4362.
5. M. Zhang, X. Guo, W. Ma, H. Ade and J. Hou, *Adv. Mater.*, 2014, **26**, 5880-5885.
6. K. Li, Z. Li, K. Feng, X. Xu, L. Wang and Q. Peng, *J. Am. Chem. Soc.*, 2013, **135**, 13549-13557.
7. J. Wolf, F. Cruciani, A. El Labban and P. M. Beaujuge, *Chem. Mater.*, 2015, **27**, 4184-4187.
8. L. Huo, T. Liu, X. Sun, Y. Cai, A. J. Heeger and Y. Sun, *Adv. Mater.*, 2015, **27**, 2938-2944.
9. M. Zhang, X. Guo, W. Ma, H. Ade and J. Hou, *Adv. Mater.*, 2015, **27**, 4655-4660.
10. Z. Li, H. Lin, K. Jiang, J. Carpenter, Y. Li, Y. Liu, H. Hu, J. Zhao, W. Ma, H. Ade and H. Yan, *Nano Energy*, 2015, **15**, 607-615.

Dear Editor, Dr. Carri Cotton,

First of all, I, along with my coauthors, would like to express appreciation to all the reviewers for their valuable comments and constructive suggestions. Here, we submit the revised version of our manuscript entitled "High-efficiency photovoltaic cells with wide optical band gap polymers based on fluorinated phenylene-alkoxybenzothiadiazole" (Manuscript ID: EE-ART-10-2016-003051.R1) for publication in *Energy & Environmental Science* as a full paper. The revised manuscript fully addresses the concerns raised by the reviewers in the previous round of review. Revisions were highlighted in yellow in the manuscript, and we have additionally included a point-by-point response to the reviewers' comments below.

Referee: 3

Comments to the Author
The authors have carefully revised the manuscript and addressed the concerns raised by the reviewers. I therefore recommend it for publication in EES without change.

Answer: We are grateful to the referee for the careful evaluation of our manuscript and for the positive review.

Referee: 1

Comments to the Author
In this manuscript, the authors synthesized and compared a series of PDTBTBz polymers containing different numbers of fluorine atoms in terms of their optical, electrical and morphological properties. By the synergetic effect of introducing the alkoxy group and optimizing the number of fluorine atoms, PDTBTBz-2Fanti achieved a high VOC of 0.97V and the highest efficiency of 9.8% for fullerene-based devices, which is reasonably high for a large-bandgap (>1.9 eV) polymer. The morphology characterizations agreed well with the device results, which provided a clear understanding of their structure-property-performance relationship. The rational design of the large-bandgap polymers should promote the further development of OSCs, especially for those non-fullerene OSCs based on low-bandgap acceptors and tandem cells. Therefore, I recommend this manuscript be published in Energy & Environmental Science after minor revisions.

Answer: We thank the reviewer for the positive review and the helpful comments.

1. The authors mentioned their previous report on the structurally similar polymer (PPDT2FBT) with comparable performances (9.4%). I think the author should also compare PPDT2FBT and PDTBTBz-2Fanti regarding the absorption, energy levels and photovoltaic parameters to further demonstrate the structure-property-performance relationship.

Answer: According to reviewer comments, we have compared the optical, electrochemical and photovoltaic properties of PDTBTBz polymers and the previously reported PPDT2FBT, and the

related discussions were included in the manuscript.

In section 2.3 (pages 9-10), we have modified the following discussions.
"The UV-vis absorption spectra of the polymers in chloroform and in thin film are shown in Fig. 1 and summarized in Table 1. The polymers show two absorption bands in which the first absorption peak below 450 nm is attributed to characteristic π-π* transition and the low-energy absorption band in the range of 450-650 nm is attributed to the ICT interaction. With compared to the similarly structured PPDT2FBT reported previously (based on 2FBT and dialkoxy-substituted dithienylbenzene, optical band gap of 1.76 eV),[39] the newly synthesized PDTBTBz series polymers show a blue-shifted absorption due to the decreased ICT from dithienylbenzene (with or without fluorine) to DOBT.[41]"

In page 11, we have revised the manuscript as follows.
"The HOMO energy levels of PDTBTBz polymers are clearly down-shifted (up to -5.67 eV) and the LUMO levels are up-shifted (up to -3.40 eV) based on the weaker donor and acceptor pairs, resulting in wider band gap, compared to PPDT2FBT (HOMO: -5.45 eV, LUMO: -3.69 eV).[39]"

In page 13, we have also revised the manuscript as follows.
"Compared to PPDT2FBT, PDTBTBz-2F_{anti} shows the lower J_{SC} (16.3→14.0 mA cm^{-2}) due to narrower absorption range but higher V_{OC} (0.79→ 0.97 V) with deeper HOMO. Both polymers show similarly high *FF*, showing well distributed nano-fibrillar, semi-crystalline BHJ film morphology.[39]"

2. In the introduction, the authors mentioned several representative examples of large-bandgap polymers with high performances (7~9%) and claimed that the PCEs in this manuscript are among the highest. They should specify that those are all fullerene-based devices, as some large-bandgap polymers in non-fullerene OSCs exhibit higher efficiencies (~11%).

Answer: We agree with the reviewer's comments. The sentence was changed as follows in the introduction.
"To the best of our knowledge, the PCE of 9.8 % is one of the highest values reported so far for fullerene-based single-junction BHJ PSCs using polymers with an optical band gap above 1.9 eV.".

The sentence was changed as follows in the Abstract.
"To our knowledge, this PCE is one of the highest values for fullerene-based single BHJ device with WBG polymers having a band gap over 1.90 eV."

The sentence was also changed as follows in the section 2.4 (page 13).
"To the best of our knowledge, the PCE of 9.8 % is one of the highest values yet reported for fullerene-based single BHJ PSCs using polymers with band gaps over 1.90 eV."

3. "In addition, the symmetric substitution of fluorines (PDTBTBz-2Fanti) showed a higher melting than the asymmetric one (PDTBTBz-2Fsyn). The symmetric F substitution may improve the crystalline interchain organization with a close and tight packing." The author should clarify that both difluorobenzene units are symmetric (anti – C2-symmetric /syn – mirror-symmetric), as proven by single crystal characterization from the previous report. (Nature Communications, (2016), 7, 13094.)

The impact of anti/syn should be related to the regularity of the polymer backbone.

Answer: We thank the reviewer for the valuable comment. As the reviewer mentioned, both PDTBTBz-2F$_{anti}$ and PDTBTBz-2F$_{syn}$ have symmetric substitution of fluorine atoms. We modified the discussion as follows in page 8.
"In addition, the different symmetry in the fluorine substitution for PDTBTBz-2F$_{anti}$ (C2-symmetric) and PDTBTBz-2F$_{syn}$ (mirror-symmetric) may influence interchain organization in a solid state. According to the DSC data, PDTBTBz-2F$_{anti}$ with C2-symmetric F substitution is expected to improve the crystalline interchain ordering with a close and tight packing.[12]"

4. It is interesting that the PDTBTBz-4F showed poor performances but similar absorption, energy levels and morphology (from AFM/GIWAXS) to the PDTBTBz-2F polymers. Can the authors propose some possible reasons? For instance, low domain purity (from Fig S10) can dramatically affect the charge generation and separation process.

Answer: According to reviewer comments, the discussions are included as follows in page 16.
"With compared to PDTBTBz-2F polymers, PDTBTBz-4F has the most rigid structure with 4 fluorine atoms in the polymeric backbone and shows the strongest tendency of interchain aggregation with relatively poor solubility. As shown in Fig. S10, the PDTBTBz-4F:PC$_{71}$BM blend exhibits a larger average domain size. The quick and excessive segregation of PDTBTBz-4F may decrease the domain purity (see Fig. S10) in the blend with PC$_{71}$BM, resulting in poorer photovoltaic performance."

We sincerely appreciate you and the reviewers for their valuable comments and hope that our revised manuscript is now acceptable for publication in *Energy & Environmental Science*.

Thank you in advance and we look forward to future correspondence.

With best regards,

Jin Young Kim, Ph. D.

Department of Energy Engineering, School of Energy and Chemical Engineering
Ulsan National Institute of Science and Technology (UNIST)

Broader Context

Renewable and eco-friendly energy sources such as photovoltaic cell technologies have been tremendously improved and extensively implemented in order to replace environmentally harmful energy sources over the past several decades. In particular, polymer solar cells (PSC) have attracted increasing attention because their many advantages such as mechanical flexibility, solution processability and low cost, which make them an attractive technology to satisfy future energy demands. As a result of a collective worldwide endeavor to develop PSCs, device efficiency has improved considerably over a short period of time. Despite significant improvements in device efficiency, current power conversion efficiencies (PCEs) of PSCs have not yet been sufficient for their widespread commercialization. To solve this challenge, multi-junction bulkheterojunction (BHJ) PSCs are considered a promising route for further improvement of device performance, by utilizing optimal combinations of both wide and small band gap polymers. In this work, we report new series of semi-crystalline conjugated polymers with wide band gaps over 1.90 eV, which demonstrate a high PCE of 9.8 % in single-junction BHJ device as well as a PCE of 10.3 % in tandem devices. We believe that our results provide an effective pathway realize the of commercial application of PSCs.

RSC publishing group

NAME OF JOURNAL: Energy & Environmental Science

TITLE OF MANUSCRIPT: High-efficiency photovoltaic cells with wide optical band gap polymers based on fluorinated phenylene-alkoxybenzothiadiazole

MANUSCRIPT NUMBER: EE-ART-10-2016-003051

CORRESPONDING AUTHORS NAME: Han Young Woo, Won Suk Shin and Jin Young Kim

PREVIOUS AUTHOR NAMES:
Seo-Jin Ko, Quoc Viet Hoang, Chang Eun Song, Mohammad Afsar Uddin, Song Yi Park, Byoung Hoon Lee, Seyeong Song, Sang-Jin Moon, Sungu Hwang, Eunhee Lim, Pierre-Olivier Morin, Mario Leclerc, Han Young Woo,* Won Suk Shin* and Jin Young Kim*

UPDATED AUTHOR NAMES:
Michael L. Chabinyc, Gregory M. Su

CHANGE TO AUTHOR LIST: Seo-Jin Ko, Quoc Viet Hoang, Chang Eun Song, Mohammad Afsar Uddin, Eunhee Lim, Song Yi Park, Byoung Hoon Lee, Seyoung Song, Sang-Jin Moon, Sungu Hwang, Pierre-Olivier Morin, Mario Leclerc, Gregory M. Su, Michael L. Chabinyc, Han Young Woo,* Won Suk Shin* and Jin Young Kim*

All co-authors approved final manuscript and addition of authors to make the manuscript clearer as follow. All co-authors have sent approval to editor's email.

Updated Author Contributions

S.-J.K. and Q.V.H. contributed equally to this work. S.-J.K. proposed the research, conducted most of the characterizations, fabricated solar cells and also contributed to data analysis and preparation of manuscript. Q.V.H and C.E.S. synthesized and five kinds of WBG polymers and conducted characterization related to synthesis. M.A.U. contributed to data analysis, participated to the discussion and manuscript preparation with S.-J.K. S.Y.P. performed HR-TEM and B.H.L fabricated PFET. S.S. measured AFM. S.-J.M. designed WBG polymers. S.H. conducted DFT calculation. E.L. and M.L.C. measured and analysed 2D-GIWAXS and also fully revised manuscript. G.M.S. measured and analysed RSoXS. P.-O.M and M.L. prepared LBG polymer for tandem device fabrication. W.S.S. supervised synthesis of five kinds of WBG polymers. H.Y.W. and J.Y.K. supervised the whole project. All authors discussed the results and commented on the manuscript.

High-efficiency photovoltaic cells with wide optical band gap polymers based on fluorinated phenylene-alkoxybenzothiadiazole

Seo-Jin Ko,‡[ab] Quoc Viet Hoang,‡[cd] Chang Eun Song,[cd] Mohammad Afsar Uddin,[e,f] Eunhee Lim,[g] Song Yi Park,[b] Byoung Hoon Lee,[a] Seyeong Song,[b] Sang-Jin Moon,[cd] Sungu Hwang,[f] Pierre-Olivier Morin,[h] Mario Leclerc,[h] Gregory M. Su,[i] Michael L. Chabinyc,[g] Han Young Woo,*[e] Won Suk Shin*[cd] and Jin Young Kim*[b]

[a] Center for Polymers and Organic Solids, University of California Santa Barbara (UCSB), Santa Barbara, CA 93106, USA

[b] School of Energy and Chemical Engineering, Ulsan National Institute of Science and Technology (UNIST), Ulsan 44919, Republic of Korea. E-mail) jykim@unist.ac.kr

[c] Energy Materials Research Center, Korea Research Institute of Chemical Technology (KRICT), 141 Gajeong-ro, Yuseong-gu, Daejeon 305-343, Republic of Korea. E-mail) shinws@krict.re.kr

[d] Department of Nanomaterials Science and Engineering, University of Science & Technology (UST), 217 Gajeong-ro, Yuseong-gu, Daejeon, 305-350, Republic of Korea.

[e] Department of Chemistry, Korea University, Seoul 136-713, Republic of Korea. E-mail) hywoo@korea.ac.kr

[f] Department of Nanomechatronics Engineering, Pusan National University, Miryang 627-706, Republic of Korea

[g] Materials Department, University of California Santa Barbara (UCSB), Santa Barbara, CA 93106, USA

[h] Department of Chemistry, Laval University, Quebec City, QC, G1V 0A6, Canada

[i] Advanced Light Source, Lawrence Berkeley National Laboratory, Berkeley, CA 94720, USA

KEYWORDS: wide band gap polymer, semi-crystalline, fluorine, noncovalent interactions, polymer solar cell, tandem solar cell

ABSTRACT

A series of semi-crystalline, wide band gap (WBG) photovoltaic polymers was synthesized with varying number and topology of fluorine substituents. To decrease intramolecular charge transfer and to modulate the resulting band gap of D-A type copolymers, electron-releasing alkoxy substituents were attached to electron-deficient benzothiadiazole (A) and electron-withdrawing fluorine atoms (0 ~ 4F) were substituted onto 1,4-bis(thiophen-2-yl)benzene unit (D). Intra- and/or interchain noncovalent coulombic interactions were also incorporated in the polymer backbone to promote planarity and crystalline intermolecular packing. The resulting optical band gap and the valence level were tuned to 1.93 ~ 2.15 eV and -5.37 ~ -5.67 eV, respectively, and strong interchain organization was observed by differential scanning calorimetry, high-resolution transmission electron microscopy and grazing incidence X-ray scattering measurements. The number of fluorine atoms and their position significantly influenced the photophysical, morphological and optoelectronic properties of bulk heterojunctions (BHJs) with these polymers. BHJ photovoltaic devices showed high power conversion efficiency (PCE) up to 9.8 % with an open-circuit voltage of 0.94 ~ 1.03 V. To our knowledge, this PCE is one of the highest values for fullerene-based single BHJ device with WBG polymers having a band gap over 1.90 eV. A tandem solar cell was also demonstrated successfully to show a PCE of 10.3% by combining a diketopyrrolopyrrole-based low band gap polymer.

1. Introduction

During the last several decades, organic bulk heterojunction (BHJ) polymer solar cells (PSCs) have attracted considerable attention as a portable and flexible energy source because of their light weight, mechanical flexibility and potential for low cost solution fabrication onto a large-area flexible plastic substrate.[1-4] Over the past few years, structural optimization of photovoltaic polymers (or small molecules) and device architecture, morphological control using processing additives and/or thermal (or solvent) annealing, as well as interlayer engineering, have led to power conversion efficiencies (PCE) over 10% in single and multi-junction PSCs.[5-11] The design strategy of Donor-Acceptor (D-A) type alternating copolymers using intramolecular charge transfer (ICT) interactions is an effective way to tune the band gap of photovoltaic materials in PSCs. According to the optical band gap, photovoltaic polymers can be classified into low band gap (LBG, $Eg < 1.6$ eV), mid band gap (MBG, $1.6 < Eg < 1.8$ eV) and wide band gap (WBG, $Eg > 1.8$ eV) polymers.[12-20] Because the optical absorption of a single polymer is relatively narrow with respect to the solar spectrum, tandem or ternary blend solar cells have been often tried as an alternative method to cover a broader spectral range by combination of polymers with complementary optical absorption.[21-25] It has been predicted that the ultimately achievable PCE of a tandem PSC with two absorbing layers is 15–20%.[26, 27] To achieve such a high PCE in tandem PSCs, it is essential to have both highly efficient WBG and LBG-polymers with deep highest occupied molecular orbital (HOMO) and complementary optical absorption.[26, 27] Various types of MBG and/or LBG polymers have been reported, but relatively fewer WBG polymer have been examined in BHJs.[28, 29]

Development of new WBG conjugated polymers with excellent photovoltaic properties is important for efficient tandem or ternary PSCs. In the most efficient tandem cells reported previously, poly(3-hexylthiophene-2,5-diyl) (P3HT) is a common WBG polymer. However, the open-circuit voltage (V_{OC}) of BHJs with P3HT can be limited by its high-lying HOMO level.[22] Hou *et al*. recently pushed forward the highest PCE of tandem (11.6%) and ternary (12.2%) organic solar cells by utilizing a deep HOMO, WBG polymer instead of P3HT along with complimentary LBG polymer/small molecules with broad absorption spectra; this work demonstrated the importance of using high-efficiency, deep-HOMO WBG polymers in tandem and ternary solar cells.[30] However, very few high-efficiency, deep-HOMO WBG polymers have been currently reported. To design new WBG polymers with deep HOMO level, it is necessary to finely control the ICT interaction in the D-A copolymer structures while still allowing the morphology of BHJs to provide good charge mobility and charge generation to achieve high PCE. It is quite challenging to design an ordered WBG polymer with a deep HOMO that has a planar polymeric backbone. Although increasing the torsional angle between units in the polymer main chain can increase the band gap, the interchain organization can become significantly disturbed and this can disrupt the morphology.

There have been several successful reports on the WBG photovoltaic polymers (see Fig. S1 and Table S1, ESI†). Beaujuge *et al*. and co-workers designed poly(4,8-bis((2-ethylhexyl)oxy)benzo[1,2-b:4,5-b']dithiophene-3,4-difluorothiophene) (PBDT2FT) as an alternative WBG polymer to P3HT based on 3,4-diflurothiophene motifs to extend the optical gap (2.1 eV) and achieved 7% PCE in BHJs.[31] Hou *et al*. developed a new WBG polymer, PM6 by fluorination of a donor segment in the D-A alternating structure and achieved over 9% PCE.[32] Wang *et al*. also developed an alternative copolymer, PBDTTS-

FTAZ with a band gap 1.9 eV by using fluorinated benzotriazole and alkylthio side-chains, showing a PCE over 8% PCE.[33] Jo and coworkers investigated the fluorination (on the D unit) effect in the D−A polymers and obtained ~7% PCE.[34] Recently, Sun *et al*. reported a highly efficient WBG polymer (1.9 eV band gap) with the highest PCE of 9.8% reported so far by extending π-conjugation of benzodithiophene unit of poly[dithieno[2,3-d:2′,3′-d′]benzo[1,2-b:4,5-b′]dithiophene-co-1,3-bis(thiophen-2-yl)-benzo-[1,2-c:4,5 c′]dithiophene-4,8-dione] (PDBT-T1) polymer.[35]

Inspired by the previous reports, we designed new WBG polymers based on our previous design concept using intra- and/or interchain noncovalent coulombic interactions.[31-40] In this contribution, we have designed and synthesized a series of semi-crystalline WBG D-A type conjugated copolymers with fluorine substitution of varying number and position, based on the similar backbone of the previously reported poly[(2,5-bis(2-hexyldecyloxy)phenylene)-alt-(5,6-difluoro-4,7-di(thiophen-2-yl)benzo[c][1,2,5]thiadiazole)] (PPDT2FBT).[39] The band gap was finely tuned by the ICT interaction from the weak donor-weak acceptor design motif. To decrease the electron-deficiency of difluorobenzothiadiazole (2FBT) in PPDT2FBT, the fluorine substituents were replaced with the electron-releasing dialkoxy groups. In addition, the phenylene ring was substituted with varying the number and position of fluorine atoms, which decreases the electron sufficiency of 1,4-bis(thiophen-2-yl)phenylene moiety, resulting in a decreased ICT interaction along the polymeric backbone. The optical gap was successfully adjusted to 1.93~2.15 eV and remarkable photovoltaic PCE up to 9.8% was measured with high V_{OC} of ~1 V. To the best of our knowledge, the PCE of 9.8 % is one of the highest values reported so far for fullerene-based single-junction BHJ PSCs using polymers with an

optical band gap above 1.9 eV. The crystalline blend morphology with nanofibrillar structure formation and face on orientation explains well-balanced charge carrier transport and the resulting photovoltaic characteristics. By combining a diketopyrrolopyrrole (DPP)-based LBG polymer, DT-PDPP2T-TT, a tandem cell was also fabricated, showing a great potential (10.3% PCE) of the WBG polymers as a front subcell component.

2. Results and discussion

2.1 Molecular Design, Synthesis and Characterization.

Synthetic routes to the dialkoxybenzothiadiazole (DOBT) monomer and final polymers are described in Scheme 1. DOBT is substituted with two 2-hexyldecyloxy side-chains for solution processibility where the electron-releasing alkoxy group decreases the electron-withdrawing ability of DOBT and resulting ICT interaction, modulating the band gap of resulting polymers. Additionally, the intrachain dipole-dipole interaction via $S^{\delta+}\cdots O^{\delta-}$ in the neighboring thiophene and DOBT moieties enhances the chain planarity and interchain orderings. The substitution of solubilizing alkoxy side-chains on the electron-deficient BT negligibly increases the HOMO level. As shown in Scheme 1, the DOBT monomer was prepared by two steps using 5,6-difluorobenzothiadiazole (10) as a starting material. First, 5,6-difluorobenzothiadiazole was reacted with 2-hexyldecanol in *N*,*N*-dimethylformamide (DMF) to form 5,6-bis(2-hexyldecyloxy)benzothiadiazole (11) almost quantitatively, and then the monomer M21 was obtained in ~80% yield by bromination of 11 with bromine in a mixture of dichloromethane : acetic acid (2 : 1 by volume). Five different kinds of dithienylbenzene intermediates (31~35) with different number and position of fluorine atoms were prepared by Stille coupling (yield: 50~80%) of dibromobenzene compounds

(with/without fluorines) and 2-(tributylstannyl)thiophene. The dialkoxy substituents on BT decrease the electron deficiency of BT, resulting in decreased ICT along the polymeric backbone. Similarly, the different number of fluorine substituents with different topology (*syn* or *anti*) modulates the ICT interaction along the polymer backbone and influences the interchain dipole-dipole interactions and intermolecular ordering. The weak donor-weak acceptor design strategy decreases the ICT and increases the band gap (~2 eV), compared to the parent PPDT2FBT (band gap 1.76 eV) structure. Successive stannylation with n-butyllithium and trimethyltin chloride yielded the final M41~M45 monomers in 70~80% yield. The synthetic details are described (see ESI†). The resulting WBG copolymers were synthesized via the Stille coupling of brominated monomer M21 and five corresponding tin monomers (M41~M45) using Pd2dba3/P(o-tolyl)3 as a catalytic system in a microwave reactor, yielding poly[(5,6-bis(2-hexyldecyloxy)benzo[c][1,2,5]thiadiazole-4,7-diyl)-alt-(5,5'-(1,4-phenylene)bis(thiophen-2-yl))] (PDTBTBz-0F) (yield: 78%), poly[(5,6-bis(2-hexyldecyloxy)benzo[c][1,2,5]thiadiazole-4,7-diyl)-*alt*-(5,5'-(2-fluoro-1,4-phenylene)bis(thiophen-2-yl))] (PDTBTBz-1F) (77%), poly[(5,6-bis(2-hexyldecyloxy)benzo[c][1,2,5]thiadiazole-4,7-diyl)-*alt*-(5,5'-(2,3-difluoro-1,4-phenylene)bis (thiophen-2-yl))] (PDTBTBz-2F$_{syn}$) (77%), poly[(5,6-bis(2-hexyldecyloxy)benzo[c] [1,2,5]thiadiazole-4,7-diyl)-*alt*-(5,5'-(2,5-difluoro-1,4-phenylene)bis(thiophen-2-yl))] (PDTBTBz-2F$_{anti}$) (81%) and poly[(5,6-bis(2-hexyldecyloxy)benzo[c][1,2,5]thiadiazole-4,7-diyl)-*alt*-(5,5'-(2,3,5,6-tetrafluoro-1,4-phenylene)bis(thiophen-2-yl))] (PDTBTBz-4F) (78%). All the polymers showed sufficient solubility in common organic solvents such as chloroform, chlorobenzene, and *o*-dichlorobenzene, etc.

Molecular weight and polydispersity index (PDI) of polymers were characterized by gel permeation chromatography (GPC) using *o*-dichlorobenzene as the eluent relative to polystyrene as a standard at 80 °C. Each polymerization was carried out three times and the three batches in the same condition showed similar molecular weights and PDI values. The number-average molecular weights (M_n) of this polymer series were measured to be in the range of 26~48 KDa (see Table 1). The thermal stability of the polymers was tested by thermogravimetric analysis (TGA) under a nitrogen atmosphere, showing decomposition temperatures (with 5% weight loss) of ~280 °C (see Fig. S2, ESI†). Differential scanning calorimetry (DSC) measurements show clear endothermic peaks at 243.3, 251.1, 253.0, 274.6, and 284.7 °C for PDTBTBz-0F, PDTBTBz-1F, PDTBTBz-2F$_{syn}$, PDTBTBz-2F$_{anti}$, and PDTBTBz-4F, respectively, which correspond the melting temperatures of each polymer (see Fig. S3, ESI†). The DSC data strongly support the crystalline nature of polymers, which may originate from strong interchain ordering via intra- and/or interchain noncovalent coulombic attractions (dipole-dipole and hydrogen bonding interaction). The melting point increases with increasing the number of fluorine atoms, suggesting stronger intermolecular interaction with fluorine substitution. In addition, the different symmetry in the fluorine substitution for PDTBTBz-2F$_{anti}$ (C2-symmetric) and PDTBTBz-2F$_{syn}$ (mirror-symmetric) may influence interchain organization in a solid state. According to the DSC data, PDTBTBz-2F$_{anti}$ with C2-symmetric F substitution is expected to improve the crystalline interchain ordering with a close and tight packing.[12]

2.2 Structural Analysis by Density Functional Theory and Electrochemical Properties

The minimum energy conformation, torsional energy barriers between units, and the frontier orbital structures of five polymers were calculated by density functional theory (DFT; Jaguar quantum chemistry software, B3LYP/6-31G** level of theory). For simplicity, methyl substituents (in place of hexyldecyl groups) were considered for all structures.[37] The torsional angles between the constituting building blocks along the polymeric chain based on a model with two repeats unit are summarized inTable S2, ESI†. Upon addition of fluorine atoms to a benzene ring, the torsional angles (θ_2, θ_3, θ_6 and θ_7) between thiophene and benzene moieties were clearly decreased through the dipole-dipole induced interaction such as $S^{\delta+}\cdots F^{\delta-}$ and $F^{\delta-}\cdots H^{\delta+}$, inducing a more planar polymeric backbone (see dihedral angle: 20 degree for PDTBTBz-0F and 0 degree for PDTBTBz-4F). This planarity of the chain is beneficial for achieving more ordered interchain packing and hence affects the resulting morphology in BHJ films and their photovoltaic properties. Interestingly, the PDTBTBz-$2F_{syn}$ and PDTBTBz-$2F_{anti}$ polymers show clearly different minimum energy conformations where PDTBTBz-$2F_{anti}$ shows more planar structure compared to PDTBTBz-$2F_{syn}$. In addition, the electronic structure of HOMO and lowest unoccupied molecular orbital (LUMO) frontier orbitals were similar for all polymers but their energy levels were gradually down-shifted with substituting more fluorine atoms due to their strong electron-withdrawing effect (see Table S4, ESI†).

2.3 Optical and Electrochemical Properties

The UV-vis absorption spectra of the polymers in chloroform and in thin film are shown in Fig. 1 and summarized in Table 1. The polymers show two absorption bands in which the first absorption peak below 450 nm is attributed to characteristic π-π* transition and the

low-energy absorption band in the range of 450-650 nm is attributed to the ICT interaction. With compared to the similarly structured PPDT2FBT reported previously (based on 2FBT and dialkoxy-substituted dithienylbenzene, optical band gap of 1.76 eV),[39] the newly synthesized PDTBTBz series polymers show a blue-shifted absorption due to the decreased ICT from dithienylbenzene (with or without fluorine) to DOBT.[41] The polymers show wide optical band gaps of 1.9-2.0 eV, depending on the number and topology of fluorine substitution. Except PDTBTBz-0F, all fluorine-substituted polymers show a vibrionic shoulder peak in solution, suggesting strong interchain interactions. In chloroform, the absorption maximum was observed at λ_{abs} = 508, 523, 558, 563 and 546 nm for PDTBTBz-0F, PDTBTBz-1F, PDTBTBz-2F$_{syn}$, PDTBTBz-2F$_{anti}$, and PDTBTBz-4F, respectively. With increasing the number of fluorine substitution, the λ_{abs} was measured to be red-shifted except PDTBTBz-4F. In film, the absorption spectra of PDTBTBz-0F and PDTBTBz-1F were further red-shifted with λ_{abs} = 569 and 571 nm. In contrary, PDTBTBz-2F$_{syn}$, PDTBTBz-2F$_{anti}$, and PDTBTBz-4F show similar λ_{abs}'s in solution and in film, which may be due to strong self-aggregation of these polymers even in solution with increasing fluorine substitution. It is noteworthy to mention that PDTBTBz-2F$_{anti}$ and PDTBTBz-4F shows the most pronounced vibrionic shoulder peak in films, suggesting the strongest interchain π–π stacking than other polymers.

Cyclic voltammetry (CV) was utilized to investigate the electrochemical properties and electronic energy levels of the polymers (see Fig. S5, ESI†). The HOMO energy levels of the polymers were determined from the oxidation onsets, by assuming the energy level of ferrocene (Fc) is -4.8 eV relative to the vacuum level. In the anodic scan, the onsets of oxidation for PDTBTBz-0F, PDTBTBz-1F, PDTBTBz-2F$_{syn}$, PDTBTBz-2F$_{anti}$, and

PDTBTBz-4F were measured at 0.57, 0.58, 0.62, 0.70, and 0.87 V, corresponding to the ionization potential values of -5.37, -5.38, -5.42, -5.50, and -5.67 eV, respectively. The LUMO energy levels were estimated similarly from the reduction onsets. In the cathodic scan, the onsets of reduction (versus Fc+/Fc) for PDTBTBz-0F, PDTBTBz-1F, PDTBTBz-$2F_{syn}$, PDTBTBz-$2F_{anti}$, and PDTBTBz-4F occur at -1.40, -1.35, -1.36, -1.31, and -1.28 V, corresponding to the LUMO level of -3.40, -3.45, -3.44, -3.49, and -3.52 eV, respectively. The results are summarized in Table 1 and the energy band diagram is sketched in Fig. 1d. It indicates that both HOMO and LUMO of polymers become deeper with increasing F substituents onto the polymer backbone, being consistent with the DFT calculation. A comparison of PDTBTBz-$2F_{syn}$ and PDTBTBz-$2F_{anti}$ reveals that the substitution of two F atoms at *anti* positions leads to a deeper HOMO energy level than that for the *syn* isomer. The HOMO energy levels of PDTBTBz polymers are clearly down-shifted (up to -5.67 eV) and the LUMO levels are up-shifted (up to -3.40 eV) based on the weaker donor and acceptor pairs, resulting in wider band gap, compared to PPDT2FBT (HOMO: -5.45 eV, LUMO: -3.69 eV).[39]

2.4. Photovoltaic Characteristics

To investigate the photovoltaic properties of PDTBTBz-based polymers, the PSC devices using a BHJ blend of PDTBTBz-based polymers as the electron donor and [6,6]-phenyl-C_{71} butyric acid methyl ester ($PC_{71}BM$) as the acceptor were fabricated in a conventional device structure of indium-tin-oxide (ITO)/poly(3,4-ethylenedioxythiophene):polystyrene sulfonate (PEDOT:PSS) /polymers:$PC_{71}BM$/Ca/Al (see Fig. 1c). First, the device fabrication was optimized at a polymer:$PC_{71}BM$ blend ratio of 1:1.5 (by weight) using

chlorobenzene as a main solvent without any processing additives. The photovoltaic characteristics were tested under illumination condition of AM 1.5G (100 mW cm^{-2}). Fig. S6a† and S6b† show optimal current density and voltage (*J*-*V*) curves and external quantum efficiency (EQE) spectra, respectively. As summarized in Table S4†, the device with PDTBTBz-2F_{anti} showed the highest PCE of 5.4 % with J_{SC} of 10.6 mA cm^{-2}, V_{OC} of 0.93, and fill factor (FF) of 0.55. The use of processing additives can modify the BHJ morphology, resulting in improvement of device properties in many cases.[42, 43] We therefore further tested devices with diphenyl ether (DPE) as a processing additive.[39, 44] The devices processed with the solvent mixture of CB and DPE (97:3 vol. %) led to a remarkable increase in all device parameters compared to devices without DPE as shown in Fig. 2 and Fig. S6†. In addition, we investigated the use of other processing additives such as 1,8-diiodooctane and 1-chloronaphthalene with PDTBTBz-2F_{anti}:$PC_{71}BM$ blends (morphologies are reported in Fig. S7). These results confirmed that DPE was the most effective processing additive. PDTBTBz-2F_{anti}:$PC_{71}BM$ blends processed with DPE exhibited the best performance among all of our WBG polymer blends as shown in Fig. S8† and Table S5†. In particular, PCEs of the devices with incorporation of DPE significantly increased from 2.2, 2.6, 5.2, 5.4, and 2.5% to 7.3, 7.5, 8.1, 9.8, and 4.1% for PDTBTBz-0F, -1F, -2F_{syn}, -2F_{anti} and -4F based PSCs, respectively. The detailed device parameters are listed in Table 2. Remarkably high values of the V_{OC} (over 0.9 V) and good values of the FF (0.6~0.7) were obtained for all devices. The optimized thicknesses of active layers with DPE additive were determined to be 160 nm (PDTBTBz-0F), 145 nm (PDTBTBz-1F), 150 nm (PDTBTBz-2F_{syn}), 190 nm (PDTBTBz-2F_{anti}) and 150 nm (PDTBTBz-4F).

Among five PDTBTBz-based PSC devices processed with CB:DPE, device using PDTBTBz-2F$_{anti}$:PC$_{71}$BM blend showed the best PCE of 9.8 % with J_{SC} of 14.0 mA cm^{-2}, V_{OC} of 0.97 V and FF of 0.72. The J_{SC} (14.0 mA cm^{-2}) measured from device with PDTBTBz-2F$_{anti}$:PC$_{71}$BM blend is well matched with the calculated J_{SC} (13.8 mA cm^{-2}) from EQE as shown in Fig. 2b and Table 2. To the best of our knowledge, the PCE of 9.8 % is one of the highest values yet reported for fullerene-based single BHJ PSCs using polymers with band gaps over 1.90 eV. Interestingly, difluorinated PDTBTBz-2F$_{anti}$ and PDTBTBz-2F$_{syn}$ showed higher photovoltaic performance, compared with PDTBTBz-0F, -1F and 4F. Furthermore, the *anti*-substitution of two F atoms turned out to be more beneficial for improving the photovoltaic properties. Compared to PPDT2FBT, PDTBTBz-2F$_{anti}$ shows the lower J_{SC} (16.3 →14.0 mA cm^{-2}) due to narrower absorption range but higher V_{OC} (0.79 → 0.97 V) with deeper HOMO. Both polymers show similarly high *FF*, showing well distributed nano-fibrillar, semi-crystalline BHJ film morphology.[39]

2.5. Characterization of Film Morphology

Fig. 3 shows AFM topography images of polymer:PC$_{71}$BM blend films prepared from CB and CB:DPE solvents. The BHJ film of PDTBTBz-0F prepared from CB solvent shows very smooth surface with root-mean-square (rms) roughness of 0.58. With increasing F substitution, the surface roughens with rms values increasing 1.04, 1.55, 1.83 and 2.43 nm for DTBTBz-1F, -2F$_{syn}$, -2F$_{anti}$ and 4F blend films respectively. This roughness may be related to the strong interchain interaction and self-agglomeration. In contrast, the optimal BHJ films prepared from a CB:DPE solvent mixture show significantly different nanoscale

morphologies. Among the blend films, the PDTBTBz-2F$_{anti}$:PC$_{71}$BM blend are the smoothest (rms roughness of 1.58 nm) and finely dispersed surface topology (see Fig. 3i).

To further study the BHJ film morphology of PDTBTBz-2F$_{syn}$ and PDTBTBz-2F$_{anti}$ blend films, HR-TEM images were also measured as shown in Fig. 4. Both PDTBTBz-2F$_{syn}$ and PDTBTBz-2F$_{anti}$ blend films show fibril-like structures and more finely distributed and clear fibrillar structures were observed with addition of DPE (Fig. 4c and 4d). A similar blend morphology of PPDT2FBT was reported previously,[39] which is closely related to the semi-crystalline nature of polymer *via* intra- and/or interchain noncovalent coulombic interactions. The nanofibrillar crystalline morphology can allow efficient charge transport, increasing the J_{SC} and FF values of PSCs.[36, 45] The TEM image of PDTBTBz-2F$_{anti}$ blend film (processed with DPE) showed the more developed fibrillary structures compared to the PDTBTBz-2F$_{syn}$ blend, leading to better device performance of PDTBTBz-2F$_{anti}$:PC$_{71}$BM. The morphology of PDTBTBz-2F$_{anti}$ blend film, obtained from AFM and HR-TEM measurements helps to provide the high photovoltaic efficiency compared to all polymers examined.

To further investigate the detailed film morphologies of five PDTBTBz-based polymers, the molecular orientation and packing characteristics were studied by 2D-GIWAXS.[46-48] Fig. 5 and Fig. S9† show 2D-GIWAXS images and in-plane and out-of-plane line-cut profiles of pristine polymers, polymer:PC$_{71}$BM blended films with and without DPE. The extracted 2D-GIWAXS scattering features are summarized in Table S6†. With regard to pristine films, the scattering from PDTBTBz-0F is characteristic of a glassy film, but increasing order is observed for polymers with F substituents. PDTBTBz-2F$_{anti}$ shows well-resolved lamellar scattering up to (300) in the out-of-plane direction with π-π stacking (010)

peaks in both in-plane and out-of-plane directions. The lamellar *d*-spacing for PDTBTBz-1F, -2F$_{syn}$, -2F$_{anti,}$ and -4F neat films were measured to be ~18 to 21 Å. The π-π stacking distances were ~3.7Å for all samples.

In the case of BHJs of the polymers with PC$_{71}$BM, there were no large changes in the packing structure of the polymer, but there were changes in texture of the crystallites. The π-π stacking (010) peak appears mainly in the out-of-plane direction, suggesting preferential face-on orientation in the blends (see PDTBTBz-2F$_{syn}$, PDTBTBz-2F$_{anti}$ and PDTBTBz-4F blend films). The polymer phase in PDTBTBz-0F: PC$_{71}$BM and PDTBTBz-1F: PC$_{71}$BM BHJs is disordered, and no clear alkyl or π-π stacking (010) peak are assignable. Aggregates of PC$_{71}$BM are observed in all BHJs by a characteristic glassy peak around 1.33~1.37Å^{-1} similar to observations for BHJs of PCPDTBT/PC$_{71}$BM and other systems.[49, 50] Upon addition of a processing additive, DPE, similar scattering patterns with qualitatively stronger scattering were observed. PDTBTBz-2F$_{anti}$:PC$_{71}$BM and PDTBTBz-2F$_{syn}$:PC$_{71}$BM blends show the most pronounced lamellar and π-π stacking scatterings. Interestingly, the PDTBTBz-4F:PC$_{71}$BM also showed a strong and similar 2D-GIWAXS pattern to the difluoro-polymers, but the lowest photovoltaic performance was observed.

The phase separated domain structure is closely correlated with charge separation and extraction in BHJ polymer:fullerene solar cell systems.[47, 51, 52] In-plane periodicities for five PDTBTBz-based BHJ blend thin films were probed using resonant soft X-ray scattering (RSoXS).[47, 51, 52] The five blend samples were prepared using the same film fabrication conditions used to prepare optimized solar cell devices. RSoXS data were obtained at a photon energy of 286.4 eV, which exhibited high scattering contrast. Fig. S10† shows Lorentz corrected RSoXS profiles as a function of scattering vector q. A single dominant peak located in the range of q = 0.010-0.017 Å^{-1} was

observed for all five samples, corresponding to length scales of approximately 43, 51, 44, 38, and 60 nm for PDTBTBz-0F, PDTBTBz-1F, PDTBTBz-2F$_{syn}$, PDTBTBz-2F$_{anti}$ and PDTBTBz-4F containing BHJ blend films, respectively. This length scale likely corresponds to an average domain separation distance. The PDTBTBz-2F$_{anti}$:PC$_{71}$BM blend exhibits the smallest domain separation and the highest PCE in solar cell devices, suggesting that this BHJ blend may form a phase separated morphology with more favorable length scales for charge separation and transport relative to the other BHJ blends. With compared to PDTBTBz-2F polymers, PDTBTBz-4F has the most rigid structure with 4 fluorine atoms in the polymeric backbone and shows the strongest tendency of interchain aggregation with relatively poor solubility. As shown in Fig. S10, the PDTBTBz-4F:PC$_{71}$BM blend exhibits a larger average domain size. The quick and excessive segregation of PDTBTBz-4F may decrease the domain purity (Fig. S10†) in the blend with PC$_{71}$BM, resulting in poorer photovoltaic performance.

2.6. Charge Carrier Transport and Recombination

To study the charge transport and recombination behaviors in the PDTBTBz-based PSCs, the light intensity dependence of J_{SC} was measured under short-circuit condition.[53-55] Fig. 2c exhibits logarithmic plots of J_{SC}s as a function of the light intensity, showing the power-law dependence of $J_{SC} \propto P_{\alpha}$ (where P is the incident-light intensity and α is an exponential constant, generally 0.85-1 in PSCs).[55] The α values were determined to be 0.90, 0.91, 0.94, 0.94 and 0.92 for the PDTBTBz-0F, -1F, -2F$_{anti}$, -2F$_{syn}$ and -4F BHJ devices with PC$_{71}$BM (with DPE), respectively. The devices of PDTBTBz-2F$_{syn}$ and -2F$_{anti}$ showed relatively higher value ($\alpha = 0.94$) compared to other devices. The higher α value for the PDTBTBz-2F$_{anti}$ and -2F$_{syn}$ devices suggests a weaker bimolecular recombination during charge

transport process,[55] showing a good agreement with the measured photovoltaic characteristics for both devices (see Table 2).

The charge carrier transport in both horizontal and vertical directions, was investigated by fabrication of polymer field-effect transistor (PFET) and the SCLC method. The details for PFET fabrication are described in the Experimental section (channel length L = 20 μm, channel width W =1000 μm). Transfer and output characteristics of the PFETs of five PDTBTBz-based polymers are shown in Fig. S11† and Fig. S12†, respectively. As summarized in Table S7†, the hole mobilities were determined to be 2.4×10^{-2}, 4.1×10^{-2}, 5.2×10^{-2}, 5.6×10^{-2} and 9.0×10^{-3} cm^2 V^{-1} s^{-1}, for the PDTBTBz-0F, -1F, -2F_{syn}, -2F_{anti} and -4F pristine polymer films, respectively. PDTBTBz-2F_{anti} and -2F_{syn} show the highest hole mobility. To obtain the vertical mobility, hole-only (ITO/PEDOT:PSS/polymers:$PC_{71}BM$/Au) and electron-only (FTO/polymer:$PC_{71}BM$/Al, FTO: fluorine-doped tin oxide) devices were prepared under the same fabrication condition for the optimized PSC devices. Fig. S13† and Table S8† show the *J*-*V* characteristics and extracted mobility values of hole- and electron-only devices, respectively. The vertical hole and electron mobilities were calculated based on the Mott-Gurney equation of $J_{SCL} = 9\varepsilon_0\varepsilon_r\mu V^2/(8L^3)$ (where ε_0 is free-space permittivity, ε_r is dielectric constant of the semiconductor, μ is mobility, *V* is the applied voltage and *L* is the thickness of the active layer).[56, 57] The hole (μ_h) (and electron (μ_e)) mobility values obtained from the SCLC method are 1.0×10^{-3} (7.5×10^{-4}), 1.07×10^{-3} (8.3×10^{-4}), 1.0×10^{-3} (9.0×10^{-4}), 1.15×10^{-3} (1.1×10^{-3}) and 1.15×10^{-4} (7.3×10^{-4}) cm^2 V^{-1} s^{-1}, for the BHJ devices of PDTBTBz-0F, -1F, -2F_{syn}, -2F_{anti} and -4F, respectively (see Table S8†). All the devices showed the efficient vertical transport of charge carriers, showing mobility of ~10^{-3} cm^2 V^{-}

[1] s^{-1}. The μ_h / μ_e ratio was also calculated to be 1.33 (PDTBTBz-0F), 1.29 (PDTBTBz-1F), 1.11 (PDTBTBz-2F_{syn}), 1.05 (PDTBTBz-2F_{anti}) and 0.16 (PDTBTBz-4F). The PDTBTBz-2F_{anti}:$PC_{71}BM$ and PDTBTBz-2F_{syn}:$PC_{71}BM$ blends with DPE show the most balanced μ_h / μ_e ratio of 1.05~1.11, suggesting the efficient charge transport and extraction with little electron-hole recombination in the PSC device. On the contrary, the poor photovoltaic properties of device using PDTBTBz-4F:$PC_{71}BM$ may be mainly due to an unbalanced charge carrier transport, build-up of space charges and the resulting electron-hole recombination.

2.7. Tandem Solar Cells

Based on the outstanding photovoltaic performance of a single junction PSC of PDTBTBz-2F_{anti}, we also fabricated a tandem PSC by combining the WBG polymer PDTBTBz-2F_{anti} (Eg > 1.9 eV) with a DPP-based LBG polymer, DT-PDPP2T-TT (Eg ~1.4 eV)[58] These two polymers have complementary absorption spectra such that the WBG front cell absorbs high energy photons and produces a large V_{OC}, while allowing low energy red and infrared photons to pass through to the LBG back cell which produces additional current at a lower V_{OC}. Brabec and coworkers suggested that an optimal combination of bandgaps of 1.3 eV and 1.6 eV would maximize the tandem device efficiency, however, this study did not completely account for the effects of overlapping absorption spectra.[26, 27] The tandem PSC was fabricated using a conventional device structure where the PDTBTBz-2F_{anti}:$PC_{71}BM$ and DT-PDPP2T-TT:$PC_{71}BM$ blend layers were incorporated as a front and back cell, respectively (Fig. 6a). DT-PDPP2T-TT LBG polymer was synthesized following the same synthetic method and the device was fabricated using the same condition as reported in the previous literature.[44,

[58] As shown in Fig. 6c, the PDTBTBz-2F$_{anti}$:PC$_{71}$BM and DT-PDPP2T-TT:PC$_{71}$BM blends show complementary absorption, covering a broad range of solar spectrum of UV-vis and near infrared regions up to 900 nm in a tandem device. The front (PDTBTBz-2F$_{anti}$:PC$_{71}$BM) and back subcell (DT-PDPP2T-TT:PC$_{71}$BM) showed the PCEs of 9.0 % and 8.0 %, respectively (see Fig. 6d and Table S9). By combining both front and back cells, the tandem PSC achieved the PCE of 10.3 % along with J_{SC} = 9.89 mA cm^{-2}, V_{OC} = 1.58 V, and FF = 0.66. We confirmed the great potential of tandem devices using the WBG PDTBTBz polymer and the device optimization is now under investigation by combining various LBG polymers, recombination layer and modulating thickness of each subcell. The detailed results on the tandem devices will be reported separately.

2.8. Inverted Devices and Device Stability

We prepared and characterized inverted devices (Fig. S14) using the architecture of ITO/ZnO/active layer/MoO_3/Au. These devices exhibited slightly reduced photovoltaic performance relative to that of conventional devices, showing a J_{SC} of 11.3 mAcm^{-2}, V_{OC} of 0.97 V, FF of 0.66 and PCE of 7.3%. We investigated the air stability of inverted devices and conventional devices (conventional devices with Al or Ca/Al electrodes without sealing and Ca/A1 with UV epoxy sealant; inverted structure devices using MoO_3/Au electrode without sealing). As shown in Fig. S15, the performance degradation of devices with Al and Ca/Al electrodes without encapsulation is similar within 100 h of air exposure. In contrast, the devices with MoO_3/Au without sealing and Ca/Al with UV epoxy sealing show much better long-term stability. The Ca/Al cathode is not stable and is unsuitable for commercialization of PSCs. However, we observed that conventional devices using Ca/Al

with proper encapsulation showed similar or better stability compared to inverted devices without encapsulation. These data indicate that our WBG polymers exhibit comparably good stability in the inverted geometry or in the conventional structure with proper encapsulation.

3. Conclusion

In summary, new series of semi-crystalline photovoltaic polymers with wide band gap over 1.90 eV were designed and synthesized based on weak donor-weak acceptor motif by varying number and position of fluorine substituents. In a design of a polymeric main chain, noncovalent coulombic interactions (such as H bonding and dipole-dipole interactions) were considered to enhance the chain planarity and interchain ordering. By attaching the solubilizing alkoxy side chains onto the electron-deficient benzothiadiazole, the intramolecular charge transfer was modulated to decrease with maintaining a deep conduction band. Five different polymers showed an optical band gap in the range of 1.93 ~ 2.15 eV and the HOMO level decreased gradually with increasing the number of fluorine substituents (-5.37 ~ -5.67 eV). In particular, PDTBTBz-2F$_{anti}$ showed a crystalline nanofibrillar morphology with strong face on π-π stacking in the blend film with PC$_{71}$BM. The best PCE of 9.8% was obtained with PDTBTBz-2F$_{anti}$ with remarkably high a V_{OC} of 0.97 V, J_{SC} of 13.95 mA cm^{-2} and FF of 0.72. The high horizontal mobility of 5.6 × 10^{-2} cm^2 V^{-1} s^{-1} was measured by PFET fabrication and well balanced hole and electron mobilities (μ_h/μ_e = 1.15 × 10^{-3}/1.1 × 10^{-3} cm^2 V^{-1} s^{-1}) in a vertical direction were also measured by SCLC method. In addition, PDTBTBz-2F$_{anti}$ showed a great potential as a front subcell, showing the PCE of 10.3 % in a tandem PSC device.

4. Experimental

4.1. General

^{1}H, ^{13}C and ^{19}F nuclear magnetic resonance (NMR) spectroscopy spectra were recorded on Bruker DRX-300 FT-NMR, Bruker Avance-400 MHz, and Bruker Avance-500 MHz spectrometer at 25 °C. Me_4Si and the residual solvent peak impurity are used as reference of 1H and 13C NMR spectra. Chemical shifts are reported in ppm and coupling constants in Hz as absolute values. UV-Visible spectroscopies were recorded using wither a Shimadzu UV-2550 spectrophotometer at room temperature. All solution UV-vis experiments were carried out in $CHCl_3$. Films were prepared by spin-coating $CHCl_3$ solutions onto quartz substrates. Full scan, low resolution mass spectrometry was carried out at the analytical center, Korea Research Institute of Chemical Technology. DSC was determined using a TA Instruments DSC (Model Q-1000) with about 5 mg samples at a rate of 10 °C / min in the temperature range of 0 to 300 °C, unless otherwise stated. TGA was carried out at the Analytical Center, Korea Research Institute of Chemical Technology. Samples were run under N_2 and heated from room temperature to 600 °C at a rate of 10 °C min^{-1}. All electrochemical measurements were performed using IVIUMSTAT instrument model PV-08 in a standard three-electrode, one compartment configuration equipped with $Ag/AgNO_3$ electrode, Pt wire and Pt electrode (dia. 1.6 mm), as the pseudo reference, counter electrode and working electrode respectively. Pt working electrodes were polished with alumina. The measurements were carried out in anhydrous acetonitrile with tetrabutyl ammonium hexafluorophosphate (0.1 M) as the supporting electrolyte under an argon atmosphere at a scan rate of 20 mV s^{-1}. Polymer films were prepared by drop casting onto

the Pt working electrode from chloroform solution and dried before measurements. The electrochemical onsets were determined at the position where the current starts to differ from the baseline. The potential of the $Ag/AgNO_3$ reference electrode was internally calibrated by using the ferrocene/ferrocenium redox couple (Fc / Fc+), which has a known reduction potential of −4.8 eV. The HOMO of copolymers were calculated from the onset oxidation potentials ($E_{oxonset}$) according to: HOMO= $-(E_{oxonset} + 4.8)$ (eV). The LUMO of copolymers were calculated from the onset reduction potentials ($E_{redonset}$) according to: LOMO= $-(E_{redonset} + 4.8)$ (eV).

4.2. Film characterization

AFM images were collected using a Veeco Multimode microscope with 300 kHz silicon tips operating in tapping mode. HR-TEM images were obtained using a JEOL JEM-2100 TEM operated at 200 kV. 2D-GIWAXS experiments were performed at the Advanced Light Source (ALS) at beamline 7.3.3. The incident beam energy is 10keV, and the incident angle used was 0.12-0.14˚. The sample-to-detector distance was 30cm, and a Pilatus 2M area detector was used for 2D diffraction pattern collection. Samples were kept under Helium environment during X-ray scattering was to minimize background scattering and beam damage. Exposure times were 5 to 60 seconds. Samples for 2D-GIWAXS measurements were prepared by spin-coating pristine polymer and polymers:$PC_{71}BM$ blend solutions on top of PEDOT:PSS/Si substrates.

Resonant Soft X-ray Scattering (RSoXS) was performed at beamline 11.0.1.2 at the Advanced Light Source. Thin film samples were prepared on 100 nm thick 1.5 mm x 1.5 mm silicon nitride membranes supported by a 5 mm x 5 mm silicon frame (Norcada Inc.). Scattering was collected in a transmission geometry with a 150 mm sample-detector

distance. Data was collected on an in-vacuum CCD camera (Princeton Instrument PI-MTE) thermoelectrically cooled to -45 °C. Images were taken near the carbon K edge, in the range of 280-300 eV. 2D data waere reduced by azimuthally averaging over all q values.

4.3. Fabrication and characterization of PSCs

Photovoltaic devices were fabricated according to the following procedures. First, the glass/ITO substrates were cleaned with detergent, then ultra-sonicated in acetone and isopropyl alcohol and subsequently dried in an oven overnight at 100 °C. PEDOT:PSS hole transport layers were spin-coated (after passing through a 0.45 μm cellulose acetate syringe filter) at 5000 rpm for 40s followed by baking at 150 °C for 30 min in air and then moved into a glove box. For the single-junction active layer, blend solutions of PDTBTBz-based polymers (1.0 wt%):$PC_{71}BM$ (1.5 wt%) dissolved in CB (with 1.5~3 vol% DPE) were spin-coated (1500 to 3000 rpm for optimization) on top of the PEDOT:PSS layer in a nitrogen-filled glove box. The device was pumped down in vacuum (< 10^{-6} torr), and the Ca/Al (20 nm/100 nm thick) electrode for conventional architecture was deposited on top of the active layer by thermal evaporation. The deposited Ca/Al electrode area defined the active area as 13 mm^2. Photovoltaic characteristics measurements were carried out inside the glove box using a high quality optical fiber to guide the light from the solar simulator equipped with a Keithley 2635A source measurement unit. J-V curves were measured under AM 1.5G illumination at 100 mW cm^{-2} using an aperture to define the illuminated area. EQE measurements were conducted in ambient air using an EQE system (Model QEX7) by PV measurements Inc. (Boulder, Colorado). The monochromatic light intensity was calibrated using a Si photodiode and chopped at 100 Hz. A Mask (1.70 mm^2) made of thin black plastic was attached to each cell for measurement of the *J-V* characteristics and the EQE spectra. All devices were tested in ambient air after UV-epoxy encapsulation.

4.4. Fabrication of Tandem-junction PSC

The device structure of the tandem cell is shown in Fig. 6a. The PDTBTBz-2F_{anti}(1.0 wt%):$PC_{71}BM$ (1.5 wt%) dissolved in CB (with 3 vol% DPE) was spin-cast on top of PEDOT:PSS layer at a spin rate of 2500 ~ 3000 rpm as an active layer in a front cell. The ZnO nanoparticles solution was prepared following the previous literature[59] and spin-coated at 3000 rpm on top of the front cell. The neutral PEDOT:PSS solution was also prepared as by mixing isopropyl alcohol (IPA) and deionized water (DI water) with a mixing ratio of neutral PEDOT:PSS (1.0): IPA(0.8): DI water (1.4) as volume fraction, and then spin-coated on top of ZnO layer at 4000 rpm for 40 s . The DT-PDPP2T-TT:$PC_{71}BM$ active layer was fabricated under the same condition reported in the previous literature.[44] Finally, the device fabrication was completed by deposition of 100 nm thick Al as cathode.

4.5. Fabrication and characterization of PFETs

The PFETs were fabricated onto n^{++}Si (500 μm)/SiO2 (300 nm) substrates (International Wafer Services Co.). The Ni (5 nm)/Au (50 nm) source and drain electrodes were patterned on the dielectrics by electron beam evaporation at 7×10^{-7} Torr. After ultraviolet/ozone treatment of pre-cleaned SiO_2 substrates for 10 min, the substrates were passivated with the n-decyltrichlorosilane (Gelest Inc.) in toluene solution (1% by volume) at 80°C for 20 min in air. The semiconductor solutions were then spin cast from a chloroform solution (5 mg mL^{-1}) at 1200 rpm for 40 s in a nitrogen-filled glove box. The devices were then cured at 200°C for 5 min prior to measurements, and were tested using a probe station (Signatone Co.) in a nitrogen-filled glove box. Data were collected by a Keithley 4200 system.

Acknowledgements

We thank Prof. Alan J. Heeger for guidance. This work was supported by the NASA Small Buisiness Technology Transfer (STTR) UCSB (07012013-01) and National Research Foundation (NRF) of Korea (2015R1D1A1A09056905, 2015M1A2A2057506, 2015M1A2A2056214). E.L. acknowledges support from the National Science Foundation Graduate Research Fellowship (DGE-1144085). Portions of the research were carried out at the Advanced Light Source, supported by the Director, Office of Science, Office of Basic Energy Sciences, of the U.S. Department of Energy under Contract No. DE-AC02-05CH11231.

Author contributions

S.-J.K. and Q.V.H. contributed equally to this work. S.-J.K. proposed the research, conducted most of the characterizations, fabricated solar cells and also contributed to data analysis and preparation of manuscript. Q.V.H and C.E.S. synthesized and five kinds of WBG polymers and conducted characterization related to synthesis. M.A.U. contributed to data analysis, participated to the discussion and manuscript preparation with S.-J.K. S.Y.P. performed HR-TEM and B.H.L fabricated PFET. S.S. measured AFM. S.-J.M. designed WBG polymers. S.H. conducted DFT calculation. E.L. and M.L.C. measured and analysed 2D-GIWAXS and also fully revised manuscript. G.M.S. measured and analysed RSoXS. P.-O.M and M.L. prepared LBG polymer for tandem device fabrication. W.S.S. supervised synthesis of five kinds of WBG polymers. H.Y.W. and J.Y.K. supervised the whole project. All authors discussed the results and commented on the manuscript.

References

1. N. Sariciftci, L. Smilowitz, A. J. Heeger and F. Wudl, *Science*, 1992, **258**, 1474-1476.
2. G. Yu, J. Gao, J. C. Hummelen, F. Wudl and A. J. Heeger, *Science*, 1995, **270**, 1789-1791.
3. B. C. Thompson and J. M. J. Fréchet, *Angew. Chem. Int. Ed.*, 2008, **47**, 58-77.
4. M. C. Scharber and N. S. Sariciftci, *Prog. Polym. Sci.*, 2013, **38**, 1929-1940.
5. Y. Liu, J. Zhao, Z. Li, C. Mu, W. Ma, H. Hu, K. Jiang, H. Lin, H. Ade and H. Yan, *Nat. Commun.*, 2014, **5**, DOI:10.1038/ncomms6293.
6. J.-D. Chen, C. Cui, Y.-Q. Li, L. Zhou, Q.-D. Ou, C. Li, Y. Li and J.-X. Tang, *Adv. Mater.*, 2015, **27**, 1035-1041.
7. C. Liu, C. Yi, K. Wang, Y. Yang, R. S. Bhatta, M. Tsige, S. Xiao and X. Gong, *ACS Appl. Mater. Interfaces*, 2015, **7**, 4928-4935.
8. X. Ouyang, R. Peng, L. Ai, X. Zhang and Z. Ge, *Nat. Photon.*, 2015, **9**, 520-524.
9. S. Zhang, L. Ye and J. Hou, *Adv. Energy Mater.*, 2016, **6**, 1502529.
10. J. Zhao, Y. Li, G. Yang, K. Jiang, H. Lin, H. Ade, W. Ma and H. Yan, *Nat. Energy*, 2016, **1**, 15027.
11. H. Hu, K. Jiang, G. Yang, J. Liu, Z. Li, H. Lin, Y. Liu, J. Zhao, J. Zhang, F. Huang, Y. Qu, W. Ma and H. Yan, *J. Am. Chem. Soc.*, 2015, **137**, 14149-14157.
12. Z. Li, K. Jiang, G. Yang, J. Y. L. Lai, T. Ma, J. Zhao, W. Ma and H. Yan, *Nat. Commun.*, 2016, **7**, 13094.
13. Y.-J. Cheng, S.-H. Yang and C.-S. Hsu, *Chem. Rev.*, 2009, **109**, 5868-5923.
14. P. M. Beaujuge and J. M. J. Fréchet, *J. Am. Chem. Soc.*, 2011, **133**, 20009-20029.
15. G. Li, R. Zhu and Y. Yang, *Nat. Photon.*, 2012, **6**, 153-161.
16. Y. Li, *Acc. Chem. Res.*, 2012, **45**, 723-733.
17. H. Zhou, L. Yang and W. You, *Macromolecules*, 2012, **45**, 607-632.
18. X. Guo, M. Baumgarten and K. Müllen, *Prog. Polym. Sci.*, 2013, **38**, 1832-1908.
19. J. You, L. Dou, Z. Hong, G. Li and Y. Yang, *Prog. Polym. Sci.*, 2013, **38**, 1909-1928.
20. K. Müllen and W. Pisula, *J. Am. Chem. Soc.*, 2015, **137**, 9503-9505.
21. J. Y. Kim, K. Lee, N. E. Coates, D. Moses, T.-Q. Nguyen, M. Dante and A. J. Heeger, *Science*, 2007, **317**, 222-225.
22. J. You, L. Dou, K. Yoshimura, T. Kato, K. Ohya, T. Moriarty, K. Emery, C.-C. Chen, J. Gao, G. Li and Y. Yang, *Nat. Commun.*, 2013, **4**, 1446.
23. J. Zhang, Y. Zhang, J. Fang, K. Lu, Z. Wang, W. Ma and Z. Wei, *J. Am. Chem. Soc.*, 2015, **137**, 8176-8183.
24. Q. An, F. Zhang, J. Zhang, W. Tang, Z. Deng and B. Hu, *Energy Environ. Sci.*, 2016, **9**, 281-322.
25. Z. Zheng, S. Zhang, J. Zhang, Y. Qin, W. Li, R. Yu, Z. Wei and J. Hou, *Adv. Mater.*, 2016, **28**, 5133-5138.
26. G. Dennler, M. C. Scharber, T. Ameri, P. Denk, K. Forberich, C. Waldauf and C. J. Brabec, *Adv. Mater.*, 2008, **20**, 579-583.
27. N. Li, D. Baran, G. D. Spyropoulos, H. Zhang, S. Berny, M. Turbiez, T. Ameri, F. C. Krebs and C. J. Brabec, *Adv. Energy Mater.*, 2014, **4**, 1400084.
28. J. W. Jung, J. W. Jo, E. H. Jung and W. H. Jo, *Org. Electron.*, 2016, **31**, 149-170.

29. G. Li, X. Gong, J. Zhang, Y. Liu, S. Feng, C. Li and Z. Bo, *ACS Appl. Mater. Interfaces*, 2016, **8**, 3686-3692.
30. W. Zhao, S. Li, S. Zhang, X. Liu and J. Hou, *Adv. Mater.*, 2016, DOI: 10.1002/adma.201604059, n/a-n/a.
31. J. Wolf, F. Cruciani, A. El Labban and P. M. Beaujuge, *Chem. Mater.*, 2015, **27**, 4184-4187.
32. M. Zhang, X. Guo, W. Ma, H. Ade and J. Hou, *Adv. Mater.*, 2015, **27**, 4655-4660.
33. Z. Genene, J. Wang, X. Meng, W. Ma, X. Xu, R. Yang, W. Mammo and E. Wang, *Adv. Electron. Mater.*, 2016, **2**, 1600084.
34. J. W. Jo, S. Bae, F. Liu, T. P. Russell and W. H. Jo, *Adv. Funct. Mater.*, 2015, **25**, 120-125.
35. L. Huo, T. Liu, X. Sun, Y. Cai, A. J. Heeger and Y. Sun, *Adv. Mater.*, 2015, **27**, 2938-2944.
36. H.-Y. Chen, J. Hou, S. Zhang, Y. Liang, G. Yang, Y. Yang, L. Yu, Y. Wu and G. Li, *Nat. Photon.*, 2009, **3**, 649-653.
37. H. Zhou, L. Yang, A. C. Stuart, S. C. Price, S. Liu and W. You, *Angew. Chem. Int. Ed.*, 2011, **50**, 2995-2998.
38. S. Albrecht, S. Janietz, W. Schindler, J. Frisch, J. Kurpiers, J. Kniepert, S. Inal, P. Pingel, K. Fostiropoulos, N. Koch and D. Neher, *J. Am. Chem. Soc.*, 2012, **134**, 14932-14944.
39. T. L. Nguyen, H. Choi, S. J. Ko, M. A. Uddin, B. Walker, S. Yum, J. E. Jeong, M. H. Yun, T. J. Shin, S. Hwang, J. Y. Kim and H. Y. Woo, *Energy Environ. Sci.*, 2014, **7**, 3040-3051.
40. F. Meyer, *Prog. Polym. Sci.*, 2015, **47**, 70-91.
41. Q. T. Zhang and J. M. Tour, *J. Am. Chem. Soc.*, 1998, **120**, 5355-5362.
42. J. Peet, N. S. Cho, S. K. Lee and G. C. Bazan, *Macromolecules*, 2008, **41**, 8655-8659.
43. C. Piliego, T. W. Holcombe, J. D. Douglas, C. H. Woo, P. M. Beaujuge and J. M. J. Fréchet, *J. Am. Chem. Soc.*, 2010, **132**, 7595-7597.
44. H. Choi, S.-J. Ko, T. Kim, P.-O. Morin, B. Walker, B. H. Lee, M. Leclerc, J. Y. Kim and A. J. Heeger, *Adv. Mater.*, 2015, **27**, 3318-3324.
45. X. Yang, J. Loos, S. C. Veenstra, W. J. H. Verhees, M. M. Wienk, J. M. Kroon, M. A. J. Michels and R. A. J. Janssen, *Nano Lett.*, 2005, **5**, 579-583.
46. W. Chen, M. P. Nikiforov and S. B. Darling, *Energy Environ. Sci.*, 2012, **5**, 8045-8074.
47. L. Ye, S. Zhang, W. Ma, B. Fan, X. Guo, Y. Huang, H. Ade and J. Hou, *Adv. Mater.*, 2012, **24**, 6335-6341.
48. H. Zhou, Y. Zhang, J. Seifter, S. D. Collins, C. Luo, G. C. Bazan, T.-Q. Nguyen and A. J. Heeger, *Adv. Mater.*, 2013, **25**, 1646-1652.
49. M. R. Hammond, R. J. Kline, A. A. Herzing, L. J. Richter, D. S. Germack, H.-W. Ro, C. L. Soles, D. A. Fischer, T. Xu, L. Yu, M. F. Toney and D. M. DeLongchamp, *ACS Nano*, 2011, **5**, 8248-8257.
50. F. Buss, B. Schmidt-Hansberg, M. Sanyal, C. Munuera, P. Scharfer, W. Schabel and E. Barrena, *Macromolecules*, 2016, **49**, 4867-4874.
51. S. Swaraj, C. Wang, H. Yan, B. Watts, J. Lüning, C. R. McNeill and H. Ade, *Nano Lett.*, 2010, **10**, 2863-2869.
52. H. Yan, B. A. Collins, E. Gann, C. Wang, H. Ade and C. R. McNeill, *ACS Nano*, 2012, **6**, 677-688.
53. P. Schilinsky, C. Waldauf and C. J. Brabec, *Appl. Phys. Lett.*, 2002, **81**, 3885-3887.
54. Z. Li, J. D. A. Lin, H. Phan, A. Sharenko, C. M. Proctor, P. Zalar, Z. Chen, A. Facchetti and T.-Q. Nguyen, *Adv. Funct. Mater.*, 2014, **24**, 6989-6998.
55. L. Lu, T. Xu, W. Chen, E. S. Landry and L. Yu, *Nat. Photon.*, 2014, **8**, 716-722.

56. P. W. M. Blom, M. J. M. de Jong and M. G. van Munster, *Phys. Rev. B*, 1997, **55**, R656-R659.
57. Y. Shen, A. R. Hosseini, M. H. Wong and G. G. Malliaras, *ChemPhysChem*, 2004, **5**, 16-25.
58. W. Li, K. H. Hendriks, W. S. C. Roelofs, Y. Kim, M. M. Wienk and R. A. J. Janssen, *Adv. Mater.*, 2013, **25**, 3182-3186.
59. Y. Sun, J. H. Seo, C. J. Takacs, J. Seifter and A. J. Heeger, *Adv. Mater.*, 2011, **23**, 1679-1683.

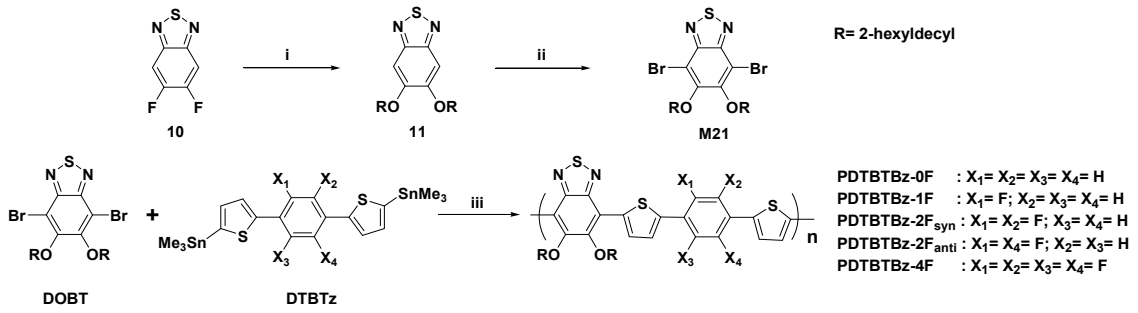

Scheme 1 The synthetic route to the monomer M21 and polymers. i) 2-Hexyldecanol, NaH (60% dispersion in paraffin), DMF. ii) Bromine, CH2Cl2:CH3COOH (1:1). iii) Pd2(dba)3, P(o-Tol)3, chlorobenzene, MW 150 ºC.

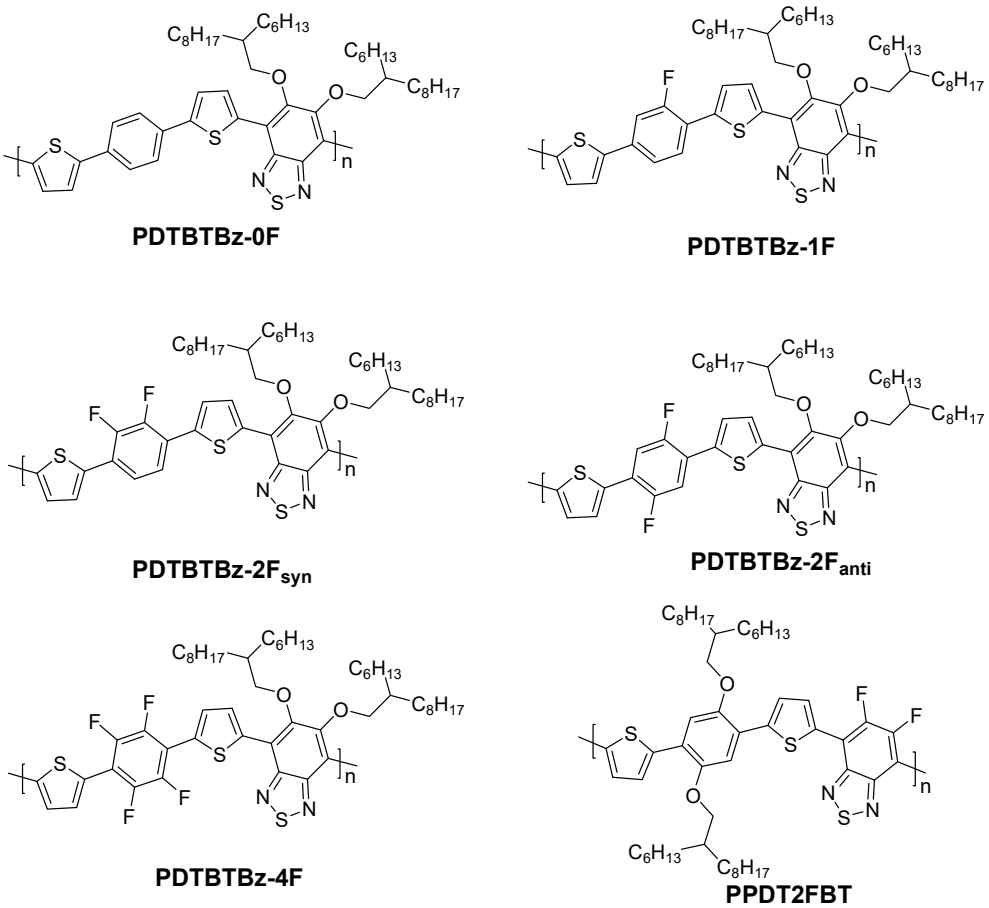

Scheme 2 Molecular structures of polymers in this study and PPDT2FBT[39]

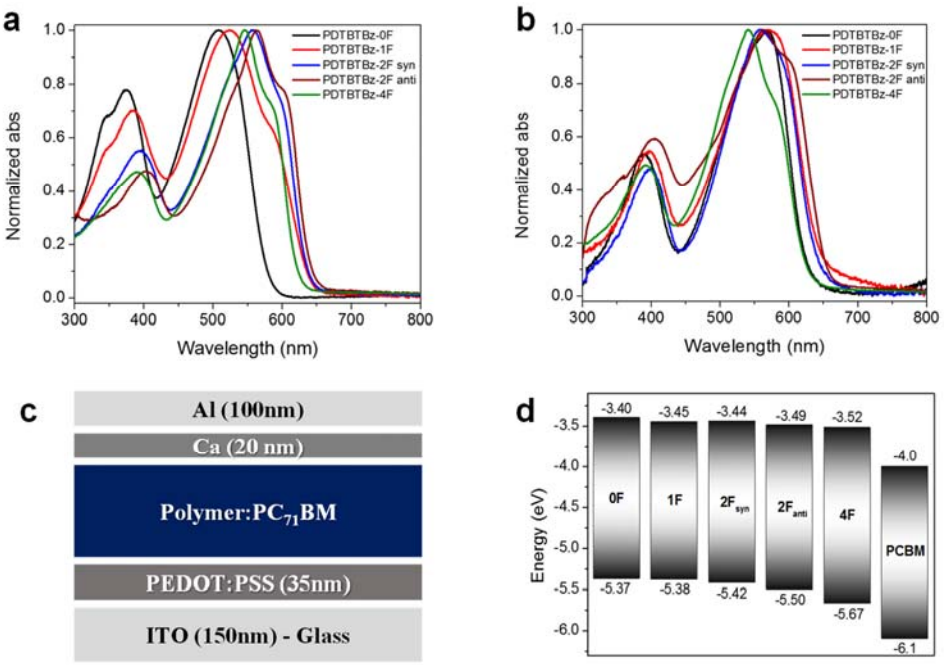

Fig. 1 Normalized optical absorption spectra of the polymers (a) in chloroform solution and (b) in thin film. (c) Device structure of PSCs used in this study. (d) Energy diagram of polymer series and $PC_{71}BM$.

Table 1 Physical properties of the WBG polymers

Polymer	M_n (M_w)[a] [kg.mol^{-1}]	T_d (^{0}C)[b]	$\lambda_{max}^{abs,sol}$ (nm)	$\lambda_{max}^{abs,film}$ (nm)	$\lambda_{onset}^{abs,film}$ (nm)	E_g^{opt} (eV)	HOMO[c] (eV)	LUMO[c] (eV)	E_g^{ec} (eV)
PDTBTBz-0F	28.6 (43.7)	283	508	569	631	1.97	- 5.37	- 3.40	1.97
PDTBTBz-1F	46.2(109.4)	283	523	571	646	1.92	- 5.38	- 3.45	1.93
PDTBTBz-2F$_{syn}$	111.9(347.2)	283	558	558	646	1.92	- 5.42	-3.44	1.98
PDTBTBz-2F$_{anti}$	182.6(382.1)	285	563	564	652	1.90	- 5.50	- 3.49	2.01
PDTBTBz-4F	182.3(557.0)	285	546	541	629	1.97	- 5.67	-3.52	2.15

[a]Number-average molecular weight (Mn) and Weight-average molecular weight (Mw) determined by GPC with o-dichlorobenzene as the eluent at 80 °C. [b]Decomposition temperature (Td) was determined by TGA in a nitrogen atmosphere (with 5% weight-loss). [c]HOMO and LUMO level was estimated from the tangential onset of oxidation ($E_{ox\ onset}$) and onset of reduction ($E_{red\ onset}$) by cyclic voltammetry using equation HOMO(eV)=-($E_{ox\ onset}$-E1/2ferrocene+4.8).

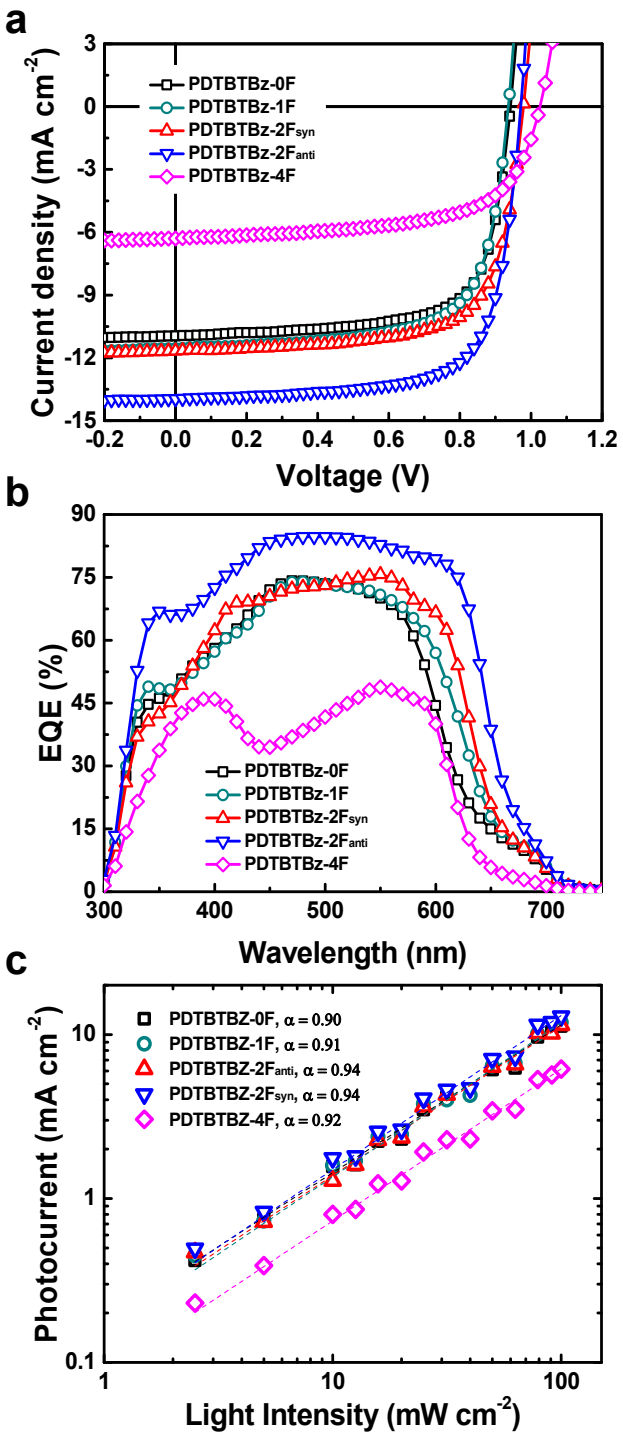

Fig. 2 (a) Current density–voltage (*J*–*V*) curves, (b) external quantum efficiency (EQE) and (c) light intensity dependence of J_{SC} for optimum devices using polymers:$PC_{71}BM$ blend prepared from CB solvent with DPE.

Table 2 Summary of device parameter for optimum device using polymers:$PC_{71}BM$ blend prepared from CB solvent with DPE.

Donor:$PC_{71}BM$	J_{SC} (mA/cm^2)	[*Cal.*] J_{SC}[a] (mA/cm^2)	V_{OC} (V)	FF	PCE (%) Best (Ave.)[b]
PDTBTBz-0F	11.0 (11.1±0.4)	10.2	0.94 (0.93±0.01)	0.71 (0.69±0.02)	7.3 (7.2±0.1)
PDTBTBz-1F	11.6 (11.5±0.5)	11.1	0.94 (0.93±0.1)	0.70 (0.69±0.01)	7.5 (7.4±0.2)
PDTBTBz-2F_{syn}	11.7 (11.5±0.1)	11.4	0.98 (0.97±0.01)	0.71 (0.70±0.01)	8.1 (7.9±0.1)
PDTBTBz-2F_{anti}	14.0 (13.8±0.2)	13.8	0.97 (0.97±0.0)	0.72 (0.72±0.01)	9.8 (9.5±0.2)
PDTBTBz-4F	6.3 (6.4±0.4)	6.4	1.03 (0.99±0.02)	0.63 (0.61±0.01)	4.1 (4.0±0.2)

a) Calculated J_{SC} from a EQE curve, [b]Average PCE values obtained from 15 devices.

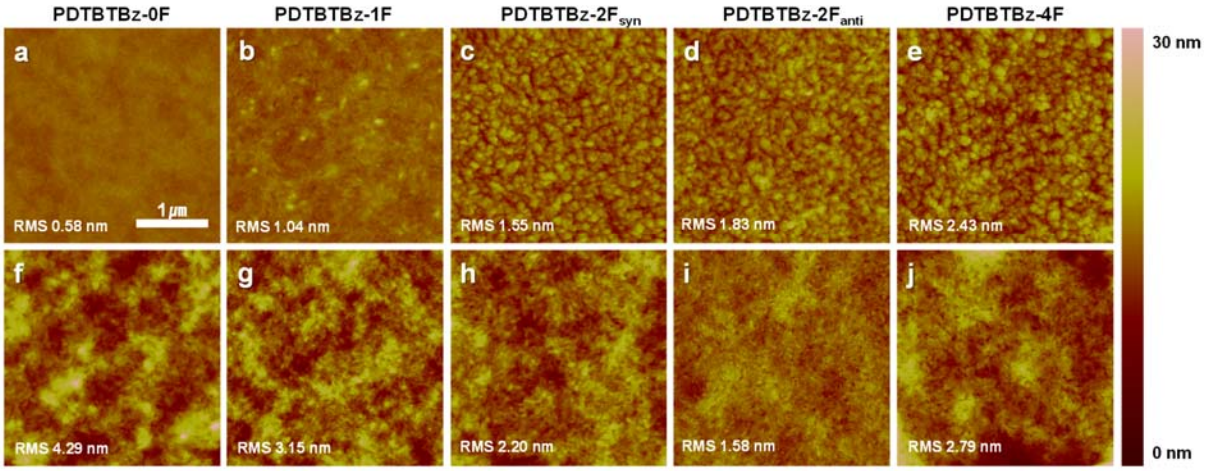

Fig. 3 Tapping-mode AFM topography of polymers:$PC_{71}BM$ blend films (solvent: CB without and with DPE). Without DPE: (a) PDTBTBz-0F, (b) PDTBTBz-1F,(c) PDTBTBz-2F_{syn}, (d) PDTBTBz-2F_{anti}, and (e) PDTBTBz-4F. With DPE: f) PDTBTBz-0F, g) PDTBTBz-1F, h) PDTBTBz-2F_{syn}, i) PDTBTBz-2F_{anti}, and j) PDTBTBz-4F. The size of all images is 3.0 μm × 3.0 μm.

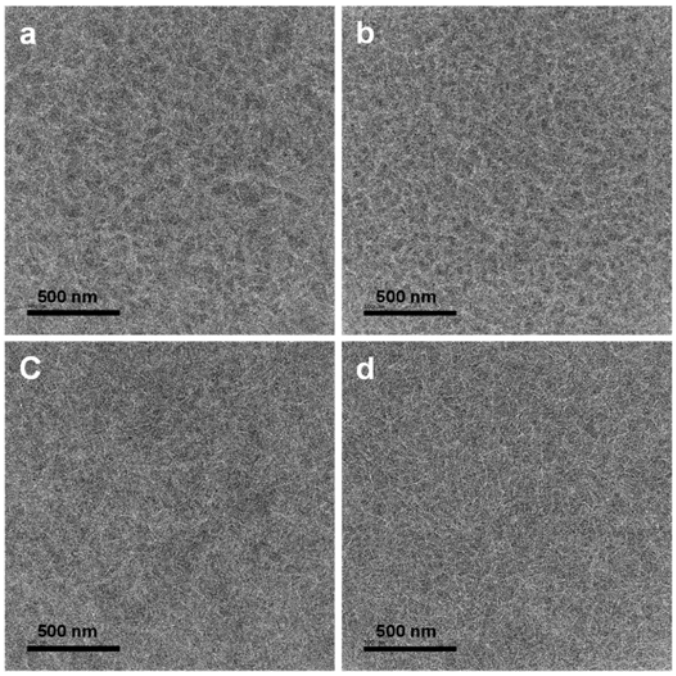

Fig. 4 HR-TEM images of PDTBTBz-2F$_{syn}$ and -2F$_{anti}$ polymers:PC$_{71}$BM films without (a and b) and with DPE (c and d), respectively. The size of all images is 1.8 μm × 1.8 μm.

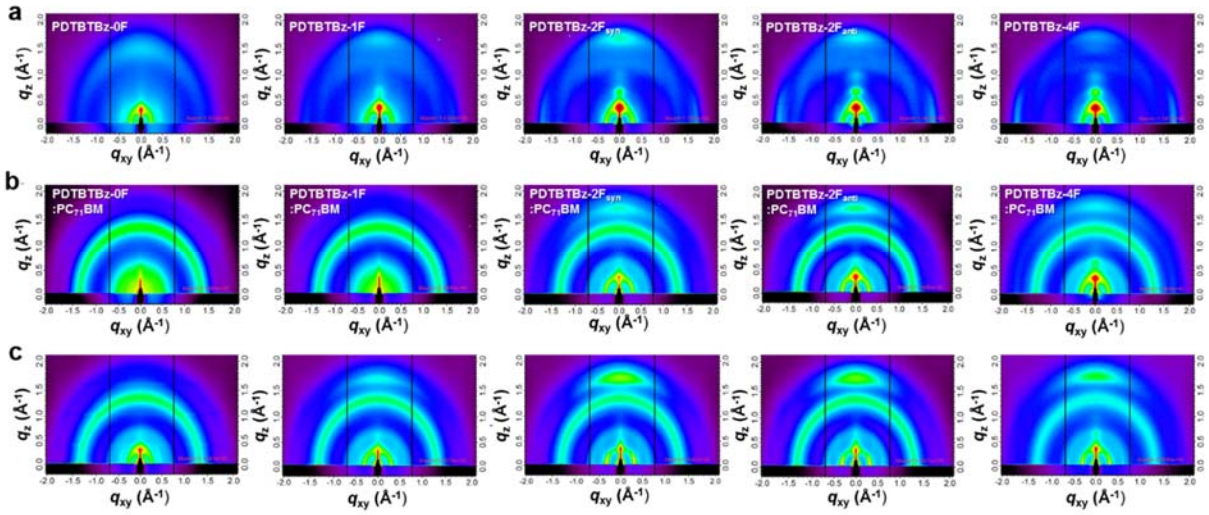

Fig. 5 Two-dimensional grazing incidence wide angle X-ray scattering (2D-GIWAXS) images. (a) 2D-GIWAXS images of pristine polymer films, (b) polymers:PC$_{71}$BM blend films, and (c) polymers:PC$_{71}$BM blend films with DPE. Each panel from left to right shows the 2D-GIWAXS images for PDTBTBz-0F, PDTBTBz-1F, PDTBTBz-2F$_{syn}$, PDTBTBz-2F$_{anti}$, and PDTBTBz-4F, respectively. Note that images have not been corrected for the inaccessible region of reciprocal space near the q_z axis.

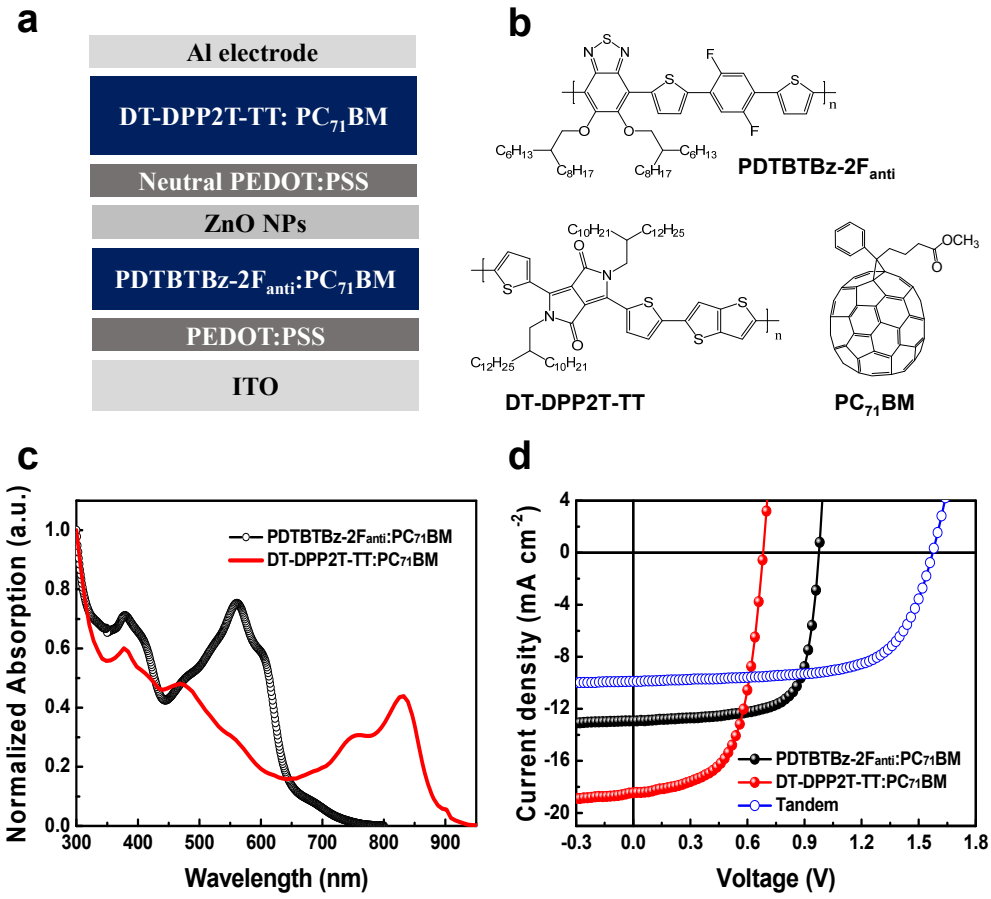

Fig. 6 (a) Tandem PSC device structure and (b) chemical structures of the active layer materials. (c) Absorption spectra of the active layers and (d) *J*–*V* curves of single (front and back) and tandem devices.

The table of contents:

A new series of wide band gap based on fluorinated phenylene-alkoxybenzothiadiazole unit with optical band gap over 1.90 eV is designed and utilized for high-performance single- and multi-junction bulk heterojunction polymer solar cells.